IR&EO measurement facilities

V11-1

THOMAS SVENSSON, ANNA SARGSYAN, ROLAND LINDELL,
JÖRGEN AHLBERG, DAVID BERGSTRÖM, STEFAN BJÖRKERT,
STAFFAN CRONSTRÖM, TOMAS HALLBERG, ROLF PERSSON

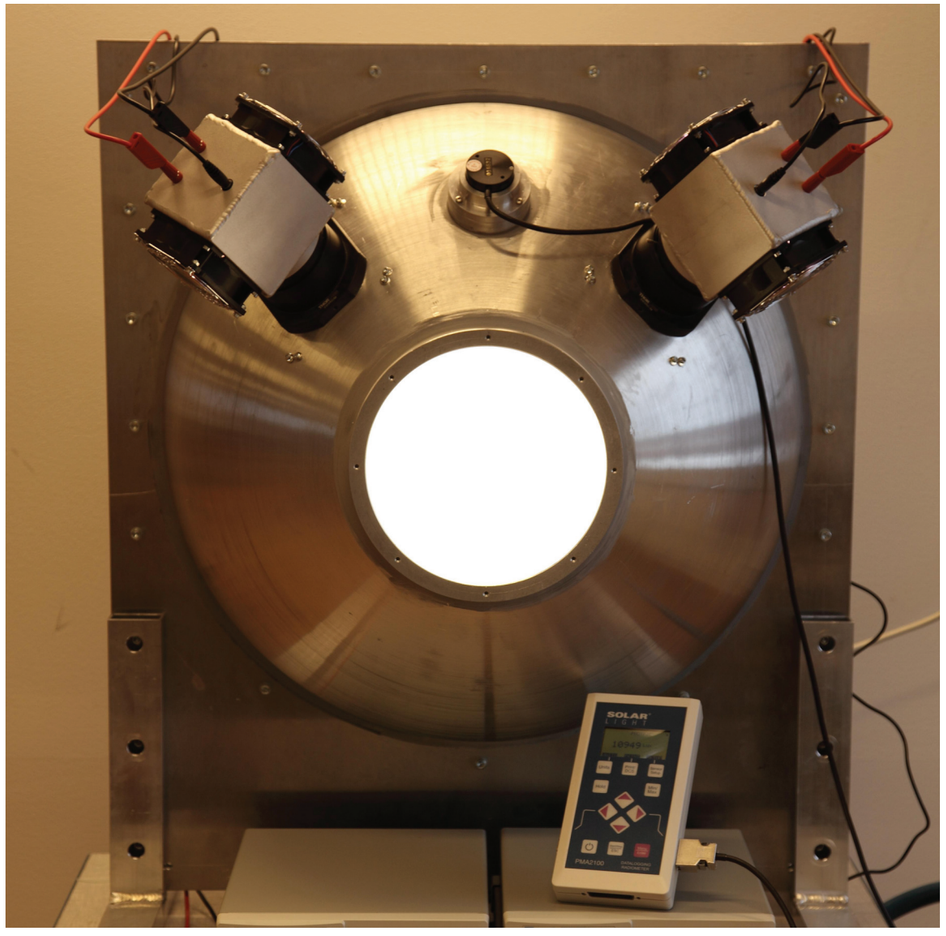

FOI
Defence Research Agency
Information Systems
Box 1165
SE-581 11 Linköping

Phone: +46 13 37 80 00
Fax: +46 13 37 81 00

www.foi.se

FOI-R--3211--SE
ISSN 1650-1942

Technical report
June 2011

Information Systems

Thomas Svensson, Anna Sargsyan, Roland Lindell,
Jörgen Ahlberg, David Bergström, Stefan Björkert,
Staffan Cronström, Tomas Hallberg, Rolf Persson

IR&EO measurement facilities v11-1

Titel	Mätinstrument och mjukvaror inom IR/EO v11-1
Title	IR/EO measurement facilities v11-1

Rapportnr/Report no	FOI-R--3211--SE
Rapporttyp Report Type	Teknisk rapport
Sidor/Pages	117 p
Månad/Month	Juni/June
Utgivningsår/Year	2011
ISSN	ISSN 1650-1942
Kund/Customer	Försvarsmakten
Projektnr/Project no	N3608, E53064
Godkänd av/Approved by	Lars Bohman

FOI, Totalförsvarets Forskningsinstitut
Avdelningen för Informationssystem
Box 1165
581 11 Linköping

FOI, Swedish Defence Research Agency
Information Systems
Box 1165
SE-581 11 Linköping

Sammanfattning

Denna rapport ger en överblick av experimentella resurser inom IR/EO-området. Instrumentbeskrivningar är oftast inkluderade i mätrapporter. Dock innehåller sällan en enskild rapport all relevant information om en sensor. Dessutom kan informationen delvis vara inaktuell på grund av uppgradering av instrument och mjukvaror.

Syftet med rapporten har varit att samla ihop all relevant information om regelbundet använda eller nyanskaffade resurser i syfte att ha ett enda dokument som referenskälla. Målet är att i framtiden göra regelbundna uppdateringar av innehållet.

Nyckelord:

mätutrustning, IR, EO, kalibrering, mjukvara, multispektral, hyperspektral, sensorprestanda, strålningsreferenser

Summary

This report presents an overview of IR/EO facilities engaged in experimental activities. Descriptions of equipment are often included in measurement reports. However, a single report does not always include all the relevant information about a sensor. In addition, the information may not be fully up to date due to upgrading of the equipment and software.

The purpose of the report has been to gather all useful information about regularly used, or newly purchased IR/EO facilities and to provide a document that can be used as a reference source containing all related information. The aim is to keep the information up to date by regularly revising the document.

Keywords: measurement equipment, IR, EO, calibration, software, multispectral, hyperspectral, sensor performance, radiation sources

Contents

1 Introduction

In 1999 a reference document was compiled at the Department of IR Systems. The document, “Measurement Equipment at the Department of IR Systems” [1] presented all the measurement equipment and related information. The purpose of [1] was to facilitate the writing procedure and gather all information in one report.

A number of experimental facilities has been purchased, modified or developed since 1999. This report gives short descriptions of current IR/EO instrumentation and corresponding software used in the analysis of collected data. It includes information on:

- Imaging sensors
- Single detector instruments
- Radiation sources
- Other measurement devices
    - Temperature measurement
    - Scintillometer
    - Collimator
    - Weather stations
    - Lux meter
- Computer softwares
    - D9: capturing of image data
    - CamViewer: reading of image data into Matlab
    - Signaturkalkyl: radiometric analysis of target signatures
    - SensorSim: addition of sensor effects to image data
    - Edgefit: calculation of MTF
    - HSI Toolbox: target detection in hyperspectral image data
    - Modtran
    - NVTherm and TRM

The report has been composed by Thomas Svensson, Anna Sargsyan and Roland Lindell. Additional contributions have been made by Jörgen Ahlberg (12.6), David Bergström (12.3-12.5), Stefan Björkert (4.3), Staffan Cronström (12.1), Tomas Hallberg (4.3-4.4, 7) and Rolf Persson (6.2, 12.7).

Figure 1-1 below shows the spectral ranges of the imaging sensors and the instruments presented in sections 3 and 4.

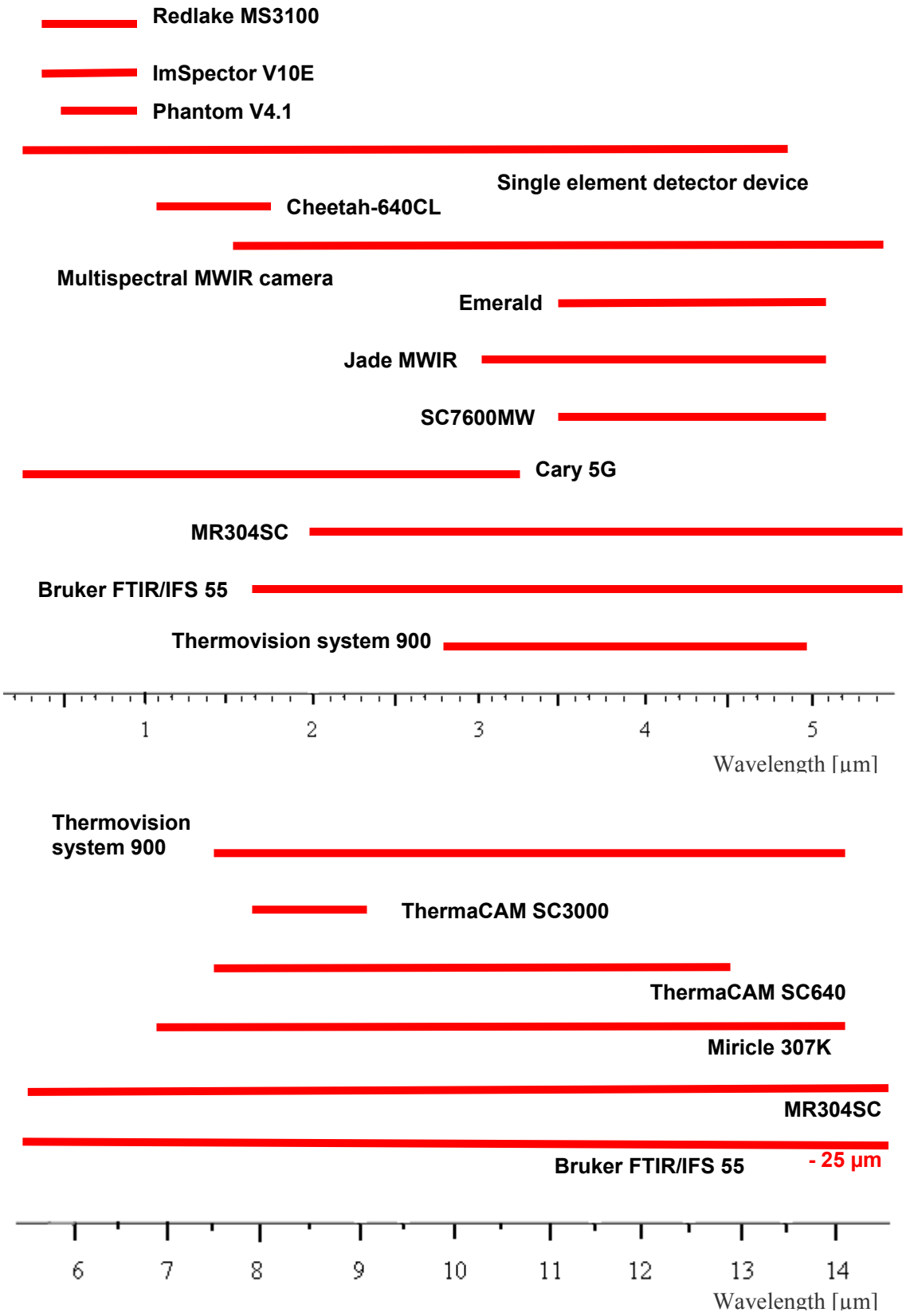

Figure 1-1. A summary of spectral ranges of the imaging sensors and the instruments in sections 3 and 4.

Abbreviations and symbols

A	area [m^2]
BRDF	bidirectional reflectance distribution function
CMOS	complementary metal oxide semiconductor
D	aperture diameter [m]
D*	normalized detectivity [$cm \cdot Hz \cdot W^{-1}$]
DHR	directional hemispherical reflectance
DN	digital number
DR	dynamic range
DSNU	dark signal non-uniformity
DTGS	deuterated triglycine sulfate
E	irradiance [W/m^2]
EMVA	European Machine Vision Association
EO	electro-optics
f	focal length [m]
F/#	f number
FOV	field of view; the angular coverage of an optical system
FPA	focal plane array
FPGA	field-programmable gate array
FTIR	Fourier transform infrared
FWHM	full width half maximum
GUI	graphical user interface
GUM	guide to the expression of uncertainty in measurements
h	Planck constant [$6.626068 \cdot 10^{-34}$ Js]
HSI	hyperspectral imaging
I	intensity [W/sr]
IFOV	instantaneous field of view
InSb	Indium Antimonide
IR	infrared
k	Boltzmann constant [$1.3806504 \cdot 10^{-23}$ J/K]
L	radiance [$W \cdot m^{-2} \cdot sr^{-1}$]
LWIR	long wave infrared (~ 8-12 µm)
M	emittance, exitance [$W \cdot m^{-2}$]
MCT	Mercury Cadmium Telluride; also written CMT
MWIR	mid wave infrared (~ 3-5 µm)
NEP	noise equivalent power [W]

NESR	noise equivalent spectral radiance [W/(cm^2·sr·cm^{-1})]
NETD	noise equivalent temperature difference; also written NEDT (noise equivalent delta temperature) [mK]
NIR	near infrared (~ 0.7-1 μm)
PE	polyethylene
PRNU	photo response non-uniformity
QWIP	quantum well infrared photodetector
R	range, distance [m]
SNR	signal-to-noise ratio; also written S/N
SWIR	short wave infrared (~ 1-3 μm)
T	temperature [K]
ε	emissivity
ρ	reflectivity
ϕ	power, flux [W]
θ	angle [radian]
Ω	solid angle [steradian]
τ	atmospheric transmission

1.1 Radiometric concepts

1.1.1 Intensity

Intensity I [W/sr] is the power radiated per unit solid angle. It is the quantity which must be used to specify the radiation from a point source (i.e. much smaller than the projected area of the detector and not resolved by the optical system). Intensity can also be used to specify an extended source (e.g. resolved by the optical system). The power ϕ [W], emitted in the solid angle Ω is given by

$$\phi = I \cdot \Omega \tag{1-1}$$

1.1.2 Irradiance

The solid angle of an optical lens with the aperture area A [m^2], as seen by a point source, is given by

$$\Omega = \frac{A}{R^2};\ A << R^2 \tag{1-2}$$

where R [m] is the distance between the point target and the sensor. The incident power on the detector is then given by

$$\phi = I \cdot \frac{A}{R^2} \tag{1-3}$$

The irradiance E [W/m^2] is the power per unit area falling on a surface

$$E = \frac{I}{R^2} \tag{1-4}$$

By including the atmospheric transmission, τ, (1-4) is modified into

$$E = \frac{I}{R^2} \cdot \tau \tag{1-5}$$

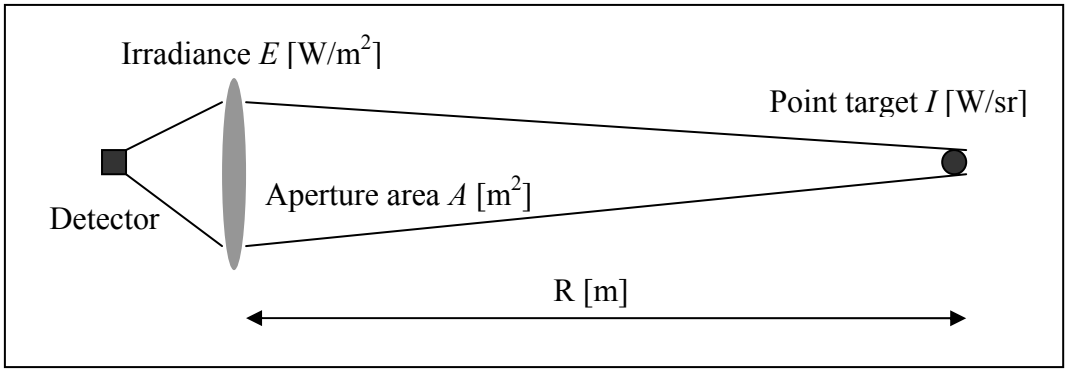

Figure 1-2. Illustration of irradiance

1.1.3 Emittance

Emittance, or exitance, [W/m^2] is the power per unit area leaving a surface. If an object's radiation is similar to a blackbody's (emissivity $\varepsilon = 1$), then the object's spectral emittance M [W/(m^2·μm)] depends on the wavelength [m] of the emitted radiation and the absolute temperature T [K] of the body. This is given by the Planck radiation law for blackbodies

$$M(\lambda,T) = \frac{2\pi hc^2}{\lambda^5 (e^{hc/\lambda kT} - 1)} \qquad (1\text{-}6)$$

where c is the speed of light, h the Planck constant and k the Boltzmann constant.

Integration over all wavelengths gives the total emittance from the object, the Stefan-Boltzmann's law

$$M_{tot}(T) = \int_0^\infty M(\lambda,T)d\lambda = \sigma T^4 \qquad (1\text{-}7)$$

where $\sigma = 5.67 \cdot 10^{-8}$ Wm^{-2}K^{-4}. At the temperature T=300 K the total emittance for a blackbody is approximately 459 W/m^2. The emittance within a specified wavelength band is obtained by integrating $M(\lambda)$ in the corresponding range:

$$M_{\lambda_1-\lambda_2}(T) = \int_{\lambda_1}^{\lambda_2} M(\lambda,T)\partial\lambda \qquad (1\text{-}8)$$

If the integration is performed (numerically) for a blackbody with the temperature T=300 K and the emissivity ε = 1 the emittance 5.9 W/m^2 is obtained for the range 3-5 μm and 121 W/m^2 for the range 8-12μm.

The maximum of the Planck radiation law is given by the Wien displacement law

$$\lambda_{\max} T = 2897.7685 \quad [\mu\text{m}\cdot\text{K}] \qquad (1\text{-}9)$$

1.1.4 Radiance

For a particular ray direction, the radiance L [W/(m^2·sr)] is defined as radiant power per unit source area (perpendicular to the ray) [m^2] and unit solid angle.

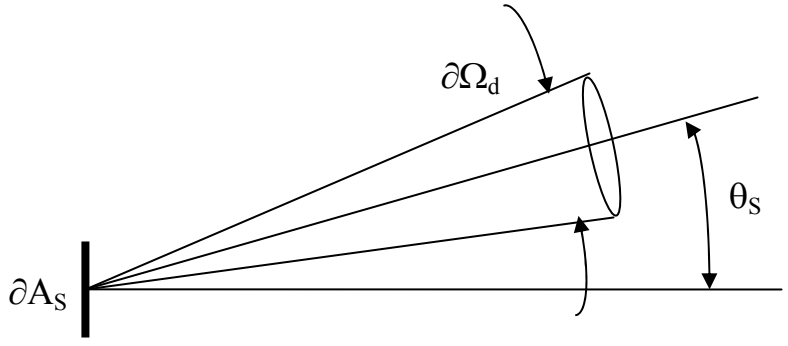

Figure 1-3. Illustration of radiance

$$L = \frac{\partial^2 \phi}{\partial A_S \cos\theta_S \partial \Omega_d} \tag{1-10}$$

where $\partial^2\phi$ is the power radiated into the cone, $\partial A_S \cdot \cos\theta_S$ is the projected area of the source and $\partial\Omega_d$ is the solid angle of the optical system. A Lambertian radiating surface is a surface for which the radiance is independent of the observation angle. For a small area A_S, small solid angle Ω_d and angle θ_S, the radiance L is approximated by

$$L \approx \frac{\phi}{A_S \Omega_d} \tag{1-11}$$

The irradiance at the aperture area A is then given by

$$E = \frac{\phi}{A} = \frac{LA_S}{R^2} \tag{1-12}$$

and the intensity from the source area A_S becomes

$$I = \frac{\phi}{\Omega_d} = LA_S \tag{1-13}$$

From (1-12) it can be noted that

$$\phi = LA\Omega_S = LA_S\Omega_d \tag{1-14}$$

For a plane Lambertian radiating surface the relation between the radiance and the emittance is expressed in:

$$L = \frac{M(T)}{\pi} \qquad \left[\frac{W}{m^2 \cdot sr}\right] \tag{1-15}$$

which can be derived from (1-10):

$$\phi = \int \partial^2\phi = \int_{\substack{hemi-\\sphere}} L\cos\theta_S \partial\Omega_d A_S = \pi L A_S;\ M = \frac{\phi}{A_S} = \pi L \tag{1-16}$$

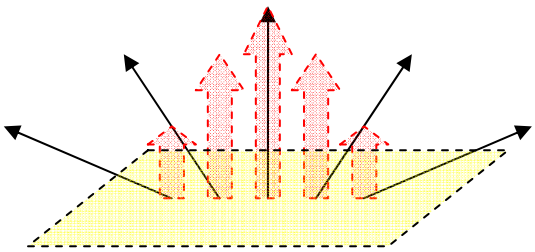

Figure 1-4. Illustration of (1-16). The source radiates into a hemisphere (2π steradians), but the proportionality to $\cos\theta_S$ introduces a factor of ½ in the integration

Figure 1-5 shows the Planck radiation law for four different temperatures: 25 °C, 250 °C, 1000 °C and 2000 °C. Note that the y-axis scale is linear in the figure.

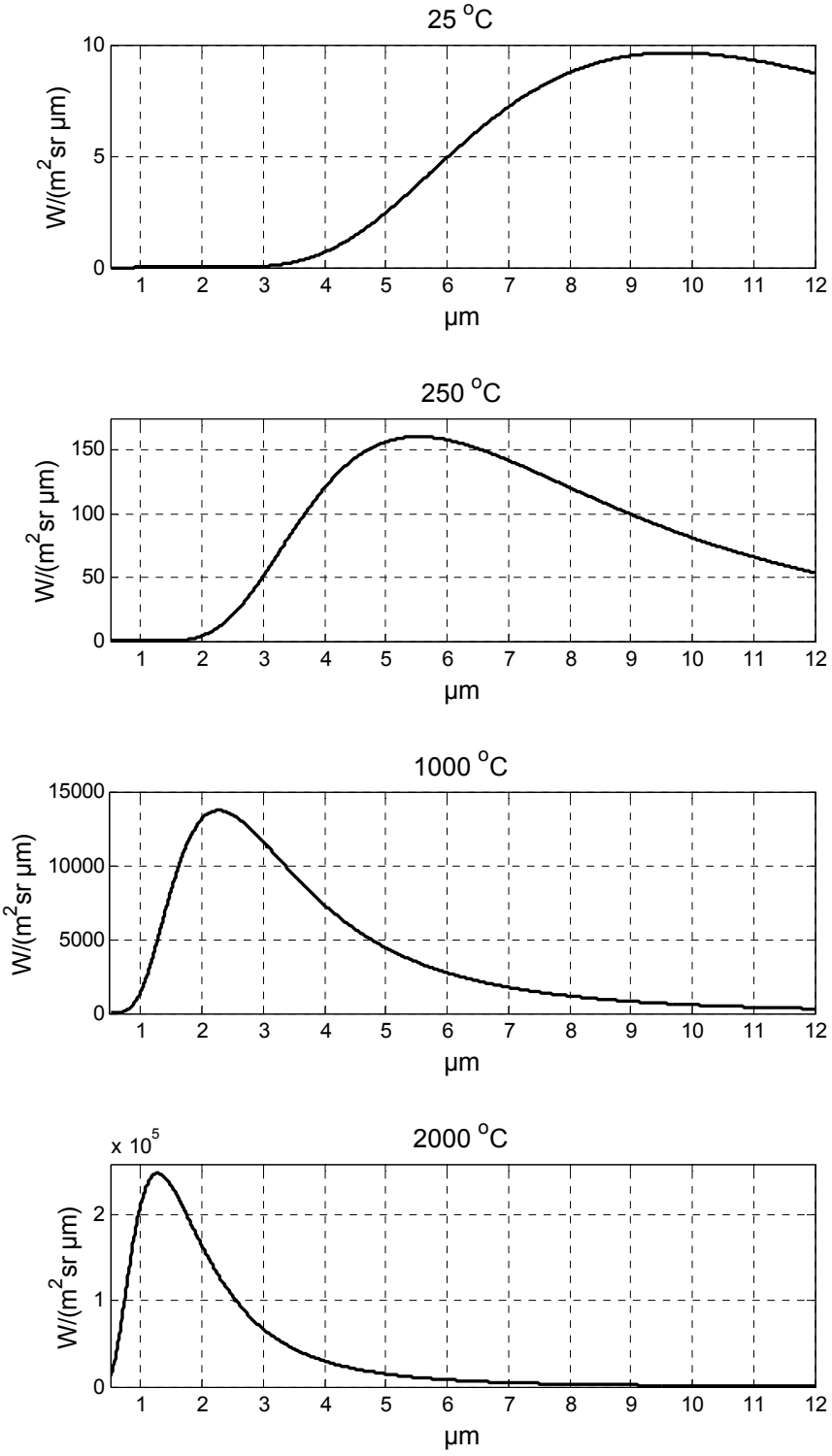

Figure 1-5. The Planck radiation law for 25 °C, 250 °C, 1000 °C and 2000 °C.

1.1.5 Emissivity and reflectivity

The maximum emittance is given by the Planck radiation law for blackbodies. The ratio between the emittance of the source, M_S, and the emittance of a blackbody, M_{BB}, at the same temperature is defined as emissivity, ε_S

$$\varepsilon_S(\lambda) = \frac{M_S(\lambda)}{M_{BB}(\lambda)} \tag{1-17}$$

If ε_S is a constant < 1 for all wavelengths the source is called a greybody.

Reflectivity is the fraction of irradiance E [W/m^2], reflected by a surface. The specular spectral reflectivity, ρ_S, is given by

$$\rho_S(\lambda) = \frac{M_S^{refl}(\lambda)}{E(\lambda)} \tag{1-18}$$

The bidirectional reflectance distribution function (BRDF) [sr^{-1}] relates the reflected radiance to the irradiance

$$\rho_B(\lambda) = \frac{L_S^{refl}(\lambda, \theta_r, \varphi_r)}{E(\lambda, \theta_i, \varphi_i)} \tag{1-19}$$

where θ is the zenith angle and φ the azimuth angle (see section 7, Figure 7-2).

Incident power on a body can either be absorbed, reflected or transmitted (Kirchoff's law):

$$\alpha(\lambda) + \rho(\lambda) + \tau(\lambda) = 1 \tag{1-20}$$

where α is the absorptance and τ the transmittance. If $\alpha = 1$ the body is an ideal blackbody.

1.2 Concepts related to imaging systems

1.2.1 F-number and FOV

A sensors F-number (F/#) is the ratio between the focal length f [m] and the aperture diameter D [m]

$$F/\# = \frac{f}{D} \tag{1-21}$$

The field of view (FOV) is the angular coverage of an optical system (Figure 1-6). Instantaneous field of view (IFOV) is the angular coverage of a single detector element.

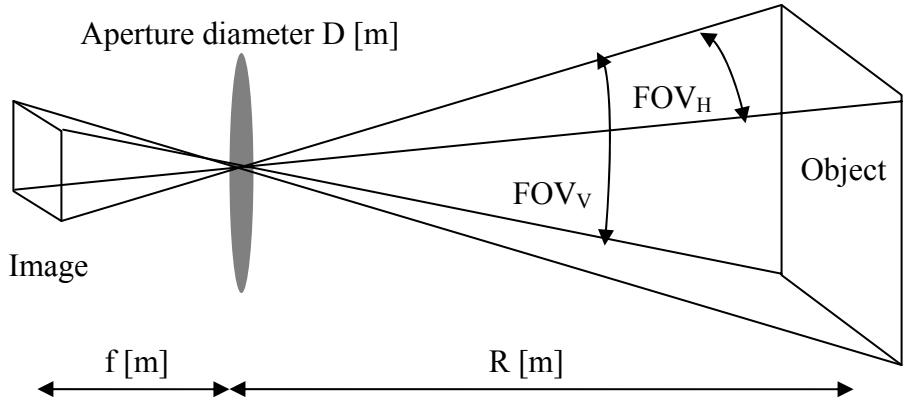

Figure 1-6. F-number and FOV

1.2.2 Diffraction and aberration

Due to diffraction, which is a fundamental consequence of the wave nature of electromagnetic radiation, an optical system with a finite-sized aperture can never form a point image and can not resolve two point targets if the angle separating the targets is smaller than

$$\theta \approx \frac{1.22\lambda}{D} \qquad (1\text{-}22)$$

Systems with low F/# (and large D) have the best potential performance, but at the same time the effects of aberrations generally produce larger spot sizes when the F-number decrease. Examples of aberrations inherent in optical systems with spherical surfaces are chromatic and spherical aberration (Figure 1-7).

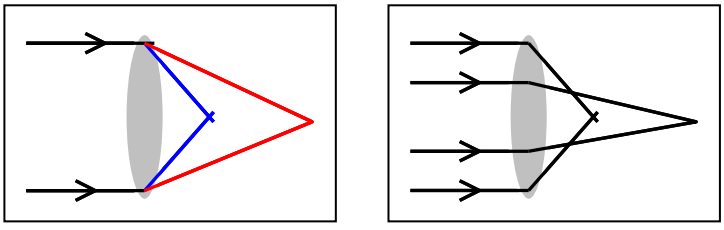

Figure 1-7. Schematic sketch illustrating aberration effects. Left: chromatic aberration; the location of the focal point is wavelength dependent. Right: spherical aberration; the location of the focal point depends on the distance between incident rays and the optical axis.

1.2.3 Modulation transfer function

An ideal image, *f(x,y)*, of an object displays the irradiance [W/cm^2] distribution in the image plane for a system with perfect image quality. The point spread function (PSF), *h(x,y)*, of an imaging system is the two-dimensional image of a point-source object and the smallest image detail an optical system can form. The image irradiance distribution, *g(x,y)*, is the ideal image, *f(x,y)*, convolved with the PSF [2, 3]

$$g(x,y) = f(x,y) * h(x,y) \tag{1-23}$$

The convolution theorem states that convolution in the spatial domain is equivalent to a product in the frequency domain

$$G(u,v) = F(u,v) \cdot H(u,v) \tag{1-24}$$

The normalized *H(u, v)* is called the optical transfer function (OTF), which generally is a complex function with both a magnitude and a phase portion. Its magnitude is called the MTF and its phase, θ(u,ν), the phase transfer function (PTF)

$$OTF(u,v) = \left|OTF(u,v)\right| \cdot \exp\left(-i\theta(u,v)\right) = MTF(u,v) \cdot PTF(u,v) \tag{1-25}$$

The MTF is an imaging systems response to sinusoids of different spatial frequencies and a measure of the systems ability to respond on and reproduce different spatial frequencies, where low frequencies correspond to larger objects and higher frequencies to smaller objects in the image. The response is given by the modulation depth, *M*

$$M = \frac{S_{\max} - S_{\min}}{S_{\max} + S_{\min}} \tag{1-26}$$

where S_{max} and S_{min} are the maximum and the minimum value of the signal. MTF is defined as the ratio between the modulation depths of the output and the input signal

$$MTF = \frac{M_{out}}{M_{in}} = \frac{M_{image}}{M_{object}} \tag{1-27}$$

(1-27) is illustrated in Figure 1-8. The spatial frequency is usually expressed in the unit cycles per milliradian [cy/mrad] (Figure 1-9).

A systems total MTF is the product of all subsystems (independent) MTFs

$$MTF_{system} = \prod_i MTF_i \tag{1-28}$$

where *i* denotes subsystems e.g. diffraction, detector, motion, turbulence etc.

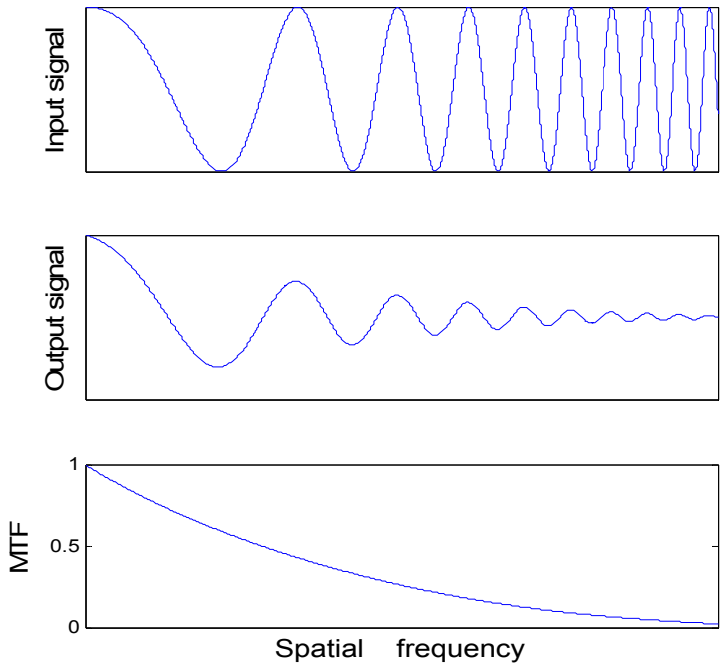

Figure 1-8. Input signal, output signal and MTF.

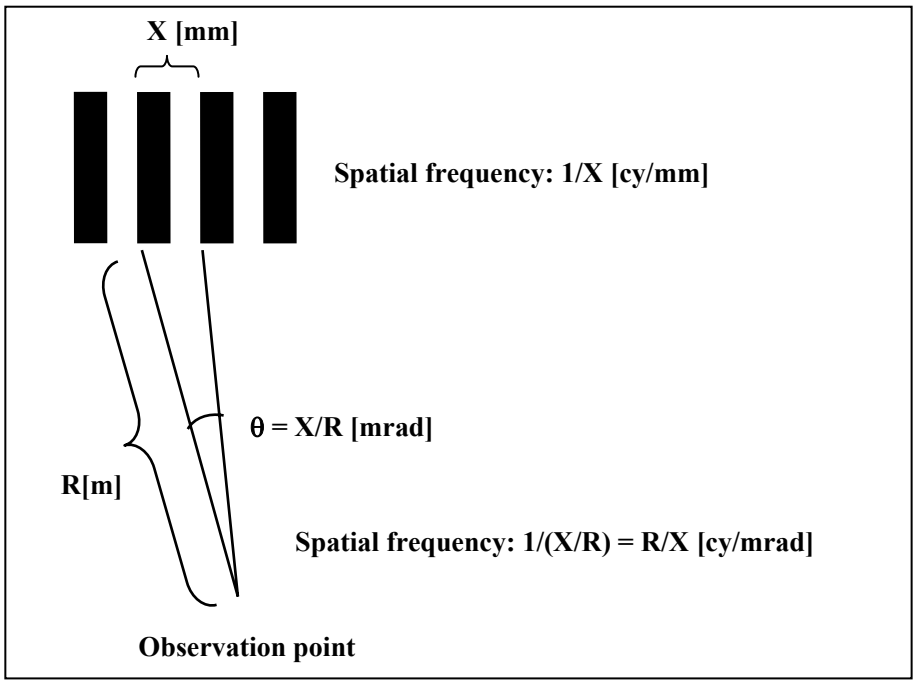

Figure 1-9. Spatial frequency: cycles per milliradian [cy/mrad] and cycles per mm [cy/mm]

The theoretically best MTF for an infrared sensor depends on detector and optics.

The MTF due to the detector is given by

$$MTF_{\det ector} = \frac{\sin(\pi\alpha v)}{\pi\alpha v} \tag{1-29}$$

where α = DAS (detector angular subtense) and ν is the spatial frequency. MTF = 0 at the spatial frequency $\nu = 1/\alpha$ (detector cut-off). DAS is defined

$$DAS = \alpha = \frac{d}{f} \tag{1-30}$$

where d = detector size and f = focal length.

The MTF is constrained by the optics due to diffraction in the circular aperture:

$$MTF_{diffraction} = \frac{2}{\pi}\left[\cos^{-1}\left(\frac{v}{v_{OCO}}\right) - \frac{v}{v_{OCO}}\sqrt{1-\left(\frac{v}{v_{OCO}}\right)^2}\right] \tag{1-31}$$

where $\nu < \nu_{OCO}$; otherwise $MTF_{diff} = 0$. ν_{OCO} is the optical cutoff

$$v_{OCO} = \frac{D}{\lambda} \tag{1-32}$$

where D is the aperture diameter and λ the wave length.

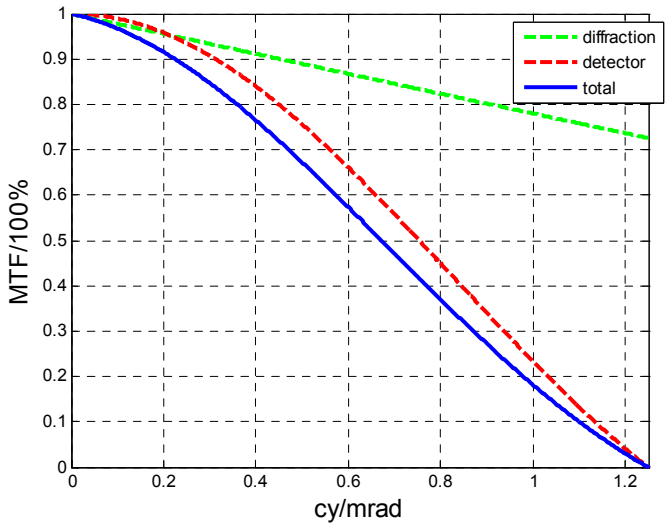

Figure 1-10 . $MTF_{diffraction}$, $MTF_{detector}$ and MTF_{system} calculated for Cheetah 640CL with the parameters given in Table 3-4 and F/#=2.8

1.2.4 Non-uniformity

The temporal noise determines the optimal resolution of radiant power by an imaging sensor. Due to non-uniform pixel responses to incident radiance, spatial noise will be added to the temporal noise (Figure 1-11). Therefore a uniform source will be non-uniformly reproduced in the image plane.

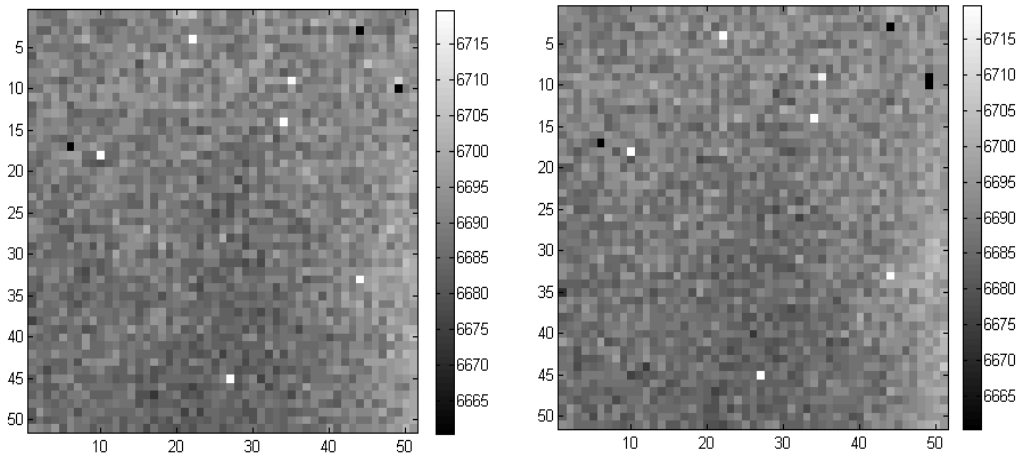

Figure 1-11. Spatial noise. The figure shows two infrared registrations of a uniform surface radiator; the time difference is 0.04 s. The mean pixel value in the (cropped) images is about 6690 [DN]. Most of the pixel deviations (too low or too high values) in the left image remain in the image to the right.

Some sources of non-uniformity are:

- Fabrication errors e.g. detector element and substrate doping variations
- Cooling system: small deviations/changes in the regulated FPA operating temperature
- Electronics: variations in the read-out electronics. A non-random source that may produce image artefacts such as striping.
- Optical effects e.g.
    - Narcissus
    - Vignetting
    - Cos^4 shading (Cosine-to-the Fourth Falloff)

Narcissus effects are due to unintended reflections of internal optical surfaces. The detector then sees sources, usually the detector itself, at lower temperatures than the background and a dark (cold) spot will appear in the image (Figure 1-12).

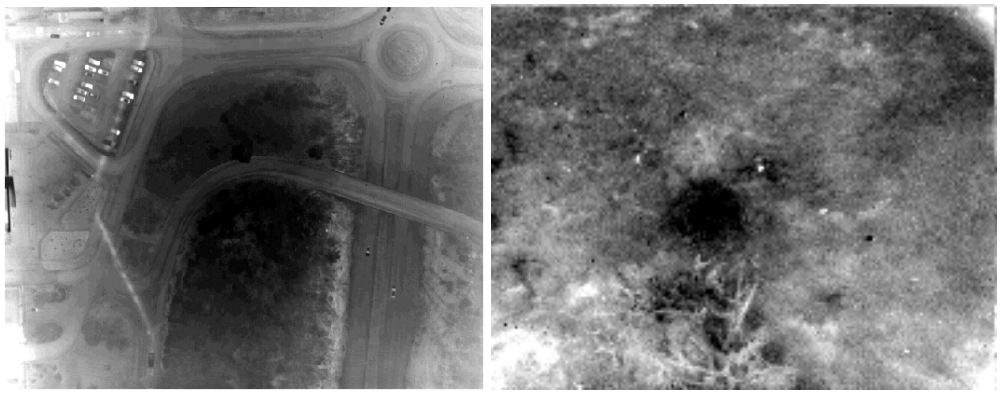

Figure 1-12. Narcissus effects are observed as dark spots in images; the degree of degradation depends on surrounding temperature changes

Vignetting are due to blockage of off-axis rays by beam-delimiting components e.g. aperture stops.

Cos^4 shading will be present when source and detector are parallel to one another, but displaced vertically according to Figure 1-13 [2].

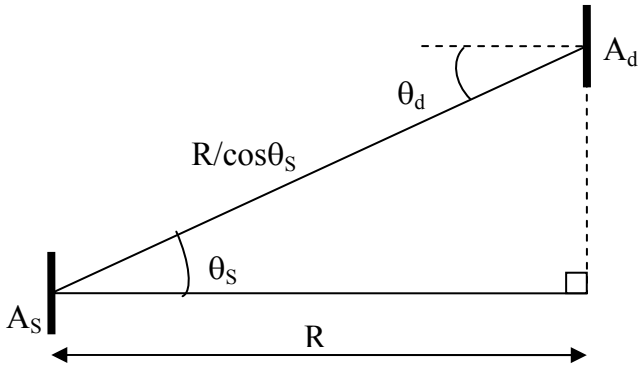

Figure 1-13. A_S = source area; A_d = detector area. The power transfer has a cosine-to-the-fourth falloff when both θ_S and θ_d are non-zero.

From Figure 1-13:

$$\phi_d = L_S \times A_S \cos\theta_S \times \Omega_d = L \times A_S \cos\theta_S \times \frac{A_d \cos\theta_d}{\left(R/\cos\theta_S\right)^2} \qquad (1\text{-}33)$$

For cases where $\theta_S = \theta_d = \theta$, $\phi_d \propto \left(\cos\theta\right)^4$

The spatial noise is often referred to as fixed pattern noise, *FPN*, which is a misleading expression because the spatial noise is not fixed (Figure 1-14).

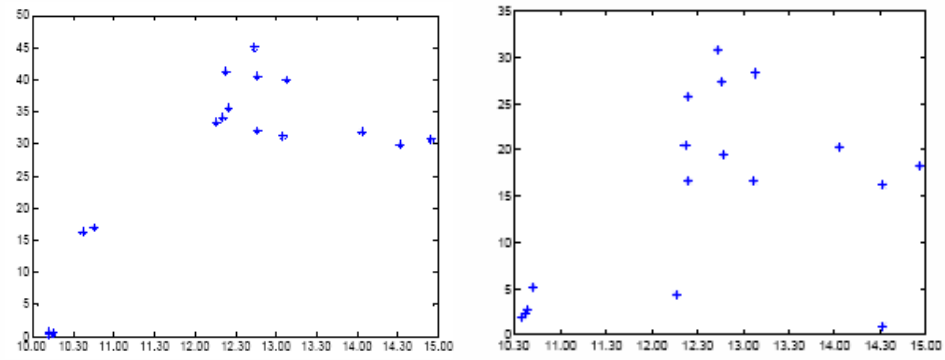

Figure 1-14. The two diagrams show the goodness value c measured for two infrared cameras vs. time. c relates the spatial noise to the temporal noise; a c value = 0 is obtained if only temporal noise remains. Non-uniformity corrections were performed for the two cameras at the time points 10.15 and 10.30 resp. For both cameras there is a dramatic increase of the spatial noise within 2 hours after the corrections were performed, which is due to sensor drift. One source of sensor drift is varying operating conditions.

1.3 Photometric units

Radiometry describes the transfer of energy [J] or power [W] from source to detector. Photometry describes the perceived brightness of a source to the human eye. The measured power is therefore weighted by a function that represents the spectral sensitivity of the eye.

Candela (cd) is defined as the luminous intensity of monochromatic radiation of frequency 540 terahertz and intensity 1/683 W/sr. 540 terahertz corresponds to a wavelength of 555 nm in the green to which the sensitivity of the human eye is at maximum.

Table 1-1. Photometric units

Quantity	**Symbol**	**Unit**	**Corresponding radiometric quantity**
Luminous intensity	I_v	candela (cd)	intensity [W/sr]
Luminous flux	F	lumen (lm) = cd·sr	power, flux [W]
Illuminance	E_v	lux (lx) = lm/m^2	irradiance [W/m^2]
Luminance	L_v	cd/m^2	radiance [W/(m^2·sr)]
Luminous emittance	M_v	lux (lx) = lm/m^2	emittance [W/m^2]

2 Characterization of imaging sensors

EMVA (European Machine Vision Association) has defined a unified method to characterize sensor parameters [4]. The model can be used to predict the signal from sensors with different sensor parameters and to compare sensors. The parameters that are calculated in the sensor model are related to the incident number of photons on the detector. Below a short description is given of the sensor model and the calculation of the parameters in the model. In Appendix A the model is applied on sensor data collected with Cheetah-640CL (section 3.1.4).

The incident power [W] due to the source under consideration, detected by one pixel is given by

$$\phi = \frac{A}{R^2}\Omega_{IFOV}R^2\int_{\lambda_1}^{\lambda_2}\left[L_S(\lambda)\tau_{atm}(\lambda)W(\lambda)+L_{atm}(\lambda)\left(1-\tau_{atm}(\lambda)\right)\right]d\lambda =$$

$$= A\Omega_{IFOV}\int_{\lambda_1}^{\lambda_2}\left[L_S(\lambda)\tau_{atm}(\lambda)W(\lambda)+L_{atm}(\lambda)\left(1-\tau_{atm}(\lambda)\right)\right]d\lambda \qquad (2\text{-}1)$$

where A = the aperture area [m^2]

$\Omega_{IFOV}=\theta^2_{IFOV}$, θ_{IFOV} is the instantaneous-field-of-view

R = the source distance [m]

λ_1 - λ_2 = the spectral range of detector, filter and optics [µm]

$L_S(\lambda)$ = the spectral source radiance [W/(m^2·sr·µm)]; for a source with blackbody characteristics, $L_S(\lambda) = L^{BB}(\lambda,T)\cdot\varepsilon_S(\lambda)$

$\tau_{atm}(\lambda)$ = the atmospheric transmission

$W(\lambda)$ = the normalized curve $\tau_o(\lambda)\tau_f(\lambda)R_{norm}(\lambda)$

where
$\tau_o(\lambda)$ = the spectral transmission of the optics
$\tau_f(\lambda)$ = the spectral transmission of the filter
$R_{norm}(\lambda)$ = the normalized spectral responsivity of the detector

L_{atm} = the atmospheric radiance

By disregarding the atmospheric influence and approximating W(λ) with a boxcar function in the spectral range λ_1 - λ_2 , (2-1) is simplified to

$$\phi = A\Omega_{IFOV}\int_{\lambda_1}^{\lambda_2}L_S(\lambda)d\lambda \qquad (2\text{-}2)$$

The mean number of photons collected during exposure time T_{exp} is given by

$$\mu_p = \frac{\phi \cdot T_{\text{exp}}}{\left(\frac{hc}{\lambda}\right)} \tag{2-3}$$

where

h = Planck constant [J·s]
c = speed of light [m/s]
λ = the wavelength of the incident radiation [m]
T_{exp} = exposure time (also referred to as integration time) [s]

The fluctuation of the collected photons is Poisson distributed and the variance, referred to as photon noise, is equal to the mean number of collected photons:

$$\sigma_p^2 = \mu_p \tag{2-4}$$

An ideal sensor has no additional noise sources (e.g. from amplifier circuits) and the quantum efficiency is equal to unity. The SNR (signal to noise ratio) of an ideal sensor therefore is given by

$$SNR = \sqrt{\mu_p} \tag{2-5}$$

In a real sensor, electrons accumulated by collected photons are converted into a voltage, which is amplified and then converted into a digital signal or digital number [DN] by an analog digital converter. The digital number μ_y [DN] is given by

$$\mu_y = K\left(\mu_e + \mu_d\right) = K\left(\eta\mu_p + \mu_d\right) = K\eta\mu_p + \mu_{y,dark} \tag{2-6}$$

where K = system gain [DN/e$^-$]
μ_e = mean number of photon generated electrons [e$^-$]
μ_d = mean number of temporal ”dark” photons
η = quantum efficiency [%/100]
$\mu_{y,dark}$ = dark signal (offset level) [DN]

μ_y is calculated according to

$$\mu_y = \frac{1}{N}\sum_{j=1}^{N} y_j \tag{2-7}$$

where y_j is the DN for pixel j in the image and N is the number of pixels in the calculation. The dark signal increases linearly with the exposure time T_{exp}

$$\mu_{y,dark} = \mu_{y,I} \cdot T_{\text{exp}} + \mu_{y,0} \tag{2-8}$$

Noise sources can be divided into temporal and spatial noise.

The temporal noise is observed as random pixel fluctuations over the array. The spatial noise is due to pixel response non-uniformity. Two basic non-uniformities are dark signal non-uniformity (*DSNU*, the variation of the offset level from pixel to pixel) and photo response non-uniformity (*PRNU*, the variation of the gain, or sensitivity, from pixel to pixel).

The variance of noise sources add up linear. The total variance of the digital numbers is given by

$$\sigma_{y,total}^2 = \sigma_{y,temp}^2 + \sigma_{y,spat}^2 = K^2\left[\eta\mu_p + \sigma_d^2 + S_g^2\eta^2\mu_p^2 + \sigma_0^2\right] \quad (2\text{-}9)$$

where

$\sigma_{y,temp}^2$ is the variance of the temporal noise

$\sigma_{y,spat}^2$ is the variance of the spatial noise

σ_d^2 is the temporal variance of dark photons

σ_0^2 is the variance of the spatial offset noise

S_g is the standard deviation of the spatial gain noise

$$\sigma_{y,temp}^2 = K^2\eta\mu_p + \sigma_{y,temp,dark}^2 \quad (2\text{-}10)$$

where $\sigma_{y,temp,dark}^2$ is the temporal variance of the dark signal (the temporal bias).

The temporal noise $\sigma_{y,temp}^2$ of pixel j is calculated according to

$$\sigma_{y,temp}^2 = \sum_{f=1}^{F}\frac{\left(y_{jf} - \langle y_j\rangle\right)^2}{F-1} \quad (2\text{-}11)$$

where F = number of images
y_{jf} = DN for pixel j in image f
$\langle y_j\rangle$ = mean value of pixel j

$$\sigma_{y,spat}^2 = K^2 S_g^2\eta^2\mu_p^2 + \sigma_{y,spat,dark}^2 \quad (2\text{-}12)$$

where $\sigma_{y,spat,dark}^2$ is the spatial variance of the dark signal (spatial bias). The spatial noise $\sigma_{y,spat}^2$ of pixel j is calculated according to

$$\sigma_{y,spat}^2 = \sum_{j=1}^{N}\frac{\left(\bar{y}_j - \langle\bar{y}\rangle\right)^2}{N-1} \quad (2\text{-}13)$$

where $\bar{y}$ = an averaged image (in order to reduce the temporal noise)
$<\bar{y}_j>$ = the mean value in the image
$\bar{y}_j$ = DN for pixel j
N = number of pixels in the calculation

By using the equations (2-10), (2-6) and (2-9) the parameters K, η and S_g are calculated according to

$$K = \frac{\sigma_{y,temp}^2 - \sigma_{y,temp,dark}^2}{\mu_y - \mu_{y,dark}} \quad (2\text{-}14)$$

$$\eta = \frac{\mu_y - \mu_{y,dark}}{K\mu_p} \quad (2\text{-}15)$$

$$S_g = \frac{\sqrt{\sigma_{y,spat}^2 - \sigma_{y,spat,dark}^2}}{\mu_y - \mu_{y,dark}} \tag{2-16}$$

By setting $\mu_p = 0$ in (2-9) it can be noted that

$$\sigma_d = \frac{\sigma_{y,temp,dark}}{K} \tag{2-17}$$

and

$$\sigma_0 = \frac{\sigma_{y,spat,dark}}{K} \tag{2-18}$$

The SNR of the signal in digital output is defined as

$$SNR_y = \frac{\mu_y - \mu_{y,dark}}{\sigma_{y,total}} \tag{2-19}$$

Using (2-6) and (2-9), the SNR is then given by

$$SNR_y = \frac{\eta\mu_p}{\sqrt{\left(\eta\mu_p + \sigma_d^2 + S_g^2\eta^2\mu_p^2 + \sigma_0^2\right)}} \tag{2-20}$$

It should be noted that spatial noise tends to be correlated (non-uniformly distributed) over the array, e.g. light and dark areas may appear in the image. The calculated spatial noise level therefore tends to be higher if all image pixels are included in the calculation instead of a selected, uniform part of the image. It should also be noted that the variations of bias and gain tend to be correlated between the pixels, which is not considered in (2-12). In order to improve both non-uniform corrections and noise models it has been suggested that the latter should be taken into account [5]. (2-12) is then modified into

$$\sigma_{y,spat}^2 = K^2 S_g^2 \eta^2 \mu_p^2 + \sigma_{y,spat,dark}^2 + 2K\eta\mu_p \rho\sigma_{y,spat,dark} S_g \tag{2-21}$$

where ρ is the correlation coefficient.

The dynamic range, DR, is the ratio of the signal at the saturation level and the smallest detectable signal level. If the sensor is linear the following relation holds true

$$DR = \frac{\mu_{p,sat}}{\mu_{p,\min}} = \frac{\mu_{y,sat}}{\sigma_{y,temp,dark}} \tag{2-22}$$

where $\mu_{p,sat}$ is the number of photons collected at the saturation level. The normalized detectivity D* [cm$\sqrt{Hz}$ W^{-1}] is a figure of merit for detector performance [2]:

$$D^* = \frac{\sqrt{A_d \Delta f}}{NEP} \tag{2-23}$$

where A_d is the detector area [cm^2] and Δf the noise equivalent bandwidth [Hz]. The noise equivalent power *NEP* [W] is the radiant power incident on a detector that yields an SNR of one

$$NEP = \frac{\sqrt{A_d \Delta f}}{D^*} \tag{2-24}$$

The higher the D*, the better SNR the detector will have. The largest potential SNR corresponds to the maximum spectral D* value.

Definition of spatial variances

EMVA has defined DSNU and PRNU values of the EMVA 1288 standard to define spatial variances:

$$DSNU_{1288} = \frac{s_{y,dark}}{K} \quad [e^-] \tag{2-25}$$

$$PRNU_{1288} = \frac{\sqrt{s^2_{y..50} - s^2_{y.dark}}}{\mu_{y.50} - \mu_{y.dark}} \cdot 100\% \tag{2-26}$$

where $PRNU_{1288}$ defines the standard deviation relative to the mean value. $DSNU_{1288}$ can be expressed in units of DN by multiplying with the system gain K.

All pixels of a sensor array are included in the calculation. $\mu_{y,dark}$ and $\mu_{y.50}$ are the mean of dark (offset) images, y_{dark}, and the mean of images registered at 50% saturation level, y_{50}

$$\mu_{y.dark} = \frac{1}{N}\sum_{j=1}^{N} y_{dark.j} \quad , \quad \mu_{y.50} = \frac{1}{N}\sum_{j=1}^{N} y_{50.j} \tag{2-27}$$

where N is the number of pixels in the image. The spatial variances are given by

$$s^2_{y.dark} = \frac{1}{N-1}\sum_{j=1}^{N} y_{dark.j} - \mu_{y.dark} \quad , \quad s^2_{y.50} = \frac{1}{N-1}\sum_{j=1}^{N} y_{50.j} - \mu_{y.50} \tag{2-28}$$

Characterization of defect pixels

The DSNU image, y_{dark}, and the PRNU image, $y' = y_{50} - y_{dark}$, are evaluated in semilogarithmic histograms. In order to eliminate effects of a non-uniform radiation sources, a highpass filtering using a box filter should be applied on the PRNU image before computing the histograms [4].

The semilogarithmic histograms are computed according to the following steps:

1. The minimum and maximum values y_{min} and y_{max} are computed

2. The interval y_{max} - y_{min} is divided into Q > 256 bins of equal width. The bin q to be incremented for a value y is

$$q = floor\left(Q\frac{y - y_{\min}}{y_{\max} - y_{\min}} \right) \tag{2-29}$$

3. A semilogarithmic histogram is drawn. The frequency value 0 is replaced with 0.1 to avoid negative infinities on the y-axis. For the DSNU image the x-axis is centered by the mean, displaying the deviation from the mean. For the PRNU the x-axis displays the deviation from the mean relative to the mean value.
4. The normal probability distribution, p_{normal}, is added to the graph:

$$p_{normal}(q) = \frac{y_{\max} - y_{\min}}{Q} \cdot \frac{N}{\sqrt{2\pi}s_{nw}} \cdot \exp\left(-\frac{y(q)^2}{2s_{nw}^2} \right) \tag{2-30}$$

where s_{nw} is the non-white variance. $y(q)$ is the y value in the middle of the bins and is given from (2-29):

$$y(q) = y_{\min} + \frac{q + 0.5}{Q} \cdot \left(y_{\max} - y_{\min} \right) \tag{2-31}$$

3 Imaging sensors

3.1 Monospectral cameras

3.1.1 Phantom V4-1

For making registrations at a high frame rate, the camera Phantom V4.1 (Vision Research, Inc.) is used. It can store full frame images (512×512 pixels) at 1000 Hz in the visual spectral region. At this frame rate and by reading out the whole image, the internal memory of the camera can store sequences that are somewhat more than 2 s long. The camera is provided with an optical zoom (can be set to e.g. 100 mm). The integration time can be set from 10 µs to an upper limit that is dependent on the frame rate. The incident radiation level can also be controlled by a variable f number.

Figure 3-1. The high speed visual camera Phantom V4.1 (Vision Research, Inc.). At FOI a different lens is used than shown in this image.

The time length of an image sequence can be increased either by decreasing the size of the images or by lowering the frame rate. A full frame rate, 400 images/s, will result in image sequences that are 5 s long.

Table 3-1. Phantom V4.1

Detector	SR-CMOS
Spectral range	400 – 1100 nm
Array size	512 x 512
Full frame rate	30-1000 Hz
Weight	2.0 kg
Size (H x W x L)	10 x 7.5 x 20 cm

Figure 3-2. An example image 512x512 with Phantom V4.1.

3.1.2 Miricle 307K

Miricle 307K (Thermoteknix Systems Ltd) [6] is an uncooled LWIR sensor based on an alpha silicon micro-bolometer detector.

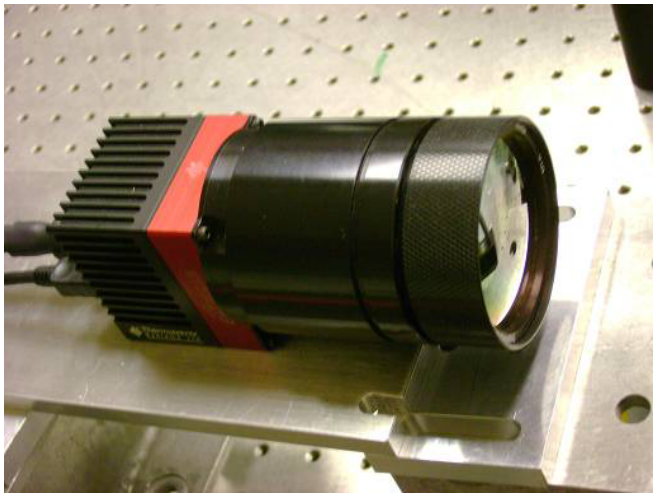

Figure 3-3. The uncooled sensor Miricle 307K (Thermoteknix Systems Ltd)

Table 3-2. Miricle 307K (Thermoteknix Systems Ltd)

Detector	uncooled Si-bolometer
Spectral range	7 – 14 µm
Array size	640 x 480
Pixel pitch	25 µm
Fill factor	80%
Standard frame rate	50 Hz
Dynamic range	14 bit
NEDT	< 85 mK
FOV	18.2°×13.7°
IFOV	0.50 mrad
F/#	1.0
Weight	86 g
Size	42 x 40 x 40 mm

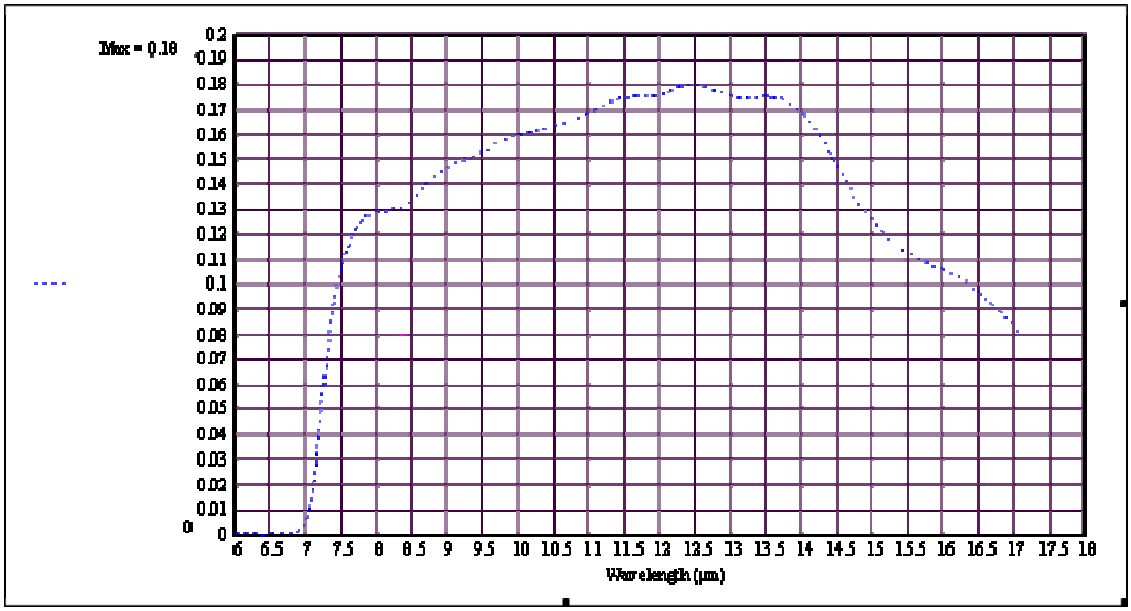

Figure 3-4 . Spectral response of Miricle307 K

Figure 3-5. An example image with Miricle 307K

3.1.3 ThermaCAM SC660

ThermaCAM SC660 (FLIR Systems) is an uncooled infrared camera in the LWIR spectral range [7]. Play-back makes it possible to view recordings without a PC. A FireWire port is available for real time image transfer to PC for image capture and analysis. A full radiometric video sequence can be recorded on a removable SD card.

Figure 3-6. Thermacam SC660 (FLIR Systems)

Table 3-3. Some data about ThermaCAM SC660

Detector	Uncooled microbolometer
FPA	640 × 480
NETD	< 30 mK
Full frame rate	30 Hz
Spectral range	7.5 µm – 13 µm
FOV (28 mm)	24°×18°
IFOV (28 mm)	0.65 mrad
Weight (incl. lens and battery)	1.8 kg
Size (L x W x H)	299 x 144 x 147 mm

Figure 3-7. An image taken with ThermaCAM SC660 (640x480 pixels)

3.1.4 Cheetah-640CL

Cheetah-640CL (Xenics) is a monochrome high speed camera with a spectral range 0.9 – 1.7 µm [7]. Its full frame rate is 1000 images/s and higher frame rates are reached by sub-windowing.

The camera head interfaces to a frame grabbing system via two parallel CameraLink interfaces. Cheetah-640CL is delivered with a software development kit which offers direct access to various camera settings and allows integration with high speed image grabbing systems. Cheetah-640CL also offers the flexibility of using C-mount lenses.

Figure 3-8. Cheetah-640CL (Xenics)

Table 3-4. Some data about Cheetah-640CL (Xenics)

Detector	InGaAs
FPA	640x512 pixels
Operability	> 99%
Pixel pitch	20 µm
Focal length	25 mm
FOV	29.3°x23.5°
IFOV	0.80 mrad
F/#	0.95 – 16.0
Spectral range	0.9 – 1.7 µm
Dynamic range	12 bit (0-4095)
Full frame rate	1000 Hz
Weight	2 kg
Size (W x H x L)	140 x 135 x 90 mm

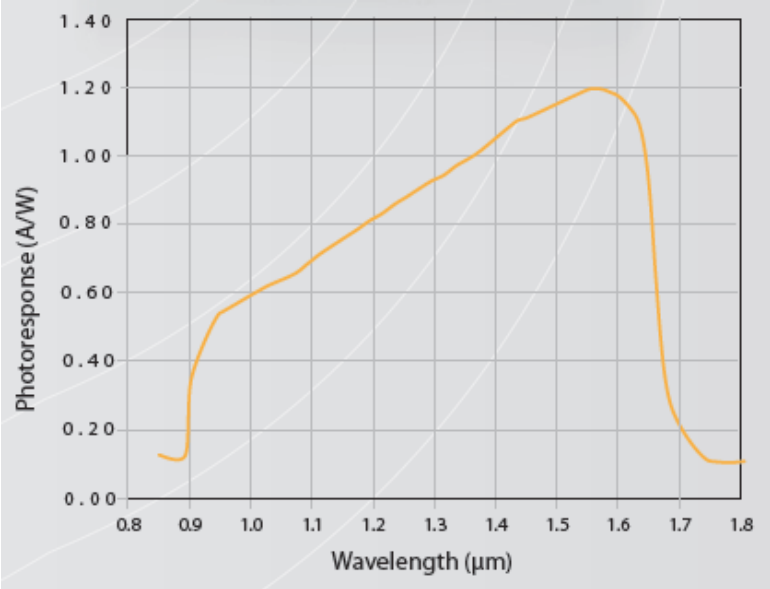

Figure 3-9. Spectral responsivity of Cheetah-640CL

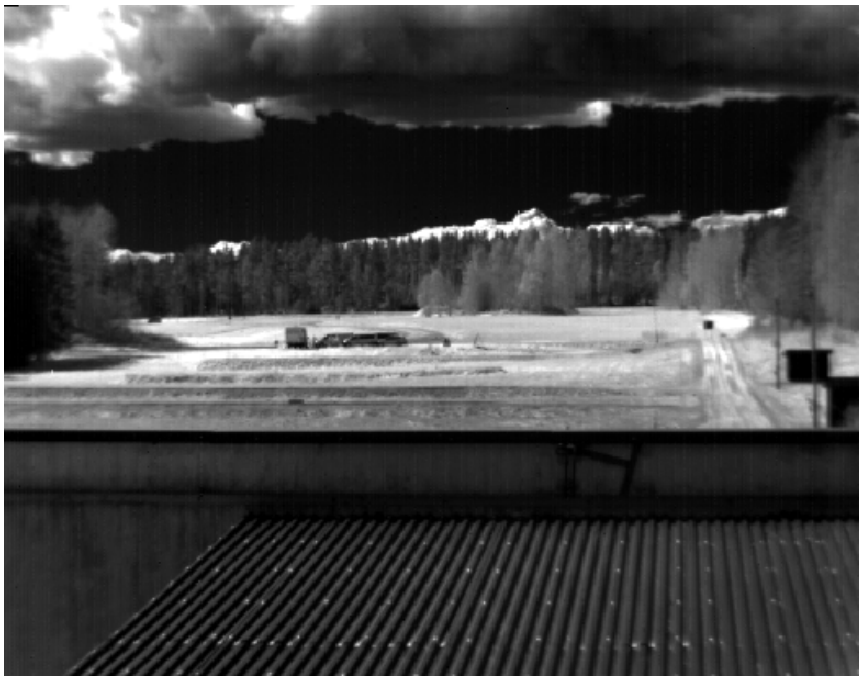

Figure 3-10. Image taken with Cheetah-640CL with a high pass filter > 1.36 µm

3.1.5 Rolera MGI

Rolera MGI (QImaging) is a back illuminated EMCCD camera for low light imaging (Figure 2-11) [9]. The specification states 90 % quantum efficiency between 500-650 nm (Figure 2-12). Binning increases sensitivity for imaging of very low light levels.

Figure 3-11. Rolera MGI (QImaging)

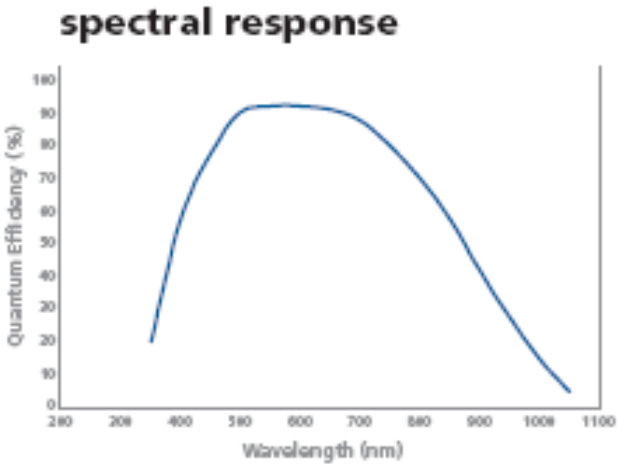

Figure 3-12. The quantum efficiency of Rolera MGI

Table 3-5. Some data about Rolera MGI

Detector	CCD
FPA	512x512
Spectral range	350 nm – 1000 nm
Binning modes	2,3,4,5,6 horisontally, arbitrary vertically
Detector size	16 µm
Dynamic range	14 bit
Frame rate	30 Hz (full frame rate) 300 Hz with 6 by 6 binning
Integration time	10 µs – days
Weight	3.18 kg
Size (L x H x W)	19 x 14 x 10 cm

Figure 3-13. Image taken with Rolera MGI

3.1.6 ThermaCam SC3000

ThermaCam SC3000 (FLIR Systems) is a cooled infrared camera in the LWIR spectral region. The camera can be mounted on a gyro-stabilized turret (Figure 3-14). Some data about the camera are presented in Table 3-6.

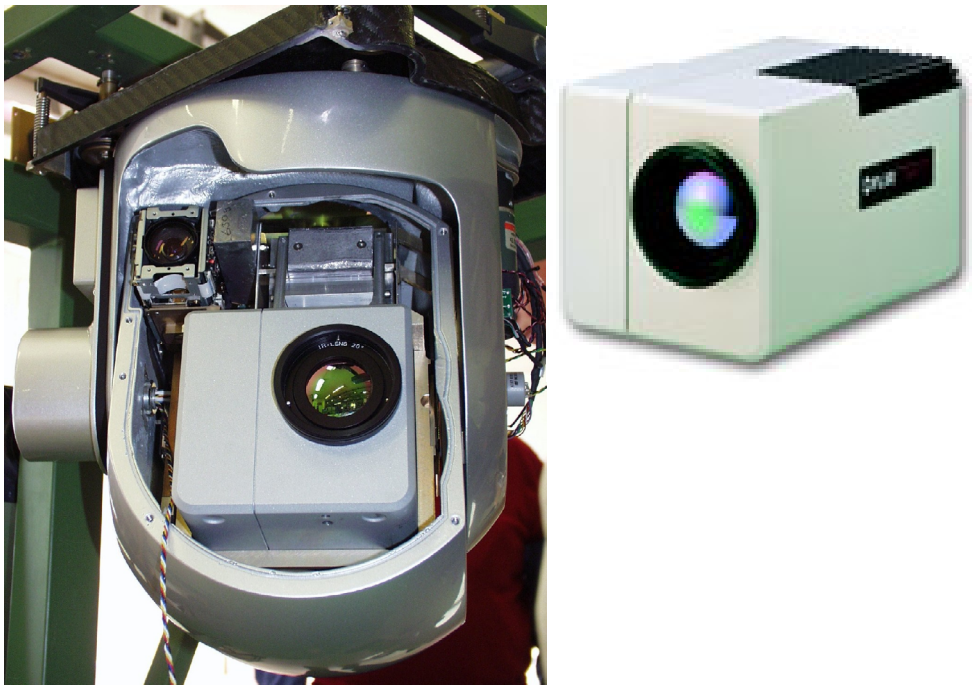

Figure 3-14. ThermaCam SC3000

Table 3-6. Some data about ThermaCam SC3000

Detector	QWIP
FPA	320x240
Spectral range	8-9 µm
NETD	< 20 mK
Frame rate	60 Hz (full frame rate) Up tp 750 Hz in subframe mode
Weight	3.2 kg
Size	220 x 135 x 130 mm

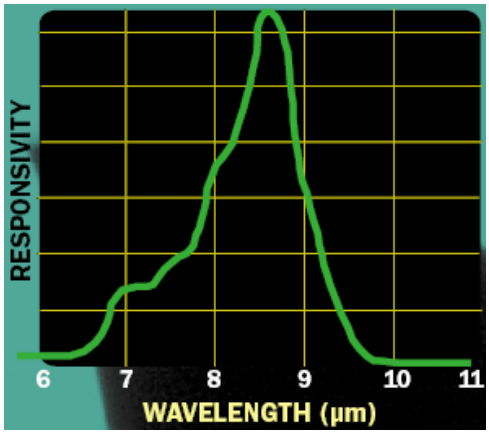

Figure 3-15 . Spectral responsivity of the QWIP detector

3.2 Multiband cameras

3.2.1 Emerald

Emerald (Cedip Infrared Systems) [10, 11] is a multiband sensor equipped with a filter holder with four positions (Figure 3-16). There are filters in three of the positions and one position is left open (Figure 3-17). The full frame rate is 50 Hz. Higher frame rates are possible by reading out sub frames, 800 Hz is reached with a 160×128 sub frame.

The exit window of the dewar has a coating limiting the response to 3.6-5.1um. This is to avoid atmospheric absorption by water vapour below this wavelength.

Figure 3-16. Left: Emerald with a 50 mm lens, right: Emerald with the lens removed revealing the filter holder in the middle.

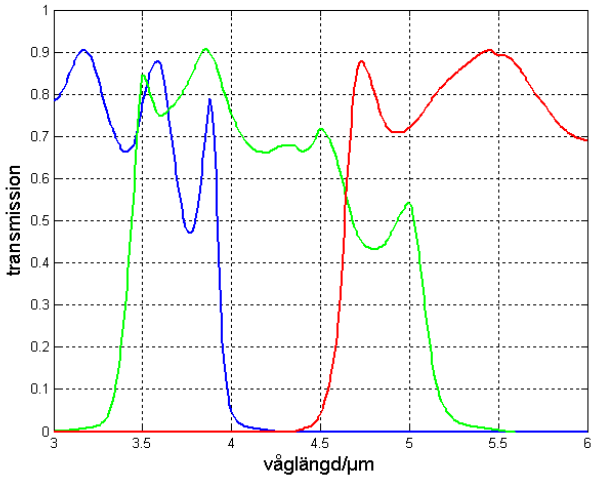

Figure 3-17. Transmission data of the three filters in Emerald. Filter 1: < 3.9 µm (low pass filter), Filter 2: 3.4 – 5.0 µm (band pass filter), Filter 3: > 4.6 µm (high pass filter)

Figure 3-18. The images show two Emerald registrations in a spectral band 4.6-5.0 µm using two different lenses. Left: FOV = 18x14°, focal length = 50 mm. The white square corresponds to the right image. Right: FOV = 4x3°, focal length = 250 mm

Table 3-7. Some data about Emerald. Note that the spectral range is 3.6-5.0 µm when both detector and optics are considered.

Detector	InSb (77 K)	
FPA	640×512	
Detector size	20 µm	
Dynamic range	14 bit	
Full frame rate	50 Hz	
Spectral range	3.6 – 5.1 µm	
NETD (300 K)	20 mK	
Integration time	75 µs – 10 ms	
Weight	5.5 kg	
Size (L x W x H)	275 x 130 x 162 mm	
	Lens 1	***Lens 2***
Focal length	50 mm	250 mm
F/#	2	2.9
FOV	18°×14°	3.5°×2.8°
IFOV	0.48 mrad	0.096 mrad
Transmission	3.5-5.0 µm	3.5-5.0 µm

3.2.2 Jade MWIR

Jade MWIR (Cedip Infrared Systems) is a multiband camera based on a cooled MCT detector. Its full frame rate is 5 – 250 Hz. Significantly higher frame rates are reached by sub-windowing.

The camera is provided with a filter holder with five positions. At present, only one filter, 4.3-4.9 µm, is mounted in the wheel. The other positions are empty.

Table 3-8. Jade MWIR

Detector	MCT
FPA	320×240
Full frame rate	5-250 Hz
Spectral range	3.7-4.9 µm
NETD (298 K)	< 20 mK
Integration time	10 µs – 3 ms
Focal length	50 mm
F/#	2
FOV	11°×8°
Weight	3 kg
Size (L x W x H)	270 x 120 x 150 mm

Figure 3-19. Jade MWIR (Cedip Infrared systems).

3.2.3 Thermovision System 900

Thermovision System 900 (Agema) [1] consists of two scanning infrared cameras, Agema 900SW and Agema 900LW and a data collecting unit, Agema 900 system controller.

Table 3-9. Some data about Thermovision system 900

	Agema 900SW	**Agema 900LW**
FPA	272 x 136	272 x 136
Dynamic range	12 bit	12 bit
Spectral range	2,8-5,0 µm	7,5-14 µm
Detector	InSb	MCT
NETD	0.1 °C	0.08 °C
FOV	5 x 2,5	5 x 2,5
Weight	3.5 kg	
Size (W x H x D)	122 x 156 x 250 mm	

Figure 3-20. Agema Thermovision system 900

3.3 Multispectral cameras

A multispectral camera collects data in several spectral bands at the same time. Hyperspectral defines a multispectral system that registers in narrow bands. According to one definition, $\Delta\lambda/\lambda$ should be in the order of 0.01 where $\Delta\lambda$ is the spectral bandwidth and λ is the wavelength under study. In a hyperspectral system the number of spectral bands may be several hundred.

3.3.1 Multispectral MWIR camera

The multispectral MWIR camera, denoted Multimir [12, 13, 14, 15], is an infrared sensor based on a spinning filter wheel containing four optical band pass filters (Figures 3.21, 3.22). It was delivered from AIM (AEG INFRAROT-MODULE) and has been modified at FOI, Linköping. The spectral response of the detector is shown in Figure 3.23.

The full frame rate is 100 Hz, whereby the time needed to register the four spectral images is 0.04 s. The camera can be operated with the filter wheel in a non-rotating mode, where only one of the spectral bands is used. The temporal difference between the images is then reduced from 0.04 s to 0.01 s. Higher frame rates are possible by reading out sub frames, up to 1000 Hz with a 128×128 sub frame.

The integration time t_{int}[µs] is calculated by

$$t_{int} = 10\mu s * int + 10\mu s \qquad (3\text{-}1)$$

where *int* is a number that can be set between 0 and 255.

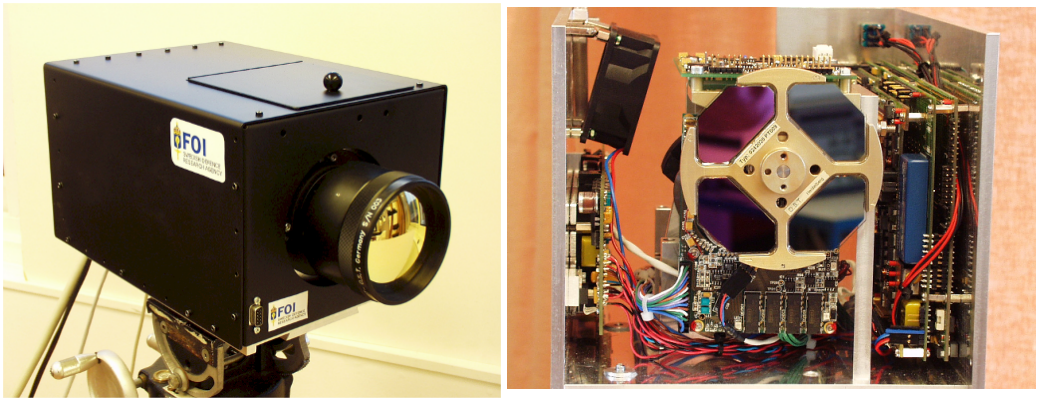

Figure 3-21. Left: the multispectral MWIR camera; a lens with the focal length 100 mm is mounted. Right: the spinning filter wheel with the four band pass filters.

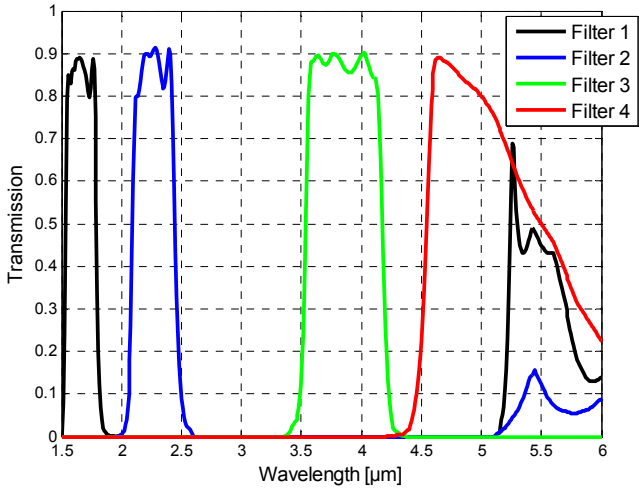

Figure 3-22. Transmission data for the four optical filters. Filter 1: 1.5 – 1.8 µm, Filter 2: 2.1 – 2.5 µm, Filter 3: 3.5 – 4.1 µm, Filter 4: 4.5 – 5.5 µm. Note that filters 1 and 2 have non-zero transmission above 5.2 µm.

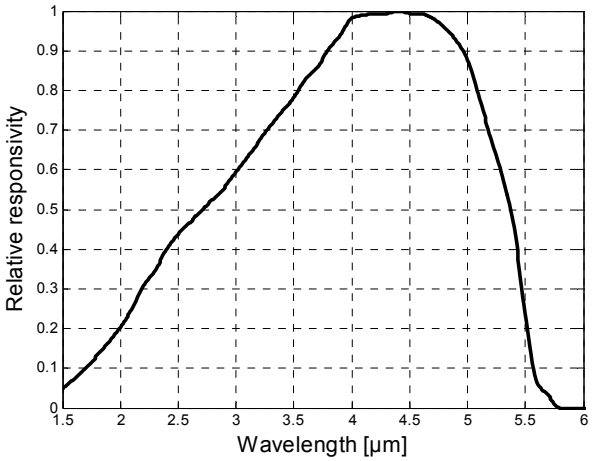

Figure 3-23. Spectral response of the MCT detector

Table 3-10. Some data about the multispectral MWIR camera

Detector	MCT		
FPA	384×288		
Detector size	20 µm		
Dynamic range	14 bit		
Full frame rate	100 Hz		
Spectral range	1.5 – 5.5 µm		
NETD (300 K)	< 25 mK		
Integration time	10 µs – 2.6 ms		
Weight (incl. lens, f = 100 mm)	11.5 kg		
Size (W x L x H)	23 x 31 x 20 cm		
	Lens 1	***Lens 2***	***Lens 3***
Focal length	100 mm	30 mm	15 mm
F/#	2	2	2
FOV	5.3°×4.0°	18°×13.0°	35°×27°
IFOV	0.24 mrad	0.80 mrad	1.6 mrad

The two SWIR filters are leaking infrared radiation above 5.2 µm (Figure 3-22). If measurements are performed at long distances, the leakages can be neglected because of the low atmospheric transmission above 5.2 µm (Figure 3-24).

At short distances the radiometric error caused by the leakage has appeared to be less than 10 %, in filter 2 for source temperatures of 900 °C or more, due to the Planck distribution. At temperatures down to 150 °C the error is significant. In filter 1 the radiometric error caused by the leakage is significant even for hot sources e.g. 1000 °C. One solution is to place an ordinary glass in front of the lens. The transmission for ordinary glass (about 2 mm thick) is shown in Figure 3-25. In rotating mode a glass placed in front of the lens will however block most of the incident radiation in filter 3 and all radiation in filter 4.

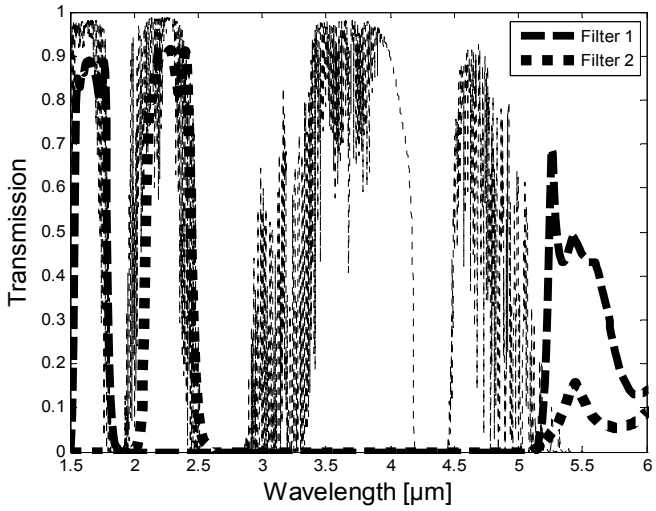

Figure 3-24. The figure shows the SWIR filter functions (taken from Figure 2-21) and the atmospheric transmission at 4 km, calculated by the Modtran model, and typical weather parameters collected at the RFN test range in Sweden in May 2008. The atmospheric transmission above 5.2 µm is very low at 4 km. At this distance the thermal leakages can be neglected.

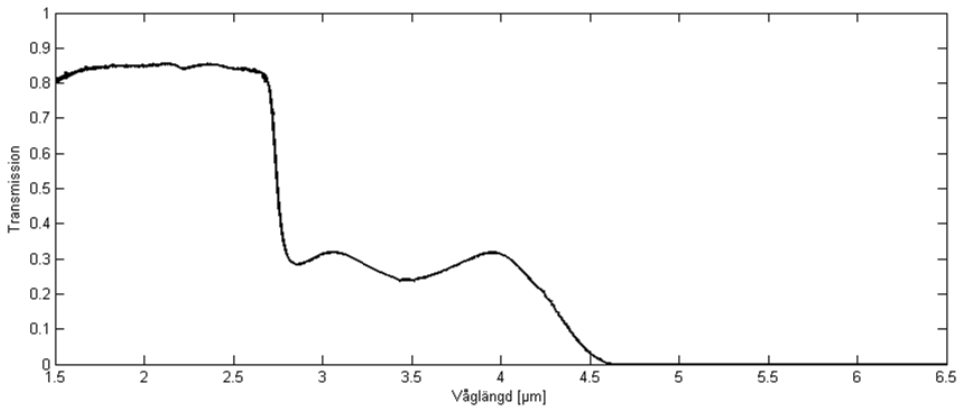

Figure 3-25. Optical transmission for an ordinary glass plate. Incident radiation above 4.6 µm is completely blocked and hence the "false" components above 5.2 µm through filters 1 and 2. However, no source signal will be detected in the filter 4 band if the camera is run in rotating mode.

Figure 3-26. Example image: a lens with 100 mm focal length is used . Upper left: filter 1 (1.5 – 1.8 µm); upper right: filter 2 (2.1 – 2.5 µm); lower left: filter 3 (3.5 – 4.1 µm); lower right: filter 4 (4.5 – 5.5 µm)

3.3.2 RedLake MS3100

Redlake MS3100 (DuncanTech) is a multispectral high resolution 3-chip digital camera [11, 16]. The camera is based on a colour separating prism with different coatings and filters (Figure 3-27). The separated light channels are imaged by three CCD sensors to acquire images in three spectral bands (Figure 3-28).

The integration time can be set independent in each channel and the aperture of the lens is adjusted manually. The table below provides more information about Redlake.

Table 3-11. Redlake MS3100

Detector	CCD
FPA	1392×1040 (each channel)
Detector size	4.65 µm
Dynamic range	10 bit
Full frame rate	7.5 Hz
Spectral range	400 – 1100 nm
Integration time	1/8000 – 1/7.5 s
focal length (optical zoom)	28-105 mm
F/#	3.5-16
FOV (28 mm)	16°×12°
IFOV (28 mm)	0.20 mrad
Weight	1.62 kg

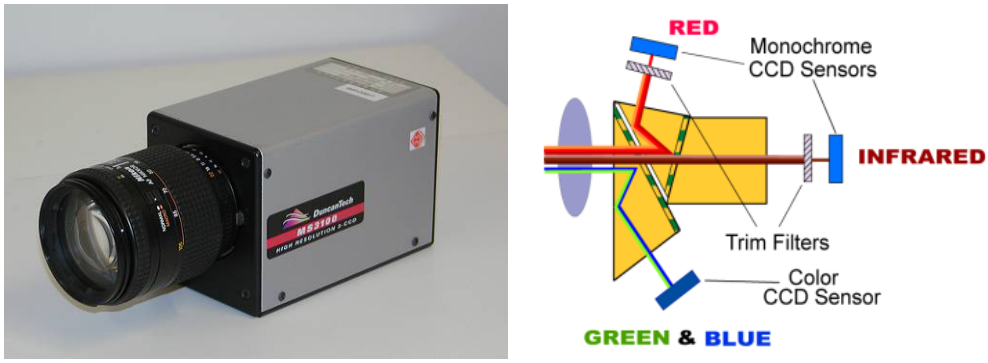

Figure 3-27. Left: RedLake MS3100 (DuncanTech); right: the colour separating prism

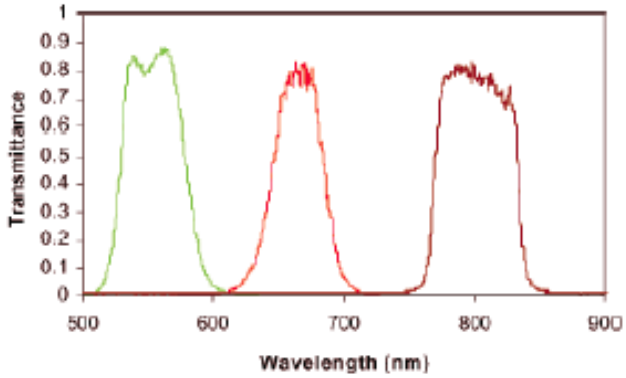

Figure 3-28. The three spectral bands in Redlake MS3100. Filter 1: 525-575 nm (green channel), Filter 2: 640-690 nm (red channel), Filter 3: 770-830 nm (NIR channel).

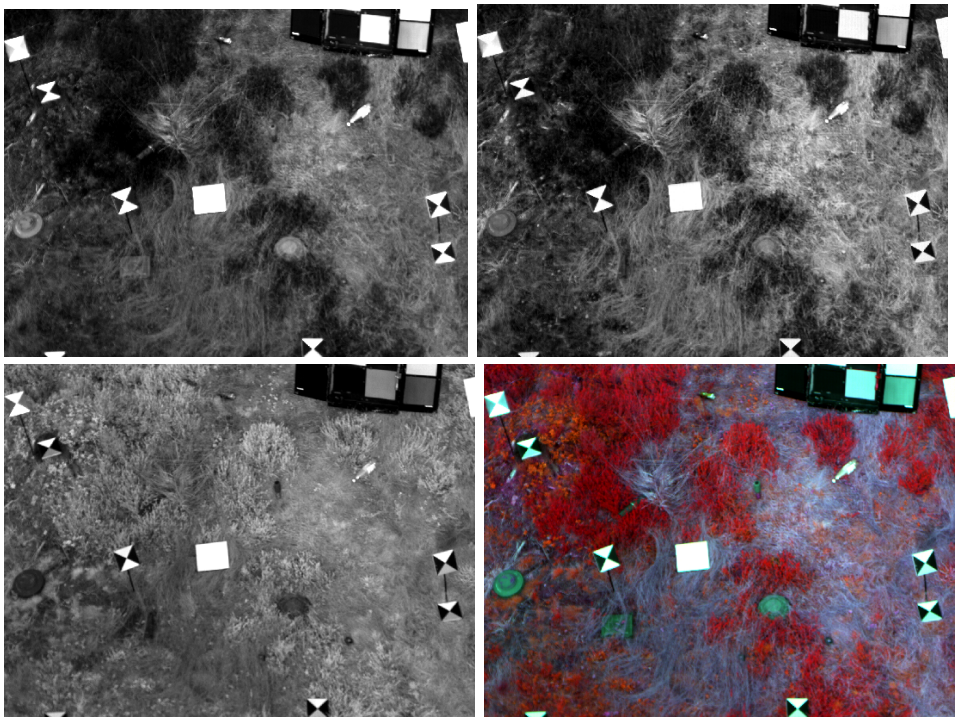

Figure 3-29. Upper left: green channel; upper right: red channel; lower left: NIR channel; lower right: the images can be represented as an ordinary RGB image where the NIR channel → R, red channel → G, green channel → B

3.3.3 ImSpector V10E

ImSpector V10E (Specim) is a hyperspectral sensor that acquires a line image and disperses it to spectra opposite to the line image (Figure 3-30, 3-31) [17, 18, 19]. Each frame contains the spatial information in one pixel dimension and the spectral information in the other pixel dimension. The frames are registered by a 1024x1024 CCD array in the back of the sensor. The highest spatial resolution is 1024 pixels while the highest spectral resolution is limited to 256 spectral bands. A binning setting combines data from several pixels into a single pixel, which will enhance the S/N ratio and the frame rate. However binning of the spatial pixels will also decrease the spatial resolution and binning of the spectral pixels will decrease the spectral resolution (and the available number of spectral bands). The possible combinations are shown in Table 3-12.

Table 3-12. Possible combinations of parameters for ImSpector V10E (approximate numbers)

Spectral resolution	2.3	4.6	9.2	9.8
Number of bands	256	128	64	60
Binned pixels	4	8	16	17
Frame rate/Hz	30	60	120	128

To acquire two-dimensional images the scene needs to be scanned, either by using the internal mirror in front of the lens, or by moving the sensor over the scene, which is performed in airborne registrations. More information about ImSpector V10E is presented in Table 3-13.

Figure 3-30. ImSpector V10E (Specim). From top to bottom: CCD array, dispersive element, scanning mirror

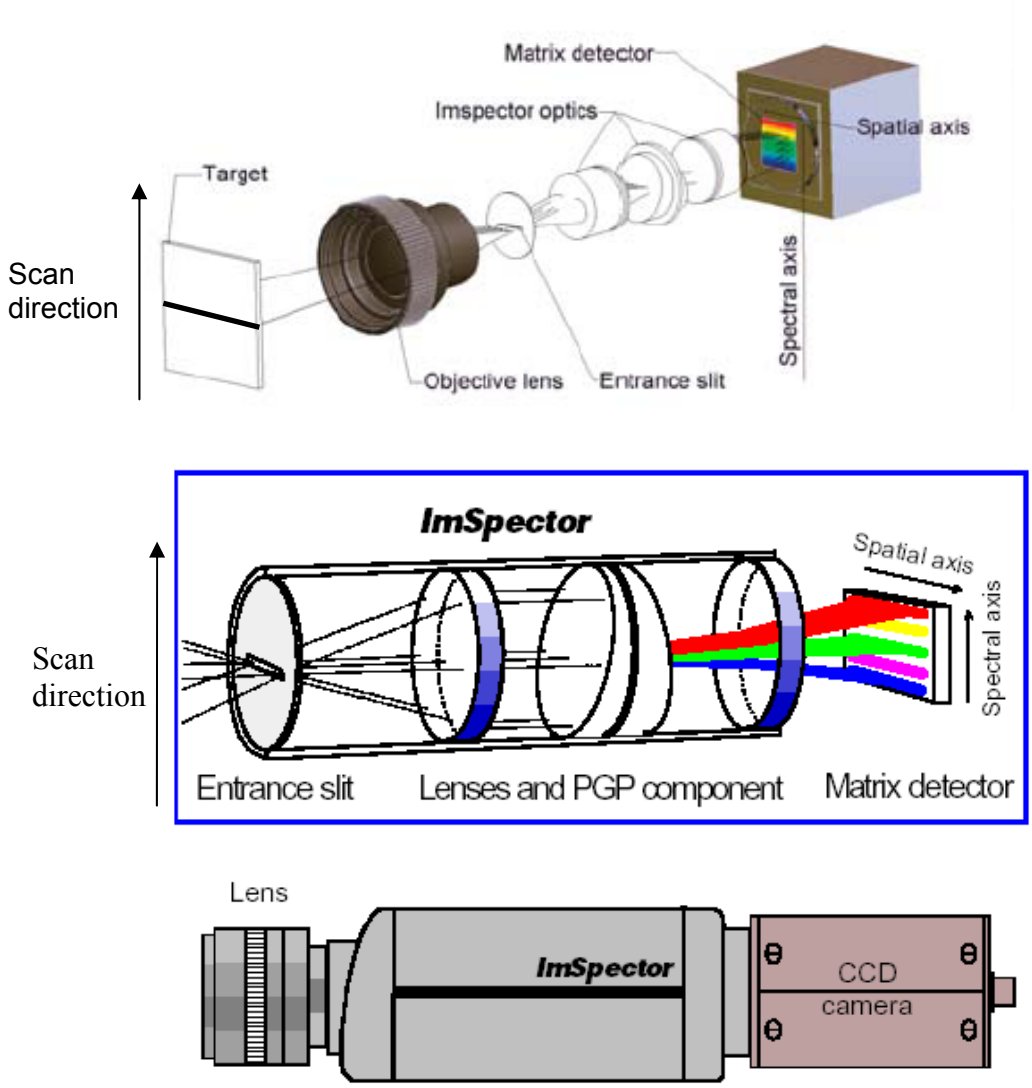

Figure 3-31. Principle sketches of ImSpector V10E

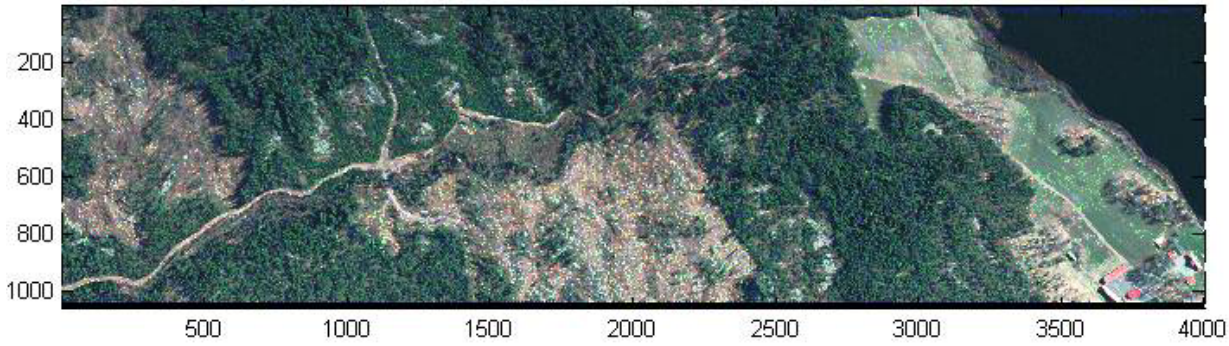

Figure 3-32. An airborne registration with ImSpector V10E. The image cube consists of 4000 lines with 1024 pixels/line and 60 spectral bands/pixel (1024x4000x60). In the figure three of the 60 bands are presented as an RGB image where 678 nm → R, 536 nm → G, 472 nm → B.

Table 3-13. ImSpector V10E

		Notes
Detector	CCD, 1024x1024	
Spectral range	391 nm – 961 nm	
Detector size	12 µm	
Dynamic range	12 bit	
Spectral bands	60 (up to 240)	Depends on pixel binning
Spectral resolution	2.8 nm	Depends on pixel binning
Pixels, one frame	1×1024/n ; n = 1 or 2	Depends on pixel binning
Pixels, one scan	up to 4000×1024	Depends on scan length and pixel binning
Frame rate	100 Hz (down to 30 Hz)	Depends on pixel binning
Integration time	7 ms	Depends on pixel binning
Size	320 x 65 x 80 mm	
Optics:		
Focal length	23 mm	
F/#	2.4	
FOV	29.9°	
IFOV	0.51 mrad	Depends on pixel binning

3.3.4 SC7000

A multispectral sensor based on two SC7000 (FLIR Systems) cameras and a semi-transparent mirror was purchased in 2010. The design allows the same path to be simultaneously registered in two spectral bands, 3.6-4.2 µm and 4.5-5.1 µm.

Table 3-14. Some data about SC7000MW

Detector	InSb
NETD	< 20 mK
Integration time	1 µs to 20 ms variable by 1 µs step
FPA	640×512
Pixel pitch	15 µm
Dynamic range	14 bit
Full frame rate	380 Hz
Spectral range camera 1	3.6-4.2 µm
Spectral range camera 2	4.5-5.1 µm
Weight	4.95 kg
Size (L x W x H)	253 x 130 x 168 mm
Lens:	
Focal length	50 mm
F/#	2.0
FOV	11° x 8.8°
IFOV	0.30 mrad

Figure 3-33. SC7000 (FLIR Systems)

3.4 Digital cameras

A digital camera takes still photographs and videos digitally. There are several digital cameras at FOI. The most advanced camera EOS 5D MarkII is described below.

3.4.1 EOS 5D MarkII

There are three EOS 5D MarkII (Canon) available; one with a 800 mm focal length and the other two with zoom lenses with focal lengths 70-200 mm (Figure 3.34). Some data about the cameras are found in Table 3-15.

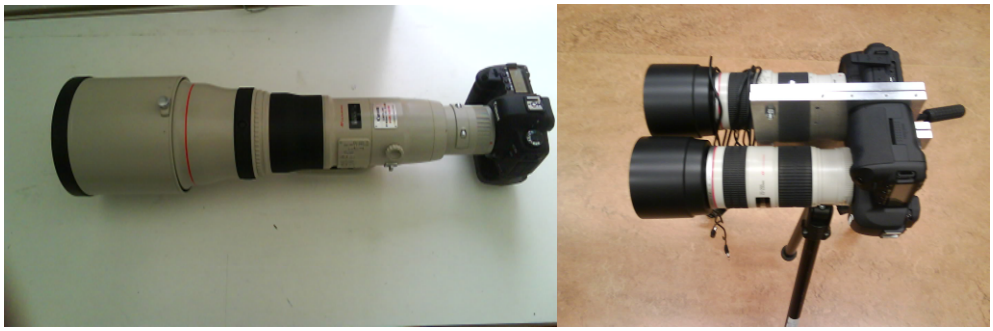

Figure 3-34. EOS 5D MarkII. Left: the camera with f = 800 mm lens; right: the two cameras with zoom lenses f = 70-200 mm.

Table 3-15. Additional information on EOS 5D MarkII

Detector	CMOS 36x24 mm		
FPA	5616×3744 (about 21.1 megapixel)		
Frame rate	3.9 JPEG images/s; 30 Hz in video mode		
	Focal length	**FOV**	**Spectral range**
Camera 1	800 mm	2.6x1.7 °	VIS
Camera 2	70-200 mm	70 mm: 29x20 °	VIS
Camera 3	70-200 mm	70 mm: 29x20 °	NIR (0.83-1 µm)

4 Single detector instruments

4.1 Single element detector device

The single element detector device, also called 6-pack, is composed of six separate single element detectors. This device is used to determine the maximal amplitude signal from very fast events, e.g. explosions, in six different wavelength bands. If the time duration of the event is in the rising order of 1 ms, a sensor with a frame rate significantly higher than 1000 Hz is needed to temporally dissolve the transient. This is beyond the frame rate of an infrared imaging sensor.

The sensors are mounted on a common fixture together with a small TV-camera to monitor the sensors direction (Figure 4-1).

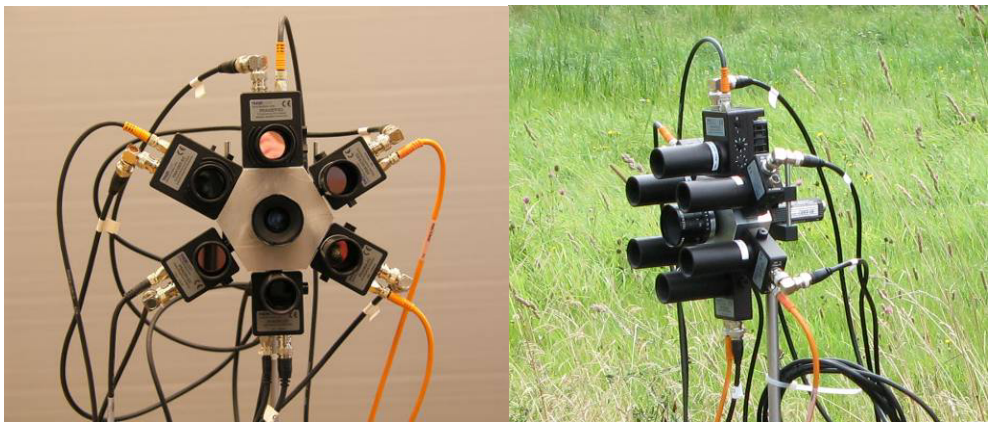

Figure 4-1. The 6-pack composed of six detectors. The FOV is individually defined by a mounted tube in front of each single detector element. A small TV-camera is placed in the middle to monitor the sensors direction.

The detector specifications and the spectral ranges of detector and filter combinations are according to Table 4-1. One of the detectors, detector 3 (4), is shown in Figure 4-2. A typical spectral responsivity curve for detector 3 (and 4) is shown in the same figure and for the other detectors in Figure 4-3 to Figure 4-6.

Table 4-1. Detector specifications of the six single element detectors. The spectral ranges of detector and filter combinations are according to the right column.

Det. nr	Thorlabs no:	Material	Spectral range (µm)	Coo-led	Resp (ns)	Electrical bandwidth up to	Detector + filter (µm)
0	PDA25K	GaP	0.15 – 0.55		46.6	7.5 MHz	0.15 – 0.29
1	PDA36A	Si	0.35 – 1.1		20.6	17 MHz	0.35 – 0.65
2	PDA10CS	InGaAs	0.70 – 1.8		20.6	17 MHz	0.79 – 1.37
3	PDA10DT	InGaAs	1.2 – 2.57	Yes	350	1 MHz	1.46 – 1.79
4	PDA10DT	InGaAs	1.2 – 2.57	Yes	350	1 MHz	2.13 – 2.57
5	PDA20H	PbSe	1.5 – 4.8		35000	10 kHz	3.00 – 4.80

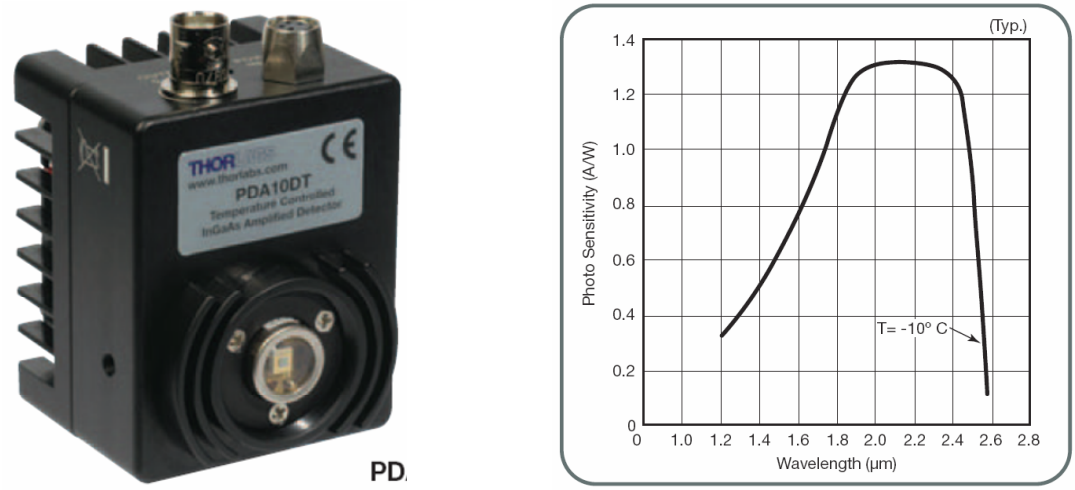

Figure 4-2. To the left a typical single element detector and to the right the responsivity for detector 3 and 4.

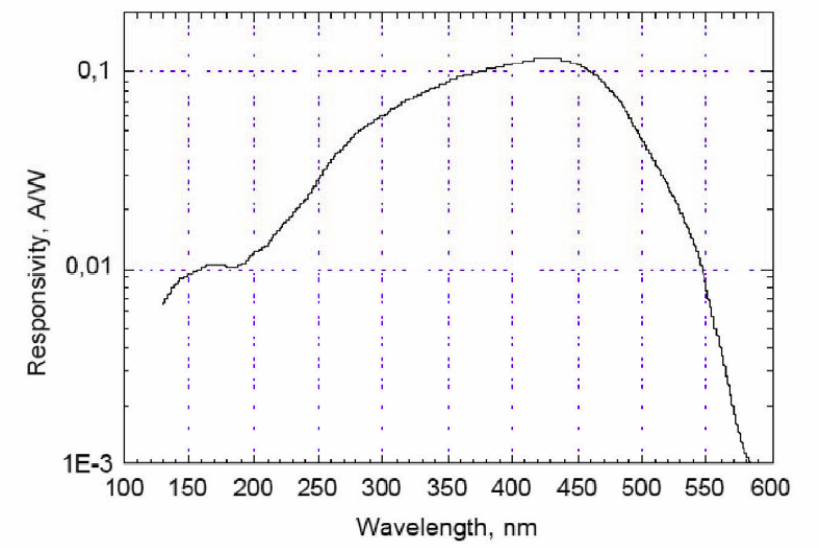

Figure 4-3. Responsivity for detector nr 0

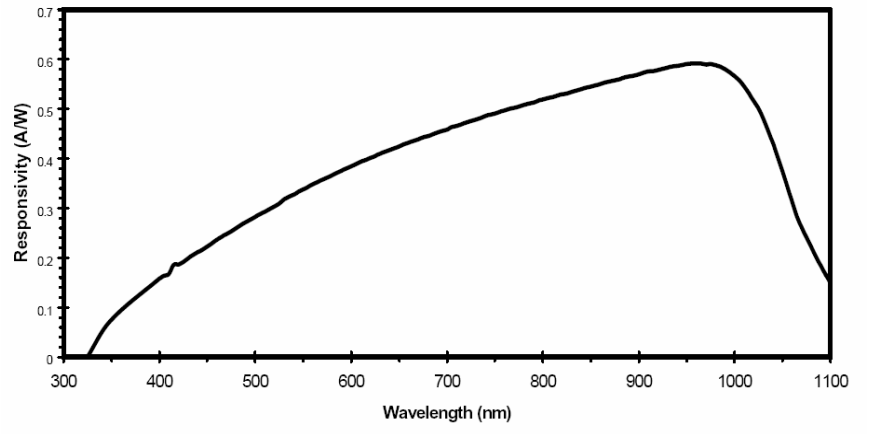

Figure 4-4. Responsivity for detector nr 1

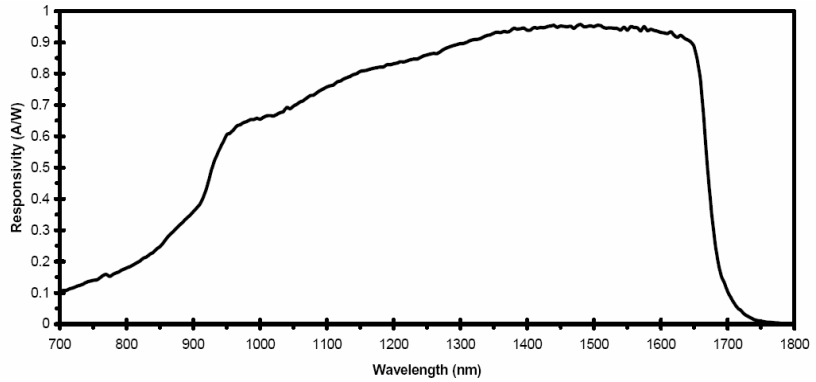

Figure 4-5. Responsivity for detector nr 2

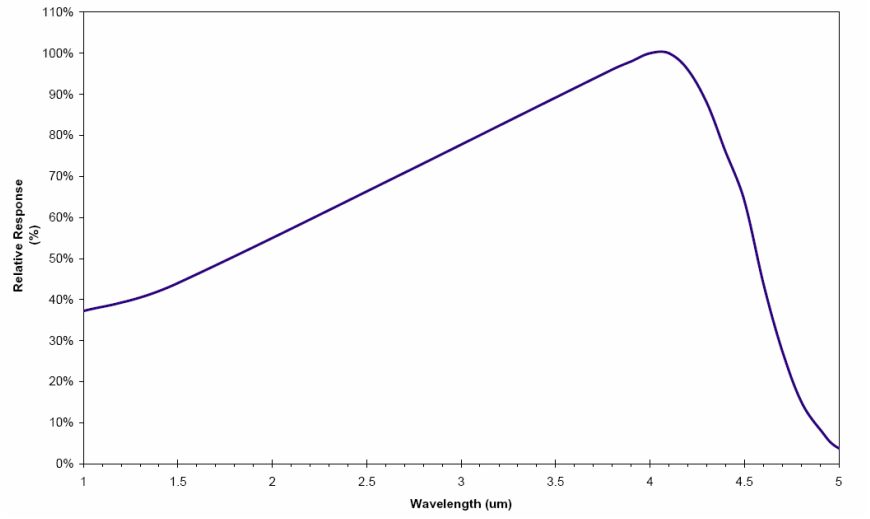

Figure 4-6. Responsivity (relative response) for detector nr 5

The measured transmission for the filters used for the different detectors are according to Table 4-2.

Table 4-2. Typical transmission for the filters used.

Detector nr	Filter type	Lower Wavelength	Upper Wavelength	Average transmission
0	Short pass	-	288 nm	
1	Short pass	-	646 nm	90 %
2	Band pass	790 nm	1370 nm	65 %: 790 – 920 nm 85 %: 920–1370 nm
3	Band pass	1456 nm	1790 nm	87 %
4	Band pass	2128 nm	2565 nm	85 %
5	Long pass	3004 nm	-	86 %

The FOV (Field of view) for the six single element detectors is individually defined by a mounted tube in front of the detector element and the actual position of the active element. The calculated FOV for the detectors is shown in Table 4-3.

Table 4-3. Calculated FOV for the 6 single element detectors.

Detector nr	FOV (°)	Detector area (mm)
0	21.3	2.54 x 2.54
1	21.0	3.6 x 3.6
2	21.6	Ø 1.0
3	23.3	Ø 1.0
4	23.3	Ø 1.0
5	21.4	2.0 x 2.0

4.2 FTIR spectrometer MR304SC

MR304SC (ABB) is a system consisting of a spectroradiometer with two input and two output ports [20, 21]. The system features simultaneous data acquisition from the two output ports (configured with an MCT and an InSb detector). One input port is used as a reference cancellation source. The other input port is designed to receive an input telescope and viewing device. The spectrometer includes:

-Real time data acquisition and data processing radiometric software (Radiance, Irradiance and Apparent Intensity)
-Input collimator
-FTIR Internal temperature control system
-Room temperature cancellation reference source

Table 4-4. MR304SC

Spectral range	2 – 15 µm
Detectors (Stirling cooled)	InSb: 2-5.5 µm MCT: 4-15 µm
Dynamic range	InSb: 16 bit MCT: 16 bit
NESR	$< 2.5 \cdot 10^{-9}$ W/(cm^2·sr$^-$·cm^{-1}) $< 2.5 \cdot 10^{-10}$ W/(cm^2·sr$^-$·cm^{-1})
Resolution	1 cm^{-1} at 10 scan/s 2 cm^{-1} at 17 scan/s 4 cm^{-1} at 34 scan/s 8 cm^{-1} at 54 scan/s 16 cm^{-1} at 82 scan/s 32 cm^{-1} at 107 scan/s
Spectral stability	Better than 0.01 cm^{-1}
Telescope	FOV = 4.9 mrad
Weight	Sensor head: 35 kg Power supply mode: 3.5 kg
Dimension	Spectroradiometer: 390 mm x 375 mm x 390 mm Power supply module: 390 mm x 255 mm x 110 mm

Figure 4-7. FTIR spectrometer MR304SC (ABB)

4.3 FTIR spectrometer IFS 55

Another single element detector is the FTIR spectrometer IFS 55 (Bruker) that measures transmittance and absorbance of solid materials and liquids, and also reflectance of solid materials.

The spectrometer can measure the directional hemispherical reflectance (DHR) for diffusely reflecting surfaces between 2-25 µm by using an integrating sphere. DHR is the sum of the diffuse and the specular reflectance.

There are two different integrating spheres. One of them is used with a fixed incident angle (9°); for solid materials or powders. The other sphere with a variable incident angle (10-80°) is only used for solid materials.

ATR (attenuated total reflection) can be applied on solid materials. ATR is a type of surface measurement which is used to increase the sensitivity in the measurement (by repeated reflections against the surface).

Other available devices:

- A microscope to measure transmittance and reflectance. The measurement range is 2-18 µm; the size of the measurement spot is 20-80 µm.
- A high temperature/high pressure cell: Specac HTHP. The spectral range is 2-20 µm; the maximum temperature is 800 °C; the maximum gas pressure is 70 bar.
- Various reflectance wavelength calibration standards

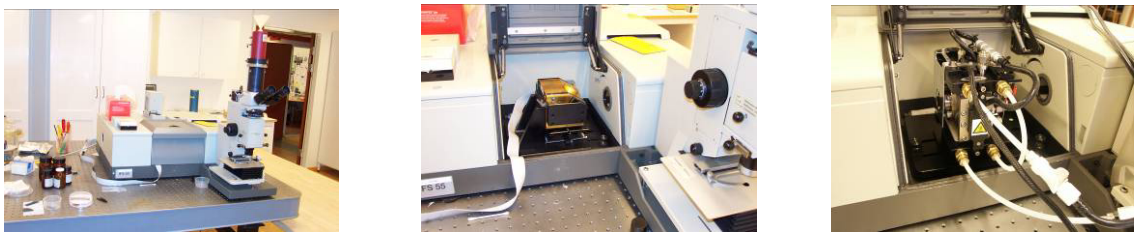

Figure 4-8. The FTIR spectrometer IFS 55

Table 4-5. Some data about IFS 55

Spectral range	0.8 – 100 µm (100-12500 cm^{-1}), range depending on detector and beamsplitter
Resolution (max)	0.5 cm^{-1}
Detectors	DTGS (KBr, PE, CsI) MCT InSb
Beamsplitters	KBr, quartz, mylar (3.5 µm)

4.4 Spectrophotometer Cary 5G

The spectrophotometer Cary 5G (Varian) is used for spectroscopic measurements in the 175-3300 nm spectral range (Figure 4-9).

- Transmission and absorption can be measured both for solid materials and liquids.
- Absolute specular reflectance is measured in a WV configuration for solid materials
- Diffuse reflectance and transmittance between 250-2500 nm. Two integrating spheres are used for this:
  - fixed incident angle (10 °); solid materials or powders
  - variable incident angle (10-70 °); only solid materials

Figure 4-9. The spectrophotometer Cary 5G

5 Radiation sources

This section presents some of the reference sources that are frequently used. Additional information about radiation sources can be found in [1].

5.1 Area radiating sources

5.1.1 Integrating sphere SR-3B

An integrating sphere contains and diffuses input light spreading it over the entire inner surface area of the sphere, producing an absolute uniform radiance level at the exit port. SR-3B (Figure 5-1) is delivered by SphereOptics [22]. The radiance level at the aperture is set by the user, and does not need to be related to another source. The inner diameter of the sphere is ca 30 cm and the diameter of the exit port is 10.16 cm. Figure 5-2 shows the spectral radiance of SR-3B between 0.3 – 2.5 μm.

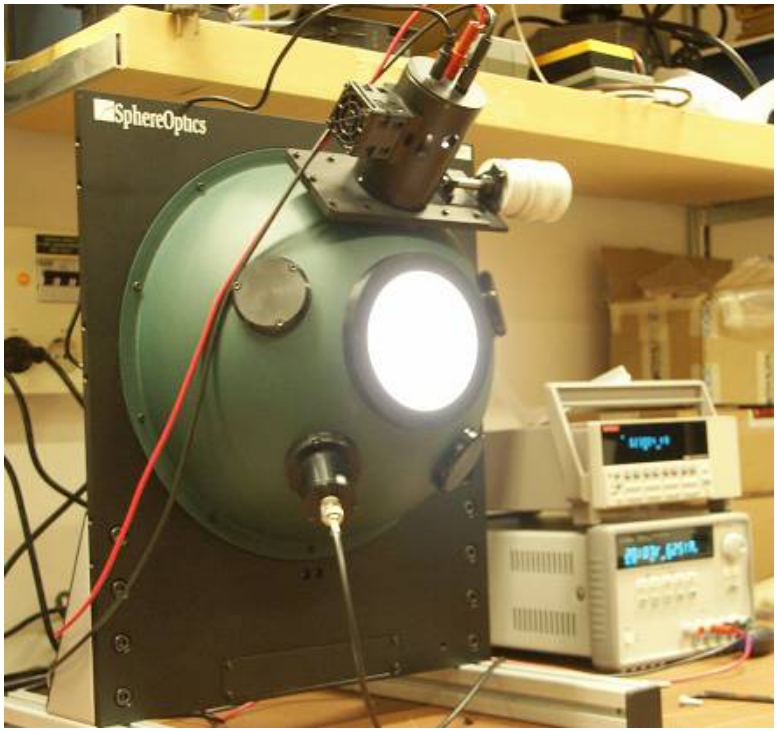

Figure 5-1. The integrating sphere SR-3B. It produces an absolute uniform radiance level at the exit port.

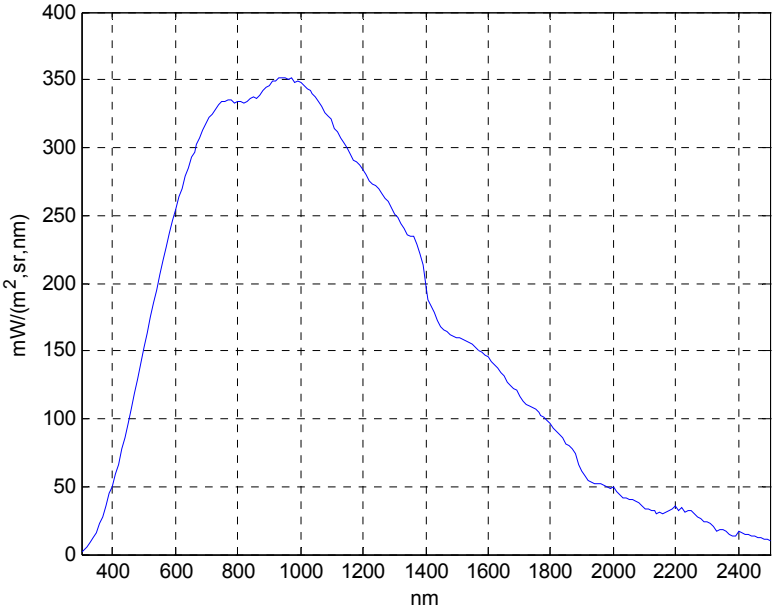

Figure 5-2. Spectral radiance of SR-3B between 300 – 2500 nm.

5.1.2 Large integrating sphere

A large integrating sphere has been constructed at FOI (Figure 5-3). The sphere consists of two connected aluminum half-spheres. The inner diameter of the sphere is 60 cm. It is irradiated with 2 lamp units, each unit consisting of a spotlight (OSRAM, 150 W, 15 V), a power supply (Instek PSP 2010, 0-20 V, 0-10 A), a glass diffuser, an iris diaphragm (Thor Labs) and a ventilator. The sphere is painted with a matt white colour inside to increase the diffusing properties of the source.

The diameter of the exit port is 20 cm. The irradiance is measured inside the sphere with a radiometer PMA2100 (Solar Light). The radiance level at the exit port is set by the two iris diaphragms. To get the radiance level at the exit port, the radiance measured by the radiometer has to be related to another source e.g. the integrating sphere SR-3B.

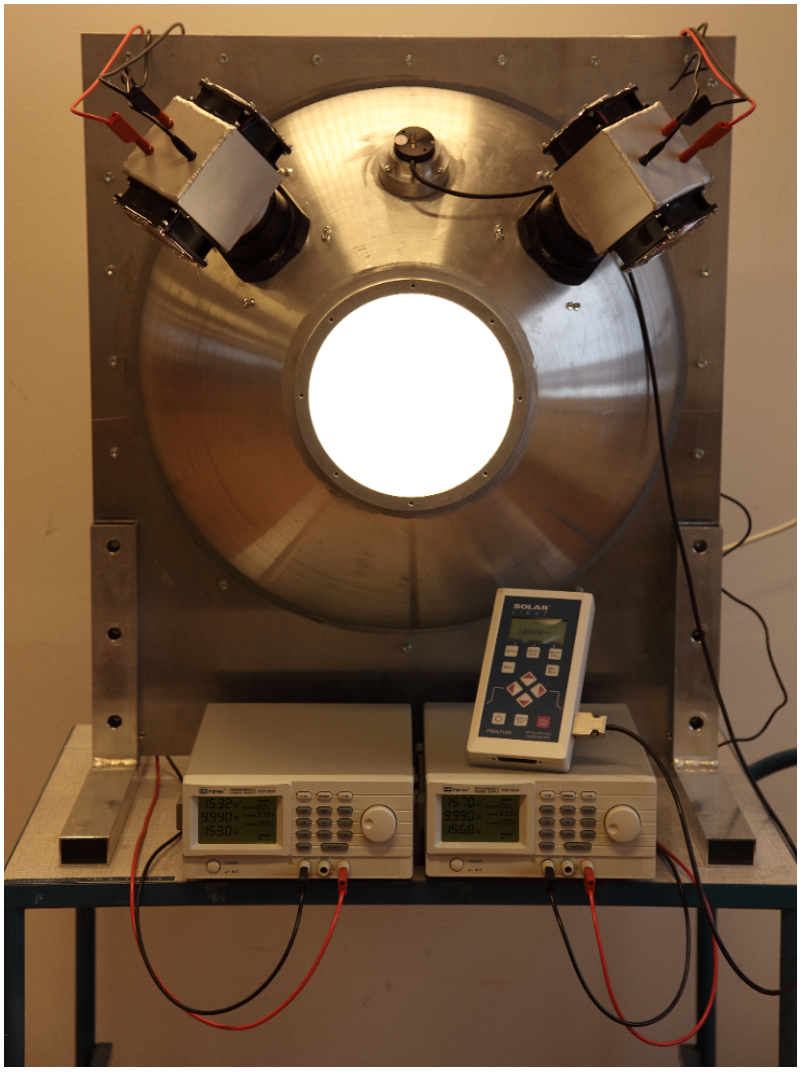

Figure 5-3. Large integrating sphere constructed at FOI.. Inner diameter = 60 cm, diameter of the exit port = 20 cm.

5.1.3 Blackbody source RCN300

RCN300 (HGH) has a large emitting surface, 0.3 x 0.3 m. The emissivity = 0.99 [1]. The temperature range is from ambient temperature up to 300 °C. The source has been calibrated by SP (Swedish National Laboratory) in Sweden (Table 5-1).

Table 5-1. Results from a calibration of RCN 300 performed by SP (Swedish National Laboratory)

Displayed temperatures °C	**HGH300**	
	Measured temperatures °C	**Differences °C**
50 °C	49.2	-0.8
100 °C	97.4	-2.6
200 °C	192.8	-7.2

Figure 5-4. Large blackbody area source RCN300 (HGH).

5.1.4 Other area radiating sources

Peltier elements

Blackbody sources like Peltier elements can be used in thermal infrared bands above 3 µm [14, 15] (Figure 5-5). The temperature can be set between 0 and 80 °C. The surface is painted black and is diffuse. Due to this, a high emissivity $\varepsilon(\lambda)$ is reached which is assumed to be constant in the wavelength bands and above 0.95.

Lamp source

In spectral bands below 3 µm, the radiation levels from Peltier elements are too low and therefore other sources have to be used e.g. a reference source based on a lamp.

The lamp source shown in Figure 5-5 [14, 15] is calibrated by relating the signal levels to an integrating sphere, SR-3B (SphereOptics). The radiance level obtained by the lamp source is adjusted by the area of an iris diaphragm placed in front of the lamp (Philips, 150 W spotlight, 17 V).

Figure 5-5. Peltier elements (left) and a lamp source (right). The temperatures of the Peltier elements are fixed and preset to 10, 25 and 50 ℃. Different radiance levels from the SWIR source are obtained by changing the aperture of an iris diaphragm in front of the lamp. The lamp is driven with 12 V generating about 100 W. In the 2.1-2.5 µm band radiance levels between 4 – 15 W/(m^2·sr) are obtained.

5.2 Cavity sources

M360 (Mikron) and M340 (Mikron) are two cavity sources with temperatures ranges between 50 - 1100 °C and -20 - 150 °C resp. [1]. The maximum size of the exit port is 25 mm for M360 and 51 mm for M340. The radiance levels are given by the Planck relation. The emissivity $\varepsilon(\lambda)$ is assumed to be approximately constant in the wavelength bands and close to 1 (> 0.99).

The cavities have been calibrated by SP (Swedish National Laboratory) in Sweden. The results are shown in Table 5-2.

Figure 5-6. Cavity sources; M360 and M340

Table 5-2. Results from calibrations of M360 and M340 performed by SP (Swedish National Laboratory) in Sweden.

Displayed temperatures °C	M360		M340	
	Measured temperatures °C	Differences	Measured temperatures °C	Differences
-17			-22.6	-5.6
10			9.3	-0.7
80			82.3	2.3
150			155.5	5.5
700	699.8	-0.2		
1000	997.5	-2.5		

IR-564 (Infrared systems) is a cavity source purchased in 2010. The temperature can be set between 50 - 1200 °C. The size of the exit port is 25 mm.

Figure 5-7. IR-564

The cavity has been calibrated by Infrared Systems. The results are shown in Table 5-3.

Table 5-3. Results from a calibration of IR-564 performed by Infrared Systems

Displayed temperatures °C	IR-564	
	Measured temperatures °C	Differences °C
50 °C	49.8 – 50.2	-0.2 - 0.2
100 °C	99.8 – 100.2	-0.2 - 0.2
200 °C	199.8 – 200.2	-0.2 - 0.2
400 °C	399.8 – 400.2	-0.2 - 0.2
600 °C	599.8 – 600.2	-0.2 - 0.2
800 °C	799.8 – 800.2	-0.2 - 0.2
1000 °C	999.8 – 1000.2	-0.2 - 0.2
1200 °C	1199.8 – 1200.2	-0.2 - 0.2

6 Temperature measurement

6.1 Pyrometer OS-86 LS

Temperatures can be measured with a pyrometer OS86-LS (Omega engineering inc.), Figure 6-1. The measurement range is -50 - 500°C and the accuracy stated is 0.1 °C, which is expected to be better than the real accuracy since the calibration error is not considered. The emissivity of the source of interest can be stated and is then corrected for by the instrument. The temperature is continuously presented in a small window and read manually.

Figure 6-1. The pyrometer OS86E-LS (Omega enginering inc.)

6.2 TinyTag Plus

The temperature can be logged with a small temperature sensor called TinyTag Plus (Intab). Each unit consists of a small box with a sensor connected to it. In a computer program it is determined how often (1 s up to 10 days) and for how long the temperature should be logged. It has a storage capacity of 16000 values. The temperature is read out after the measurement with the same software and is given with a resolution of two decimal figures. The measurement range is between -40°C and 125°C. At room temperature the accuracy is better than 0.5°C.

Figure 6-2. TinyTag Plus(InTab)

6.3 PC-logger AAC-2

PC-logger AAC-2 (Intab) is a temperature logging system with 24 channels and 24 Pt-100 resistance thermometers. The measurement range is approximately -20 °C - 200 °C (± 0.5 °C).

Figure 6-3. The figure shows one of the 24 Pt-100 resistance thermometers

7 TASC Polarimetric Scatterometer

The bidirectional reflectance distribution function (BRDF) describes the reflection from a sample surface of incident laser radiation (10.6 µm, 3.39 µm, 633 nm) over a hemispherical surface. It is measured with a BRDF reflectometer, TASC Polarometric Scatterometer (TMA), Figure 7-1. The detector can either move 180° (azimuthal angle) over the hemisphere or in the plane of incidence.

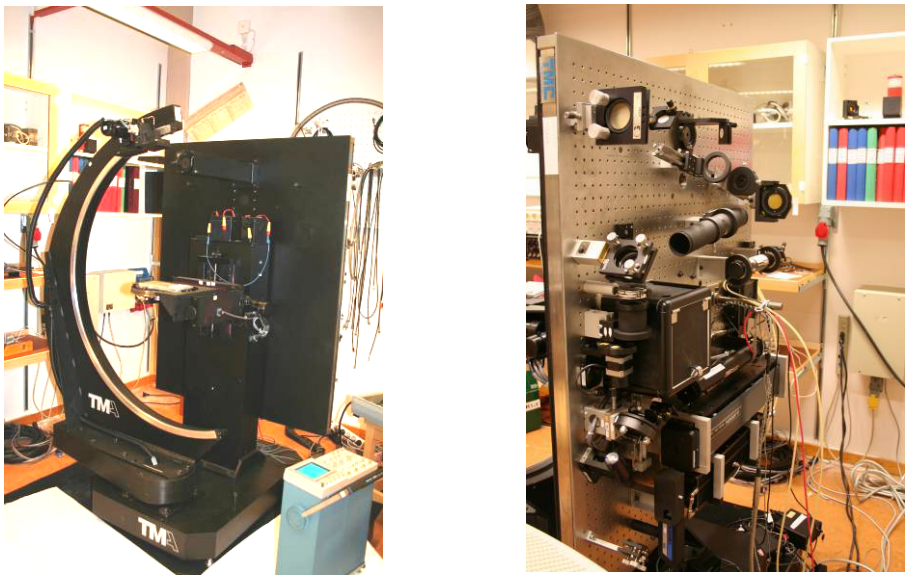

Figure 7-1. TASC Polarometric Scatterometer

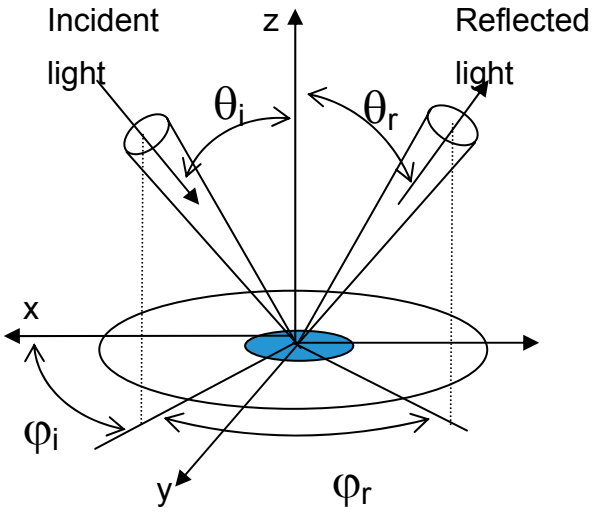

Figure 7-2. θ_i = 0-80°, θ_r = 0-89°, φ_i = 0-180°, φ_r = 0-180°

8 Scintillometer BLS2000

With the scintillometer BLS2000 (Scintec AG) [23] turbulence data such as the refractive index structure constant C_n^2 [$m^{-2/3}$], Fried's parameter r_0 [m], and the averaged scintillation index, are measured (see below). It measures the distance weighted mean between 1000 m and 10000 m.

The scintillometer consists of an optical transmitter, an optical receiver, a signal-processing unit and a data evaluation software. The transmitter consists of two units, each with 878 LEDs in NIR (880nm) and 34 red in the visual range (Figure 8-1). The receiver collimates the radiation onto 2 photodiodes. The following statistics are measured:

Average received intensity originating from unit 1	$<I_1>$
Average received intensity originating from unit 2	$<I_2>$
Variance of received intensity originating from unit 1	σ_{11}
Variance of received intensity originating from unit 2	σ_{22}
Covariance of received intensity originating from units 1 and 2	σ_{12}

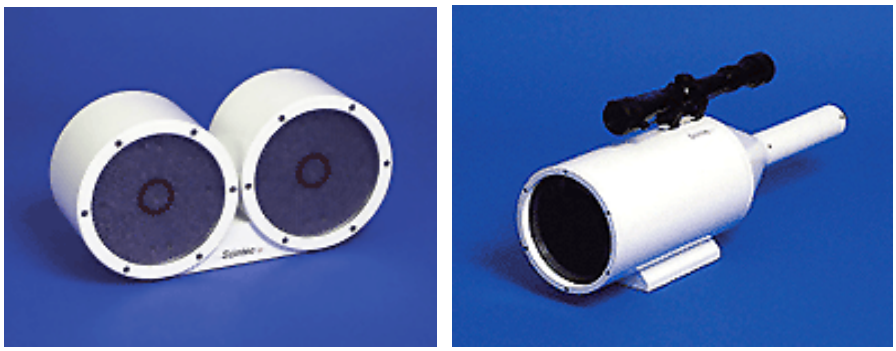

Figure 8-1. Scintillometer BLS200: transmitter (left) and receiver (right).

Table 8-1. BLS2000

Transmitter:	
Main radiation source	2 × 878 AlGaAs LEDs
Auxiliary radiation source	2 × 34 LEDs
Wavelength	880 nm
Pulse repetition rates	1 Hz, 5 Hz, 25 Hz, 125 Hz
Pulse length	8 ms
Weight	22 kg
Size	590 x 330 x 170 mm
Receiver:	
Detector	2 Si photodiodes
Focal length	495 mm
Diameter	265 mm
FOV	7.5 mrad
Weight	19 kg
Dimension	570 x 480 x 300 mm

The refractive index structure constant C_n^2 is a parameter used to describe the strength of turbulence and is defined [24, 25]

$$C_n^2 = \left\langle \left[n(r_1) - n(r_2) \right]^2 \right\rangle / \left| r_1 - r_2 \right|^{2/3} \quad (8\text{-}1)$$

where n is the refractive index in the points r_1 and r_2.

Turbulence (also referred to as scattering or intensity fluctuations) is called weak when the observed log-amplitude variance is proportional to C_n^2. If it is not proportional, the turbulence is called strong. C_n^2 values $\geq 10^{-13}$ $m^{-2/3}$ indicate a highly turbulent atmosphere with a considerable blurring as a result. C_n^2 values $< 10^{-15}$ $m^{-2/3}$ indicate low optical turbulence with negligible image-degrading blurring at distances ≤ 2 km.

The theoretical treatment is facilitated if weak turbulence conditions can be assumed. For conditions of weak turbulence C_n^2 is calculated according to

$$B_{11} = \frac{1}{4} \ln \left[1 + \frac{\sigma_{11}}{\langle I_1 \rangle^2} \right] \quad (8\text{-}2)$$

$$B_{22} = \frac{1}{4} \ln \left[1 + \frac{\sigma_{22}}{\langle I_2 \rangle^2} \right] \quad (8\text{-}3)$$

$$C_n^2 = \alpha_r \, B_{11} D_t^{7/3} R^{-3} = \alpha_r \, B_{22} D_t^{7/3} R^{-3} \quad (8\text{-}4)$$

The factor α_r depends on the ratio of the transmitting to the receiving aperture. For BLS2000, $\alpha_r = 4.49$. D_t is the size of the emitting disks = 0.26 m. R is the path length [m].

Fried's parameter r_0 [m] corresponds to the aperture diameter at which atmospheric phase perturbations begin to seriously limit the image resolution. If the aperture diameter is larger than r_0, then the resolution is independent of the diameter. r_0 is calculated by

$$r_0 = \left[0.423 \cdot k^2 \cdot R \cdot C_n^2 \right]^{-3/5} \quad (8\text{-}5)$$

where k is the optical wave number = $2\pi/\lambda$. The scintillation index σ_I^2 , also referred to as normalized irradiance variance, is given by

$$\sigma_I^2 = \frac{\langle (I - \langle I \rangle)^2 \rangle}{\langle I \rangle^2} = \frac{\langle I^2 \rangle}{\langle I \rangle^2} - 1 \quad (8\text{-}6)$$

σ_I^2 increases with increasing values of the Rytov variance, σ_R^2, at weak turbulence conditions. The Rytov variance is given by

$$\sigma_R^2 = 1.23 \cdot C_n^2 \cdot k^{7/6} \cdot R^{11/6} \quad (8\text{-}7)$$

σ_I^2 reaches a maximum >1 at strong fluctuations and finally decreases towards a value of unity for large values of σ_R^2.

9 Collimator CTS-1

The collimator system is a CTS-1 (Collimator Test System) from CI Systems in Israel [1] (Figure 9-1, 9-2). Its main parts are radiation source, target and collimator as seen in the schematic drawing in Figure 9-3. The targets consist of metal plates with one or several holes, which may be mounted on a target wheel. Radiation from a radiation source like a blackbody, placed in front of a target, is reflected by the flat mirror and then collimated at the off-axis parabolic mirror at the rear of the collimator to produce parallel radiation.

Figure 9-1. Collimator test system CTS-1; with target wheel, test targets, blackbody source and control unit.

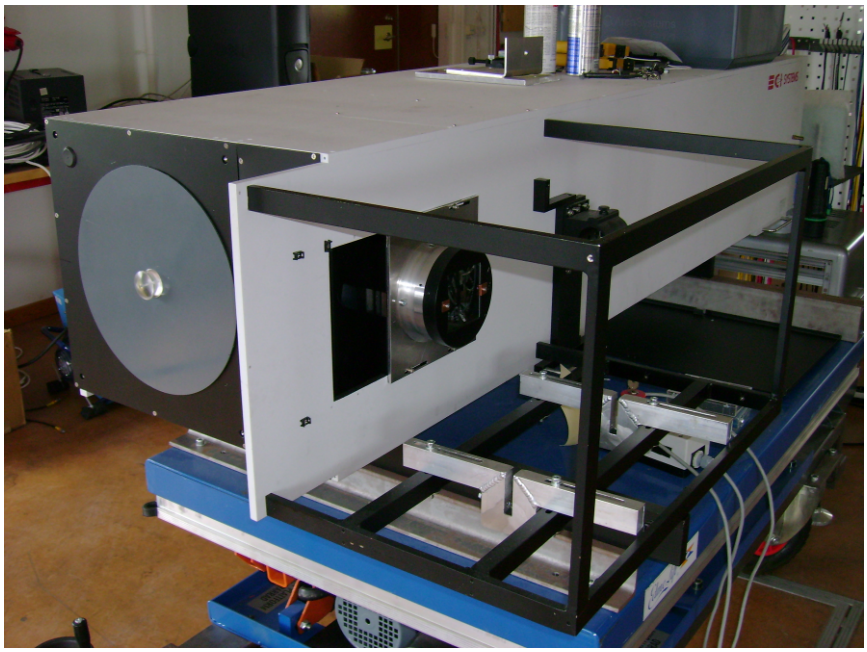

Figure 9-2. Collimator test system CTS-1; prepared for use with an integrating sphere as a radiation source and testing of cameras in the spectral range 500-2500 nm.

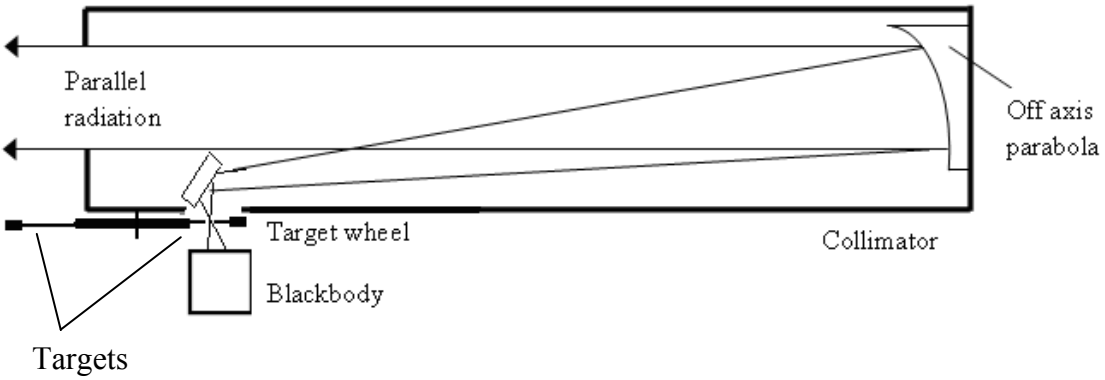

Figure 9-3. Schematic drawing of CTS-1

For small angles, which is the case below the collimator FOV of 2.9°, the following relation holds between target size *a* (meters) at the collimator focal plane and the viewing angle θ (radians) that is covered by the target as seen by the unit under test:

$$a = f_{col}\,\theta \qquad (9\text{-}1)$$

where f_{col} = 1,787 m is the collimator focal length. As alternative units, mm for *a* and mrad for θ can be used. For periodic targets, the spatial frequency *v* is related to the cycle length *d* according to

$$v = \frac{f_{col}}{d} \qquad (9\text{-}2)$$

where the units for *f* and *d* are cycles/rad and meters, or cycles/mrad and mm. *d* is the full cycle length as shown in Figure 9-3.

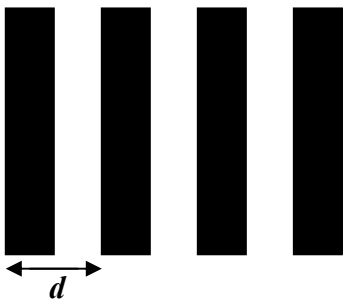

Figure 9-3. Definition of cycle length for periodic targets.

A set of standard targets are available for the collimator system, including four-bar targets, point targets (circular apertures), a slit target, and an edge target.

10 Weather stations

10.1 Milos 500

Data about the weather station Milos 500 (Vaisala) [1], are shown in the table below.

Table 10-1. Weather parameters logged with Milos 500 (Vaisala) [1]

Weather station	Parameters	Unit
Milos 500	wind direction	degrees
	wind speed	m/s
	air temperature	°C
	soil temperature	°C
	relative humidity	%
	pressure	hPa
	visibility range, 1 min mean	km
	visibility range, 10 min mean	km
	solar radiation	0.3 – 2.8 µm
	ground	0.3 – 2.8 µm
	sky radiation	3.5 – 50 µm
	ground	3.5 – 50 µm
	albedo	%
	precipitation	mm/h

Figure 10-1.Weather station Milos 500 (Vaisala)

Table 10-2 . The two left columns show the authentic output file from Vaisala (Swedish).

Parameter	**Unit**	**Translation/Note**
Vindriktning	°	Wind direction/Accuracy ± 3°
Vindhastighet	m/s	Wind speed/Accuracy ± 0.17 m/s
Lufttemperatur	°C	Air temperature
Fukt	%	Air humidity
Tryck	hPa	Air pressure
Nederbörd	ON/OFF	Precipitation
Sikt (1 min medelvärde)	KM [1)]	Visibility (1 min arithmetic mean)/km
Extension koefficient [2)]	KM^{-1} [1)]	Extinction coefficient/km^{-1}
Sikt (10 min medelvärde)	KM [1)]	Visibility (10 min arithmetic mean)/km
Extension koefficient [2)]	KM^{-1} [1)]	Extinction coefficient/km^{-1}
Nederbördstyp	REGN/SN™ [3)]	Kind of precipitation; RAIN/SNOW
Nederbördsintensitet	mm/h	Precipitation intensity
Nederbördsmängd(regn)	mm	Amount of precipitation(rain)
Nederbördsmängd(SN^{TM}) [3)]	mm	Amount of precipitation(snow)
Direkt väderkod	//////	A meteorological code
Instrålning(albedometer) [4)]	W/m^2	Direct insolation/Measured from VIS up to ~3µm
Markstrålning(albedometer) [4)]	W/m^2	Earth's insolation
Albedo	%	= Markstrålning/Instrålning
Instrålning(pyrgeometer)	W/m^2	Direct insolation /Measured > 3µm
Markstrålning(pyrgeometer)	W/m^2	Earth's insolation
Strålningsbalans (extra)	W/m^2	Radiation balance/Not in use
Strålningsbalans (Schenk)	W/m^2	Radiation balance /Not in use
PT100(1)	°C	/Inside the albedometer
PT100(2)	°C	/Inside the pyrgeometer
PT100(3)	°C	/In the ground
Markfukt 1 (tryck)	hPa	Ground humidity 1 (pressure)/Not in use
Markfukt 2 (tryck)	hPa	Ground humidity 2 (pressure)/Not in use
Extra ingång	V	Extra input/Not in use

[1)] "KM" is stated in the output file; should be: km

[2)] "extension koefficient" is stated in the output file; should be: extinktionskoefficient

[3)] SN™ = snö

[4)] "albedometer" is stated in the output file; should be: pyranometer

10.2 Vantage Pro2

Table 10-3. Weather parameters logged with the weather station Vantage Pro2 (Davis) [26]

Weather station	Parameters	Unit
Vantage Pro2	wind direction	degrees
	wind speed	m/s
	air temperature	°C
	relative humidity	%
	pressure	hPa

Figure 10-2. Weather station Vantage Pro2 (Davis)

Figure 10-3. Weather station Vantage Pro2 (Davis)

10.3 Pyranometer SPN-1

The sunshine pyranometer SPN1 (Delta-T Devices Ltd) measures the direct and diffuse components of incident solar radiation [W/m^2].

Table 10-4. Some data about SPN1 (Delta-T Devices Ltd)

Spectral range	400-2700 nm
Spectral sensitivity variation	10 % typical
Range	0 to > 2000 W/m^2
Resolution	0.6 W/m^2
Sunshine status threshold	120 W/m^2 in the direct beam
Azimuth angle accuracy	±5% over 360° rotation
Cosine correction accuracy	±2% of incoming radiation over 0-90° zenith angle
Size (diameter x H)	140mm x 100 mm
Weight	0.94 kg

Figure 10-4. Pyranometer SPN1(Delta-T Devices Ltd)

11 Minolta illuminance meter

The incident radiation from the sun can be measured manually with a lux meter, Minolta illuminance meter (Minolta) [27]. Lux meters measure lux (lx) which is the unit of illumination, E_v [W·m^{-2}]:

$$E_v = \frac{F}{A} \qquad (11\text{-}1)$$

where F is the lumens illuminating a certain surface A.

In nature, illuminance ranges from about 0.01 lx on a dark night of a new moon to about 100,000 lx on a hot summer day.

Table 11-1. Some data about Minolta illuminance meter

Receptor	Silicon photocell
Illuminance unit	Lux (lx) or foot candles (fcd)
Measuring range	Illuminance 0.01 to 299,900 lx (0.001 to 29,990 fcd)
Accuracy	± 2 %

Figure 11-1. Minolta illuminance meter

12 Software

12.1 D9

D9 is a flexible tool used for collection of data from imaging sensors [28]. It is compatible with Windows XP and later versions. It is designed for scientific applications and has been evaluated both by laboratory measurements and extended field trials. Main features of the image capturing software are:

- D9 supports monospectral, multispectral and hyperspectral cameras. A new camera is included by adding additional information in a configuration list.
- The image data acquired from D9 are standardized into formats based on the ENVI format.
- Each single image gets a timestamp with a precision of 1 ms. There is support for an FPGA board, which can improve the precision to 1 μs.
- Through D9 an arbitrary number of cameras can be temporally synchronized and the data collected. This option imitates true multi-colour cameras.

The design of the graphical user interface is compact with only two windows visible on the desktop. A large number of options are available in the main dialog with the live image being viewed in the second window. The compact design is made possible by an “active” interface that changes appearance depending on the mode. D9 is mainly run in two modes: a live image/recording mode and a play-back mode. During the play-back mode, a number of play-back controls that are not used in the live image/recording mode, become visible.

The sections 12.1.1-12.1.6 describe options often used in D9. Abbreviations used in D9 are defined in section 12.1.7.

12.1.1 Starting D9

D9 is started by double-clicking the icon “d9”. A dialog window then appears with selective options seen in Figure 12-1 below.

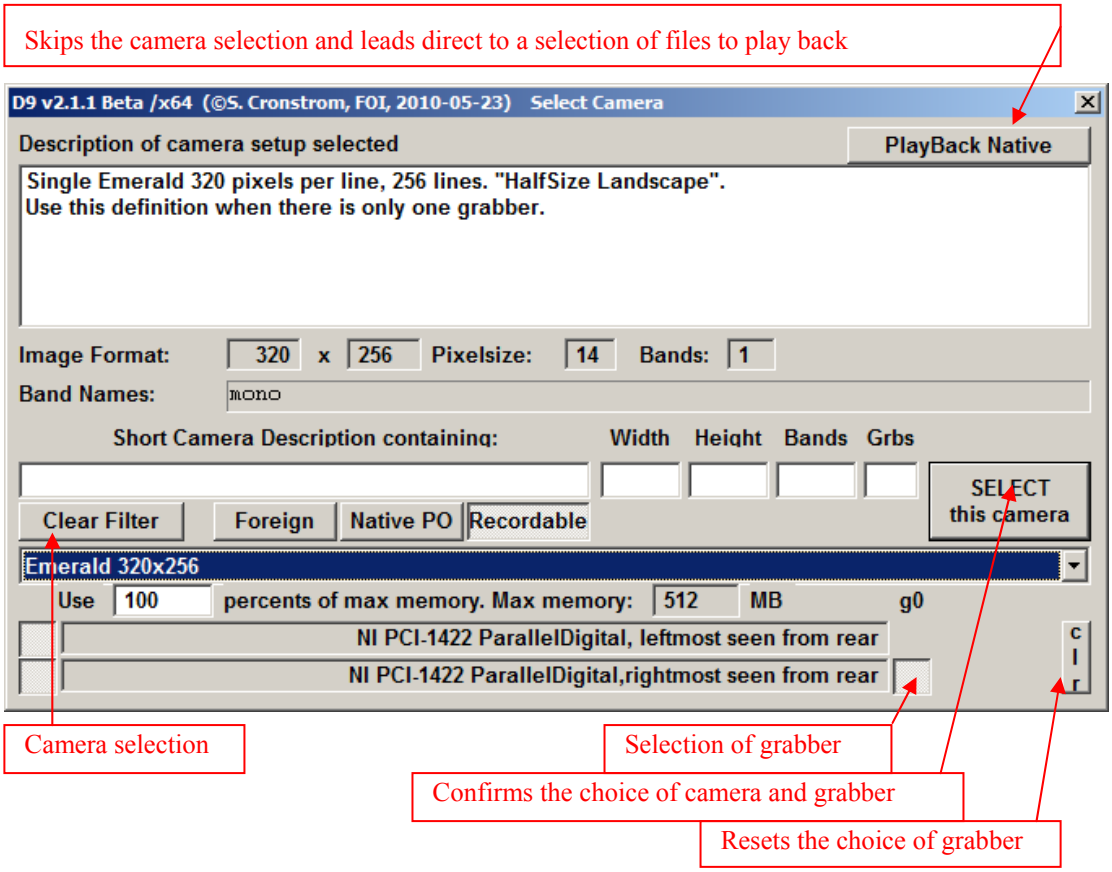

Figure 12-1. Dialog window at the start of D9

The downwards pointing arrow below “Select this camera” reveals a drop-down menu seen in the figure below.

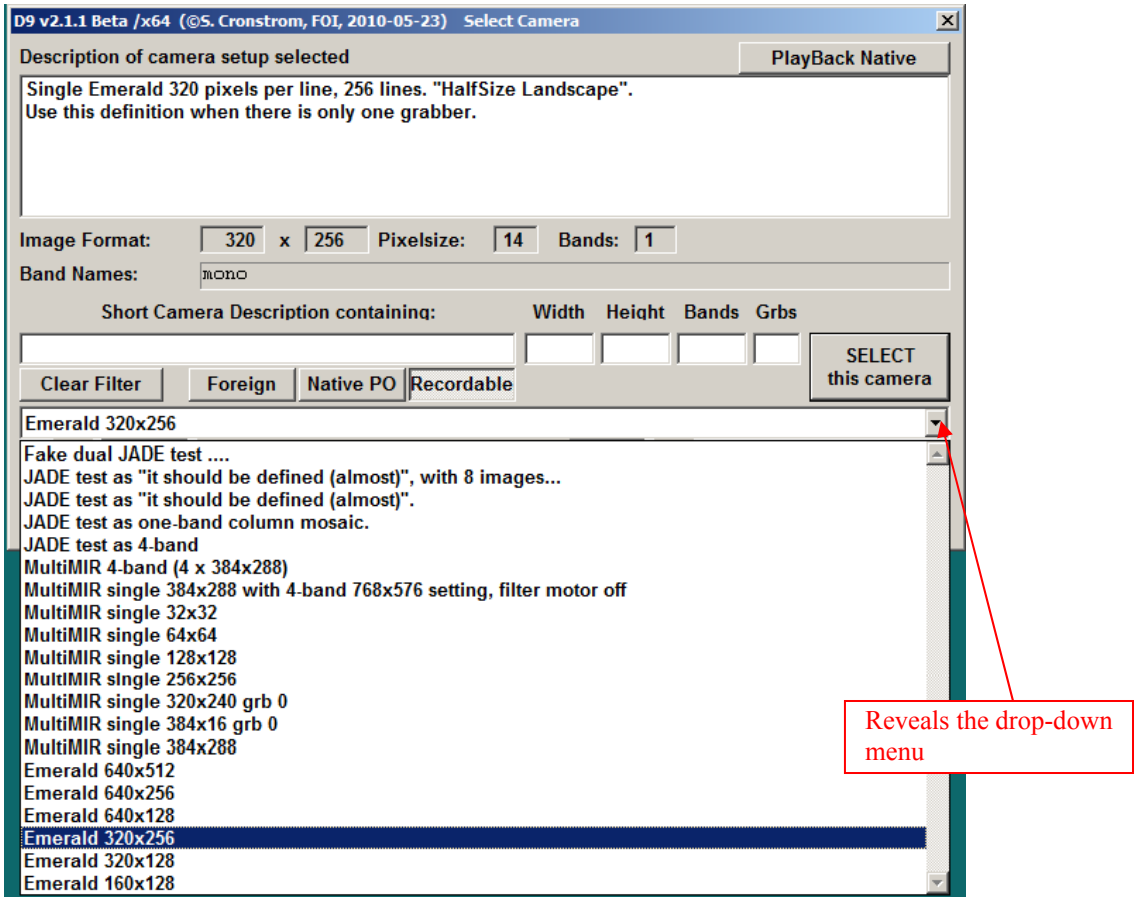

Figure 12-2. Drop-down menu

The menu list may be very long and therefore it may be difficult to get a full overview. However, the fill-in fields above the drop-down menu offer possibilities to constrain it. Figure 12-3 below shows the menu constrained to items with “emerald” (case insensitive) in the one-line description summary.

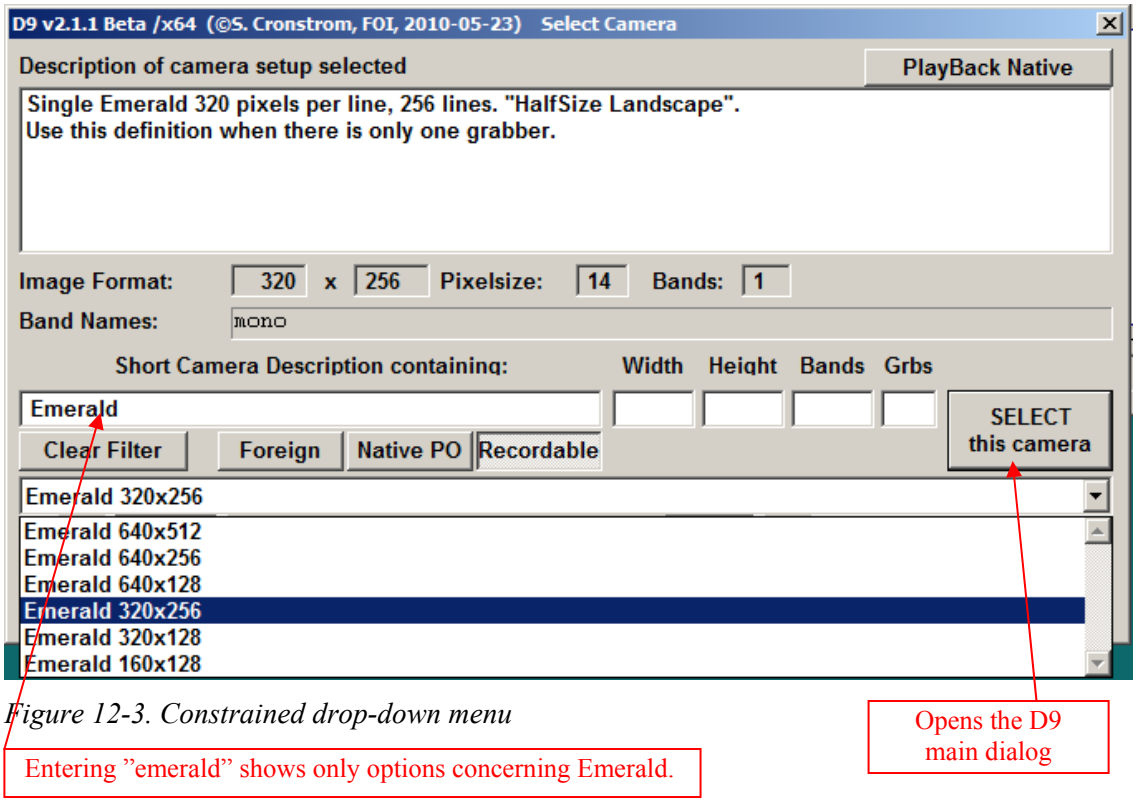

Figure 12-3. Constrained drop-down menu

If there is no camera file, the camera selection menu will not appear. Instead an "Open file" dialog will emerge. In addition, "Width" and "Height" fields constrain the menu to items with the width and the height between approximately 0.7 and 1.4 times the respective field values. In the "Grbs" box the number of grabbers is entered.

"SELECT this camera" reveals the D9 main dialog (Figure 12-4). If "PlayBack Native" is selected, it will look like in Figure 12-12. Buttons and other controls connected to grabbing and recording are then hidden.

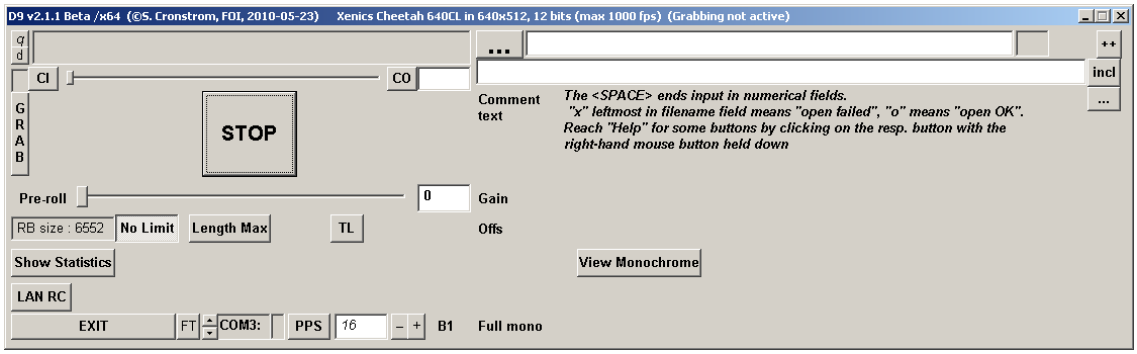

Figure 12-4. D9 main dialog

"View Monochrome" followed by "Grab" yields an image as shown in Figure 12-5 (in case of multiband images "mosaic", the individual bands are displayed as a "mosaic" of e.g. 2 rows of 2 images each.). New buttons become visible.

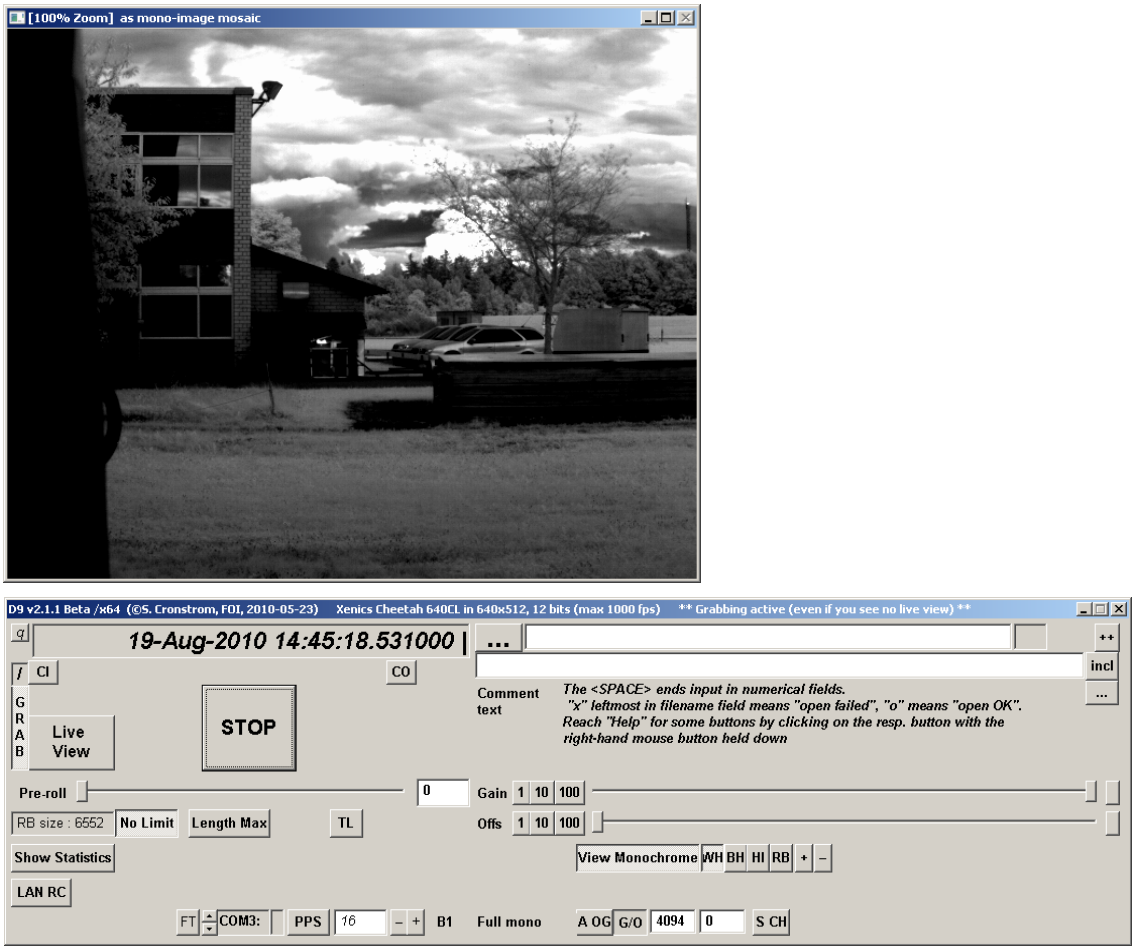

Figure 12-5. D9 main dialog and an image window

The '+' button magnifies the image-display window by a factor of 2 at the first click and by 3 at the next. A sequence 1,2,3,5,7,10,14… of magnification factors is browsed through by the '+' and '-' buttons, "upwards" and "downwards" respectively. The initial magnification is 1. Clicking '-'from unity magnification (initial or reached by '-' clicks) yields scale-down by 1/2, -1/3, 1/5, 1/7, etc.

'**WH**' ("White Hot"), '**BH**' ("Black Hot"), '**HI**' ("Hot Iron") and '**RB**' ("Rainbow") give four options to represent the monochrome image.

The last three decimal positions of the time stamp's seconds show the microseconds, and are irrelevant when only Windows' own time management is used.

'TL' reveals an empty box and a new button 'da'. By entering "2" in the box, every second image is displayed. "100" displays every 100th image. Pressing 'da' displays all images (as far as possible; the frame rate may be much higher than the updating of the live view).

The contrast and over-all brightness in the displayed image can be adjusted with the ‘Gain’ and ‘Offset’ sliders. An automatic adjustment can be activated by clicking the ‘A OG’ (“Automatic Offset and Gain control”) button. The sliders are hidden when ‘A OG’ is pressed. The two edit controls show the values of the gain and offset. It is possible to enter values into the boxes to update the sliders accordingly.

The button ‘S CH’ to the right of the edit controls activates a functionality to display all pixels with values below a “cold” limit in maximally blue, and those above a “hot limit” in maximally red. These are controlled by the slides shown in figure 12-6 below.

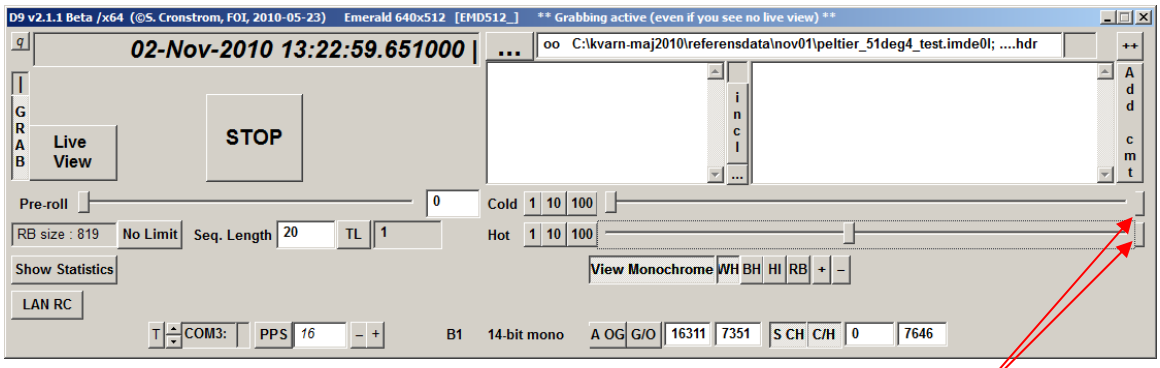

Figure 12-6.

Makes it possible to navigate “Cold” and “Hot” (or Offset and Gain) by using the arrows on the keyboard instead of the slides.

The ‘O/G’ and ‘C/H’ buttons form a radio-button group. They select which gain/offset or cold/hot limit the sliders shall control (and show). All these settings of display mode and contrast and brightness affect only the displayed image and not what is stored in the file.

The single band ‘B1’ has the name “Full mono” defined in the camera-definition file.

12.1.2 Show statistics

In addition to using the button ‘S CH’ (described in 12.1.1) a check of the signal level can also be made with help of the button ‘Show Statistics’. By clicking this button a window and a button (‘B1’, to the left of the band name ‘Full mono’ in the figure below) appear. By pressing ‘B1’ the pixel values are displayed in a histogram. The display of the pixel values is, when “density” is shown, scaled to fit the histogram by using the ‘s+’ and ‘s-‘ shown in Figure 12.7. Density is non-negative but not upward-bounded. Density values alone tell “nothing”. The ‘r-‘ and ‘r+’ buttons adjust the x-axis scale; the range is then halved or doubled respectively. ‘<<’ and ‘>>’ move the range.

‘S CH’ followed by ‘C/H’ display the cold and the hot levels as vertical blue and red lines in the histogram. By pressing ‘C’, a control value stated in the box to the left is displayed as a vertical green line in the histogram (Figure 12.8). By clicking the ‘Distribution’ a cumulated histogram is applied as seen

in Figure 12.9. The ‘s+’ and ‘s-‘ button have no effect when “distribution” is shown. Distribution is always between 0 and 1.

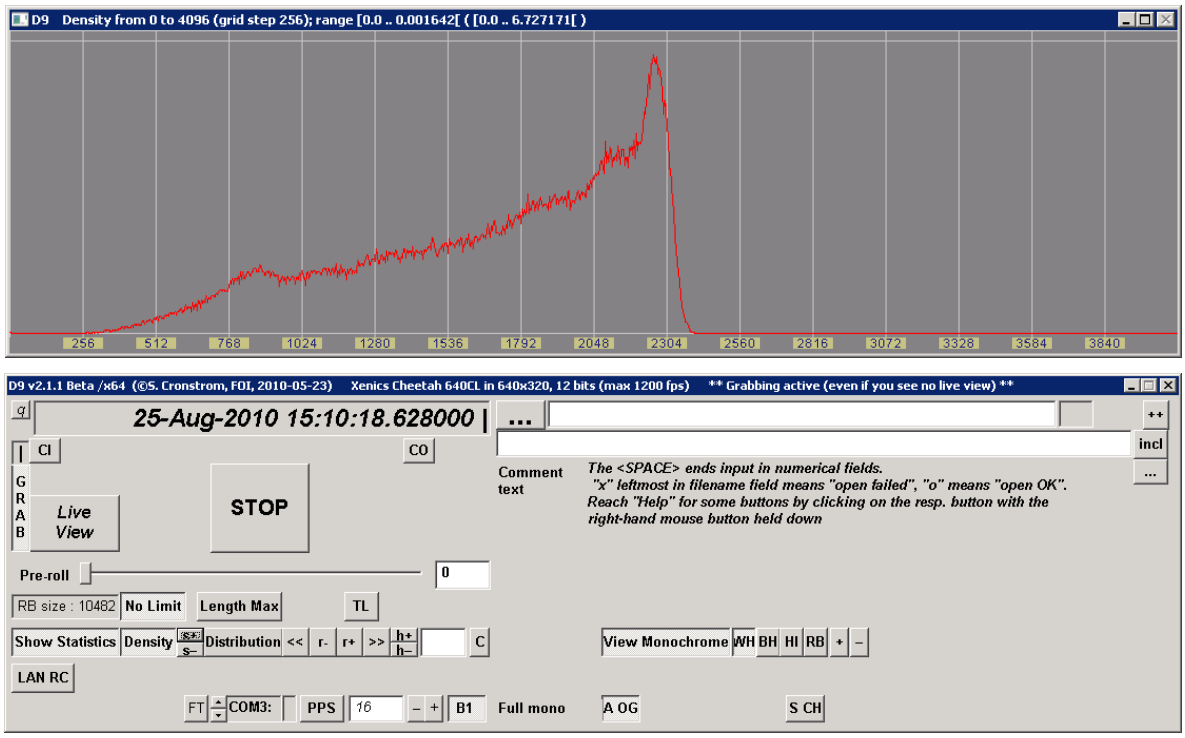

Figure 12.7. D9 main dialog and a histogram window.

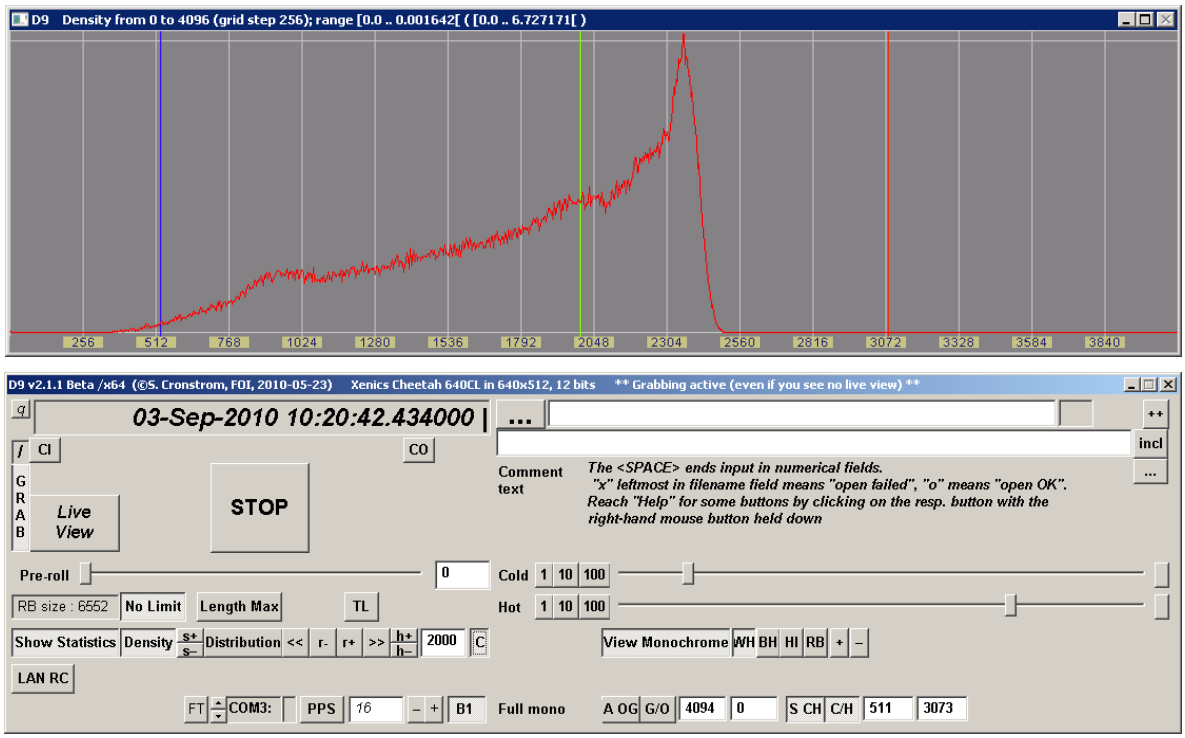

Figure 12.8. D9 main dialog and a histogram window with the cold level (blue vertical line), the hot level (red vertical line) and a control level (green vertical line).

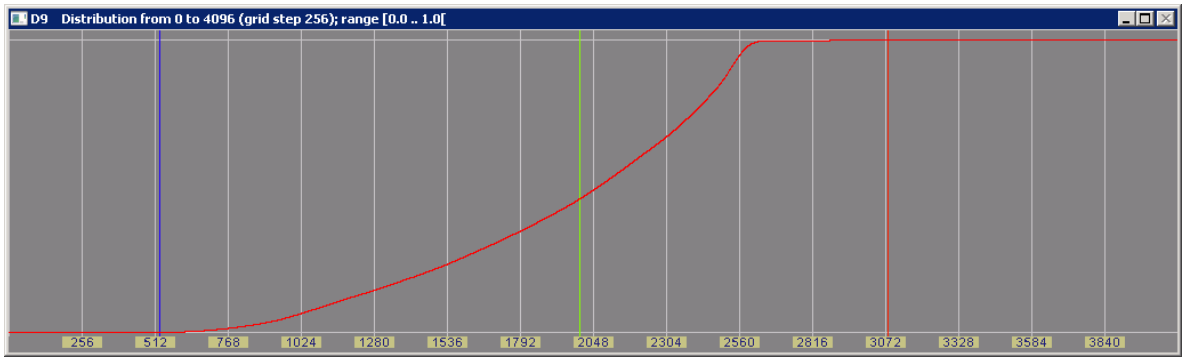

Figure 12.9. A cumulated histogram window displayed with the button 'Distribution'.

12.1.3 Making a recording

In order to make a recording it is required that a file is opened (defined) first. This is achieved by clicking the button with three dots to the right of the time stamp. The name of the new file can be entered without extension in the file-open dialog following (Figure 12-10). It is possible to select an existing file, and after deleting it, open (define) the file. Deleting is necessary because it is not possible to overwrite an existing file. The "oo" in the file name field indicates that both the header and the image data file have been opened successfully.

"Pre-roll" is a pre-trig function that makes it possible to record data before the start button is pushed and the sequence is run. This is done by putting a desired image number in the box to the left of "Pre-roll"and finishing with space bar. The number stated in the box indicates the number of images that are to be recorded before running the sequence.

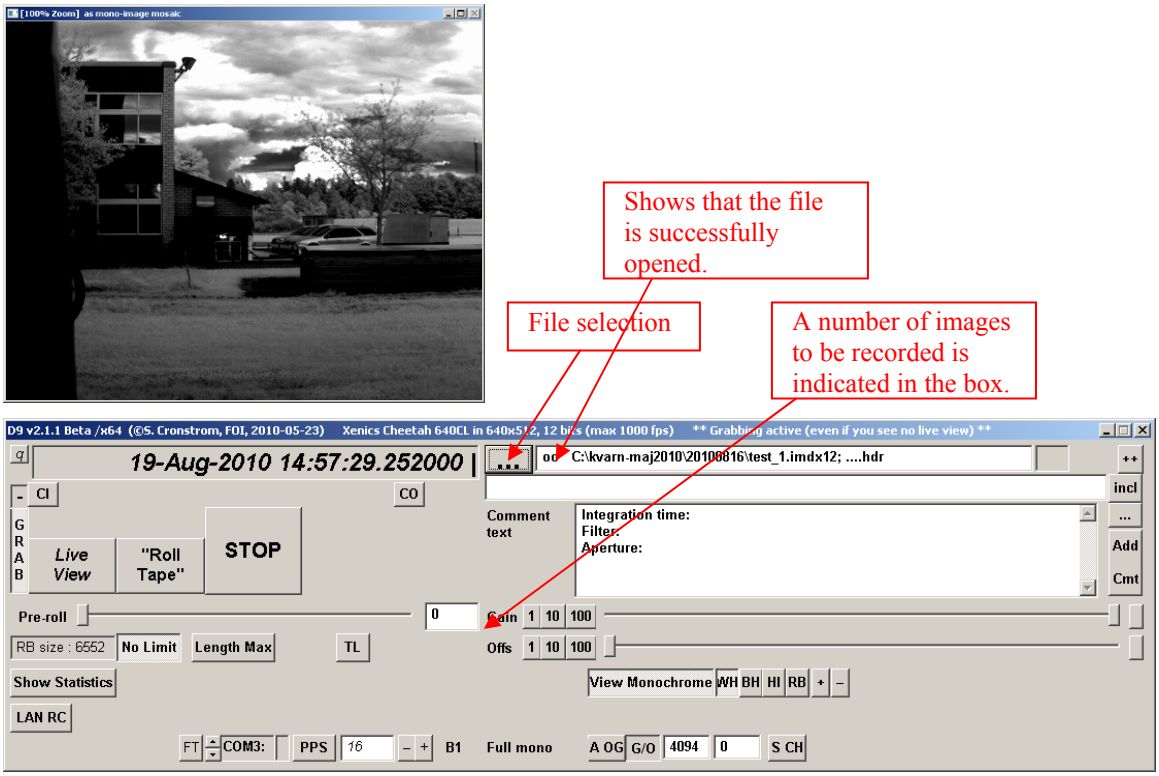

Figure 12-10. A defined file

"Roll Tape" yields a ' | ' sign that cycles to the left of the time stamp showing the recording progress (Figure 12-11). A progress indicator right of the "Stop" button shows how much image data remains to be saved on the disk. If the disks keep a good margin with the data rate from the frame grabber, the bar will be relatively thin. In cases where the disk is not able to keep up with the image data rate, the progress indicator bar will grow until a limit is reached where the grabbing is automatically stopped.

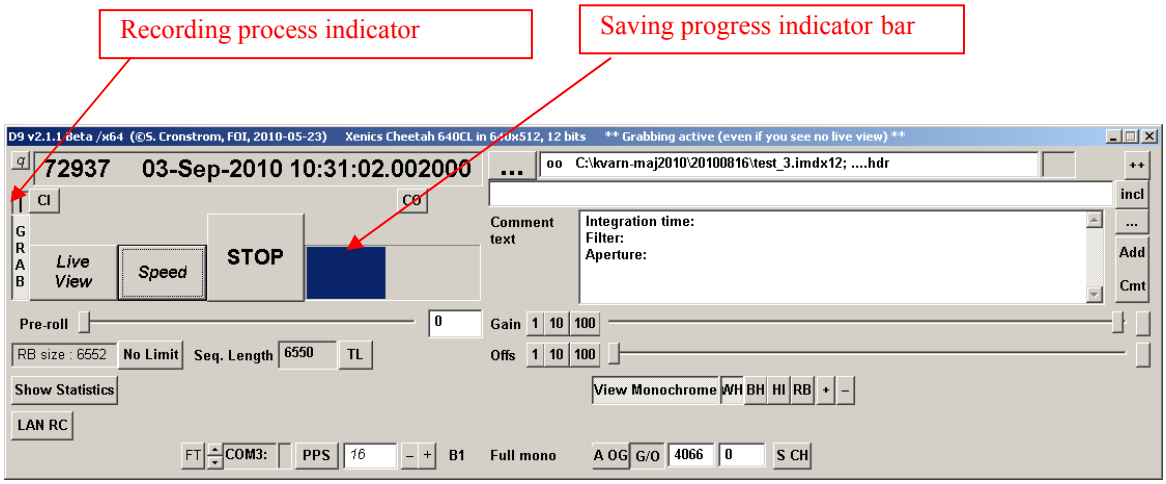

Figure 12-11. Window shown when "Roll Tape" has been selected

Figure 12-12 shows what happens after recording has stopped. The sequence can now be replayed by pressing the play controls, which appear underneath the slide. Holding <CTL>, <SHIFT>, <ALT> down when clicking one of the buttons '<|' and '|>', gives a jump to the beginning or end of the sequence. Holding one of <CTL> and <SHIFT> down when clicking a step button steps the sequence with a step greater than one. The recorded file can be over-written by clicking 'Start Grab' which once again makes 'Roll Tape' visible. After confirming the wish to over-write, 'Roll Tape' must be clicked again to make the new recording.

There is a smaller button with three dots to the right in the dialog. This button initiates a file-open dialog (not visible here) where a cfm, comment form file, is opened. Each time a recording is stopped, the contents of this file are displayed in the comment area beneath the file-name field. In the newer version of D9 this has been slightly changed. The changes are presented in **12.1.4**

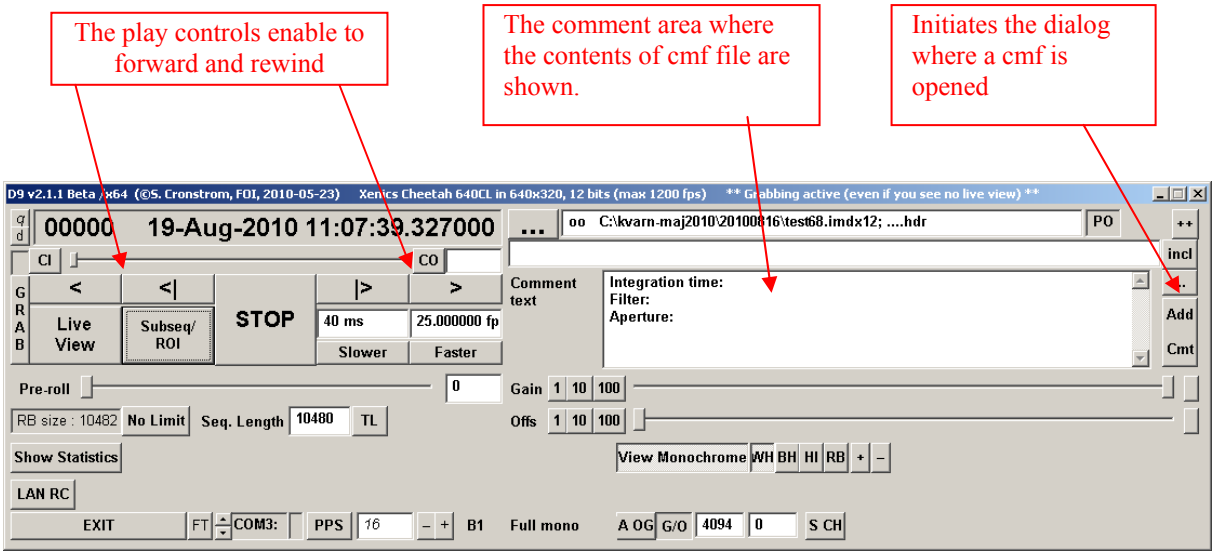

Figure 12-12. After the recording has stopped.

12.1.4 Commenting on a D9 recording

In the latest version of D9 the comment area is divided into two fields (figure 12-13). The fields can be either left empty or be loaded with comment notes.

The left comment area is provided for permanent notes, i.e. notes that will accompany all 'hdrfiles'. After filling in the comment field, "incl" should be pressed which makes the text change from cursive to bold.

The right comment area is provided for notes that are non permanent, for example: lens focus adjustments, weather etc. The notes in the right field will appear in the header after 'Add Cmt' is pressed.

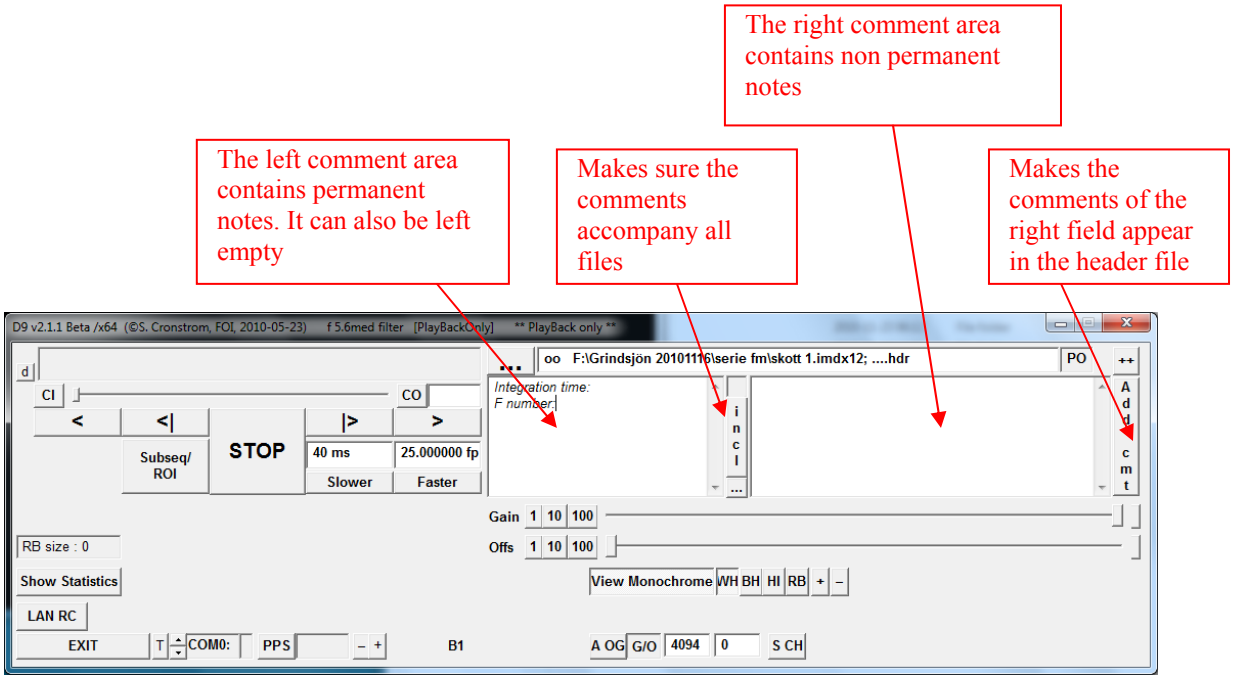

Figure 12-13. New version of figure 12-12. After a recording is stopped, two comment fields, instead of one, appear.

12.1.5 Reducing the file size

Recorded image sequences can be very large, up to 5GB. Such sequences can be difficult to read into Matlab on an ordinary computer. Typically, the number of images that are used in the analysis is small compared to the total number of images in the file. In addition, only a part of the image sequence may be of interest in the analysis. In these cases "Subseq/ROI" (subsequence/region of interest) is selected (Figure 12-14).

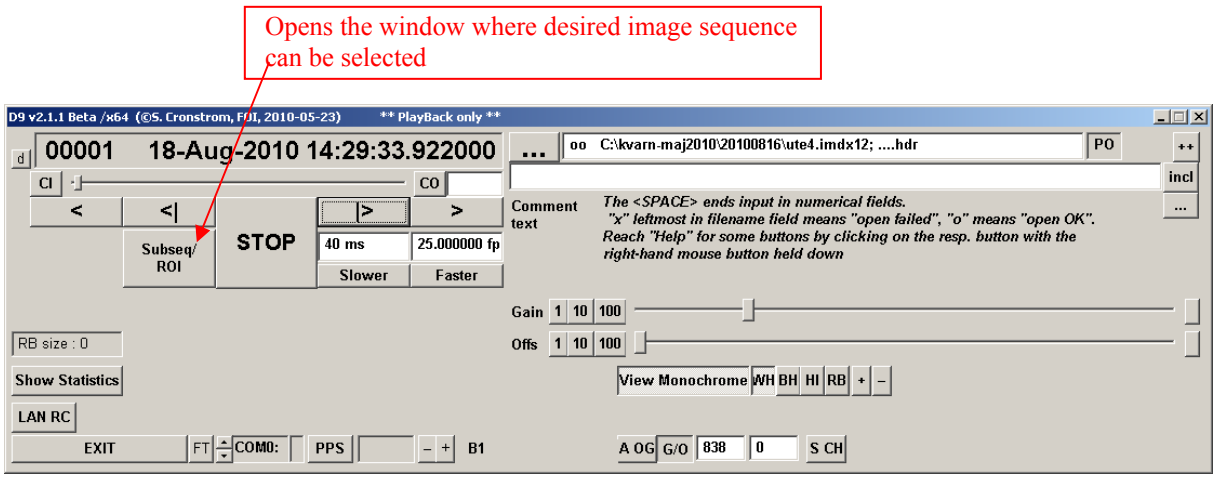

Figure 12-14. PlayBack only mode

"Subseq/ROI" opens another window shown in figure 12-15. "CI" (cut in) and "CO" (cut out) are used to cut the image sequence. "CI" indicates the lower limit of the sequence and is pressed after the first image of the required sequence is chosen, which is done by the play controls seen in the figure. In the same manner "CO" indicates the upper limit of the sequence and should be pressed after the completion image is determined. If this is not done, all images will be saved.

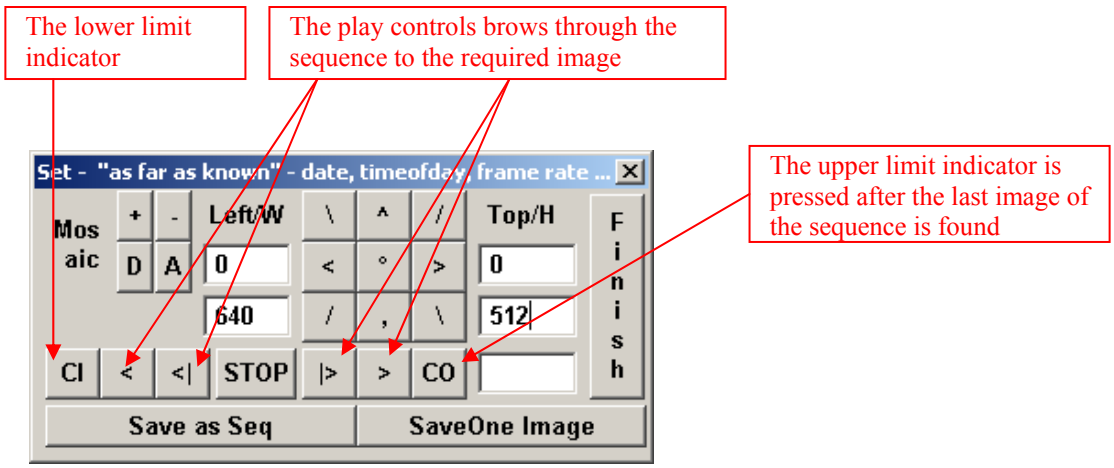

Figure 12-15. After clicking "Subseq/ROI"

The four upper white fields are used to crop the image. The upper two determine the position in the whole image from the left and from the top (Figure 12-16). The lower two determine the size of the cropped image (width and height). After cropping the image the little box around the required area appears and is saved by pressing "Save as Seq". An example is shown in Figure 12-17 and 12-18.

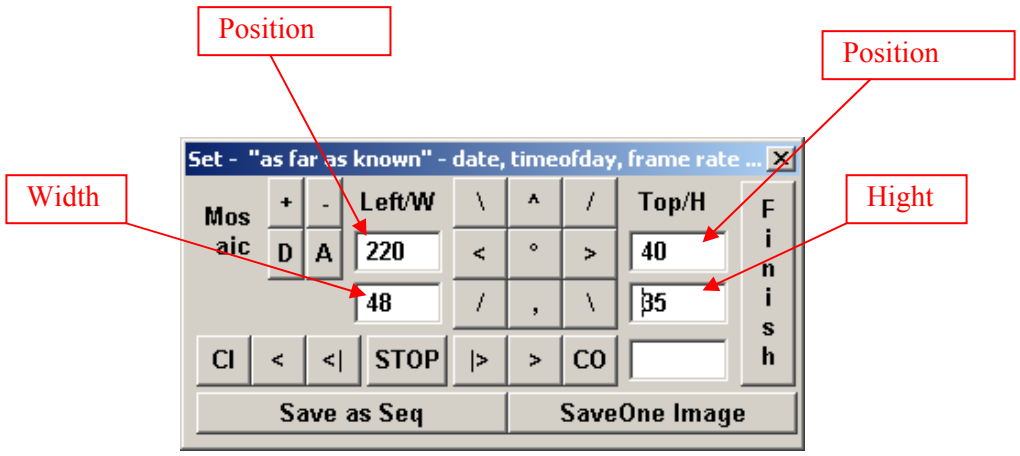

Figure 12-16. 35x48 pixels at the position (40, 220) in the image (Figure 12-17)

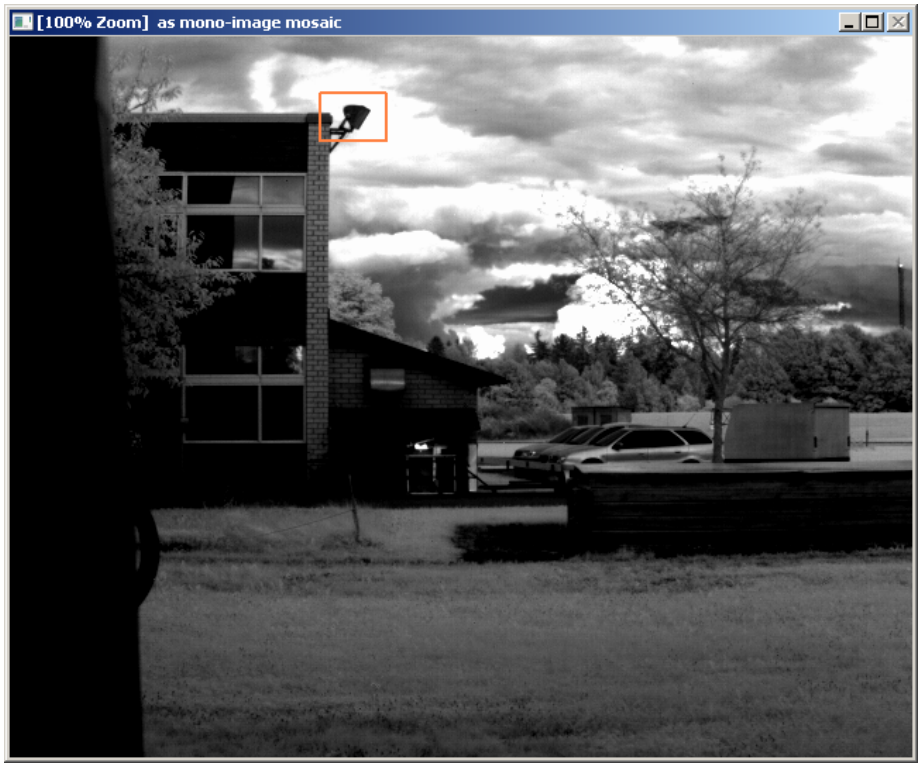

Figure 12-17. The box indicates the required area to be saved.35x48 pixels at the position (40, 220) in the image (Figure 12-16)

Figure 12-18. The cropped sequence saved

12.1.6 Master and slave option

The master and slave option allows one computer (the master) to control several cameras (the slaves). When pressing “LAN RC” (Local area network remote control), two new fields appear to the right of “LAN RC” (port@address and Slave) as seen in Figure 12-19. By pressing “P&A” the port and the address (in this case “9710@multicast_1”), are shown in the second field. The same port and address are stated on the participating computers. In the third field it is stated whether the computer will function as the master or a slave. File names given on the master will be shared by all the slaves.

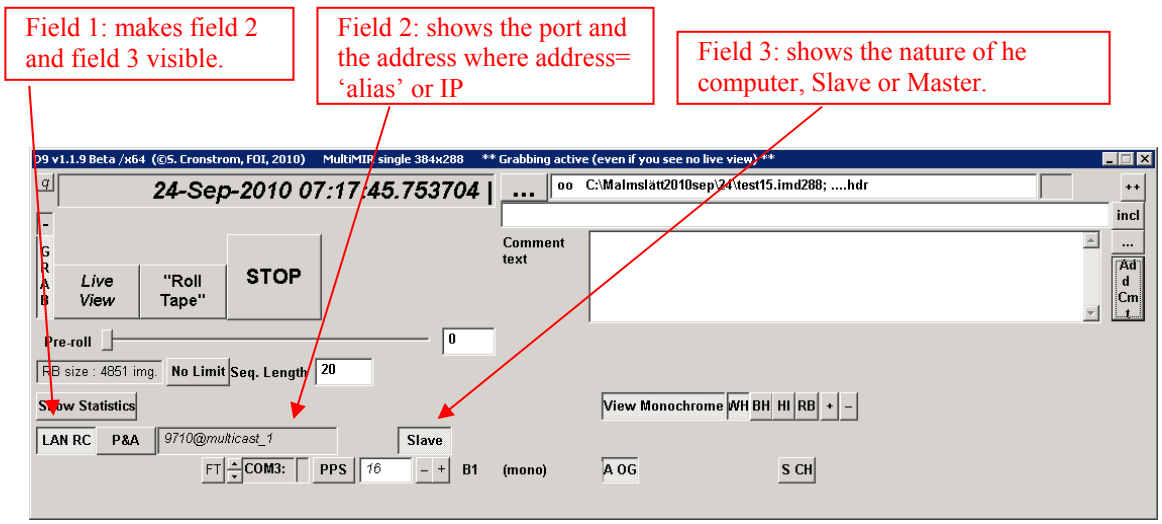

Figure 12-19. Master and slave

12.1.7 D9 abbreviations

The abbreviations in D9 are collected in the list below. Most of these are specific for D9.

A:	across (gives a row representation of a mosaic, 4x1 → 2x2 → 1x4)
A OG:	automatic offset&gain
BH:	black hot
da:	display all
C:	control value
C/H:	cold&hot
CI:	cut in
CO:	cut out
d:	difference
D:	down (gives a column representation of a mosaic, 1x4 → 2x2 → 4x1)
FT:	flow test
Grbs:	grabbers
H:	height
HI:	hot iron
LAN RC:	local area network remote control
O/G:	offset&gain

P&A:	port&address
PO:	play only
q:	quiet
r:	range
RB:	rainbow
ROI:	region of interest
s:	scale
S CH:	show cold&hot
Subseq:	subsequence
TL:	time lapse
W:	width
WH:	white hot

12.2 CamViewer

Below is a short description of the Matlab-GUI ”CamViewer” which is a reader/player with capability of simple preprocessing and saving of data [29].

12.2.1 Loading data and playing through a sequence

The GUI is started by entering the command “CamViewer” in Matlab workspace. In the main window (Figure 12-20) a scene file is selected by pressing “Select file”. After selecting a file, the player is started by pressing “>” at the very right. In order to stop the player, “>” or “<” is pressed once. By pressing the button “<” again the sequence will be read backwards, i.e. rewind. For multispectral cameras a spectral band is chosen with “Band”. All these functions are found in the box “Image”.

The square “Stretch image” gives a default setting of the contrast enhancement which also changes the pixel values in the image to values between 0 and 1. In order to retain the original pixel values and enhance the contrast, the button “Contrast Tool” is used. View settings are made in the box “Display type”. ”Multi Band” allows no more than 4 spectral images to be displayed and “RGB” a maximum of 3 spectral images to be presented as an RGB-image (Figure 12-21).

The pixel values are displayed by pressing “Pixel Info”, which opens the Matlab function “impixelinfo”

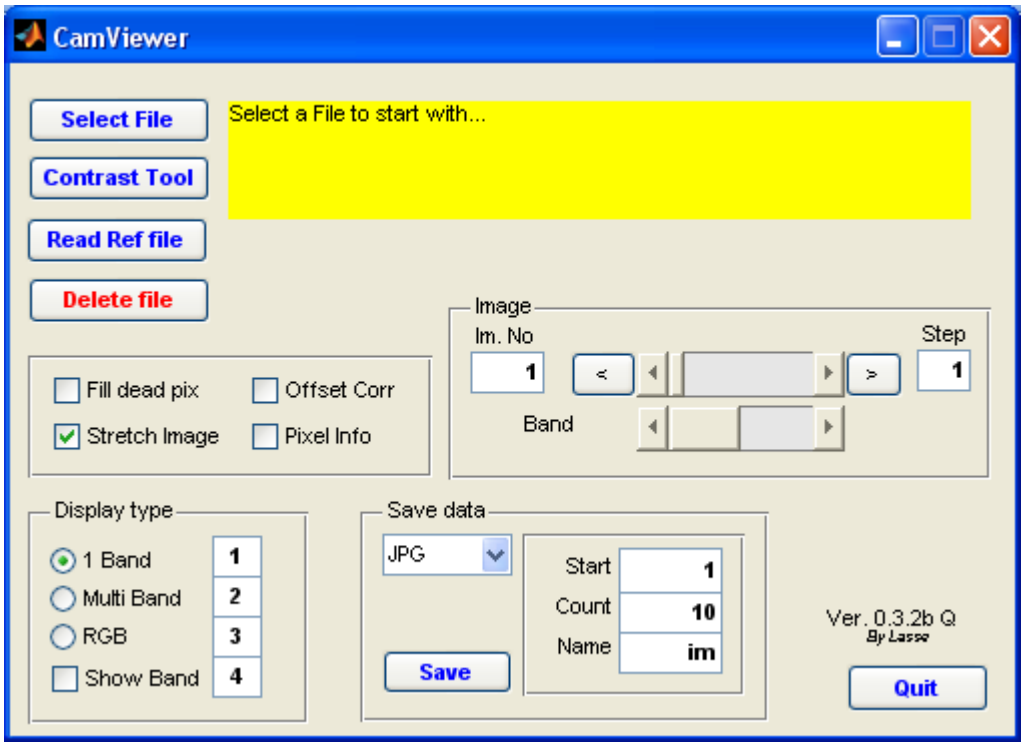

Figure 12-20. Main window

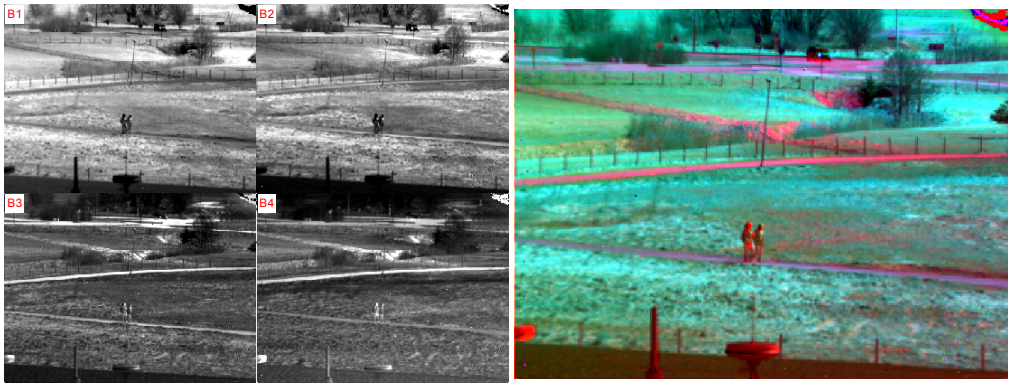

Figure 12-21. Left: ”Multi Band”; right: ”RGB” (the image is offset corrected and bad pixles have been replaced)

12.2.2 Offset correction and replacement of bad pixels

To perform an offset correction (a 1-point correction) and to replace bad pixels, a reference file is chosen by pressing “Read Ref file”. A new window appears (Figure 12-22) where the user needs to select the images to be averaged in the calculation of the the offset image. Bad pixels are identified and replaced with values provided by median filtering. In measurements with a large temperature drift between registrations of scene data and reference data (e.g. airborne registrations) the reference data will most likely not fit the scene data. In these cases the scene data file is used to calculate the offset image. For airborne data it has shown to be enough to use 100 images in the averaging.

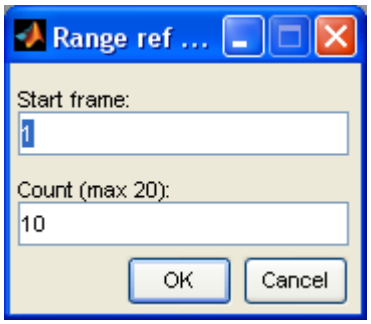

Figure 12-22. Estimation of the mean of reference data.

Offset correction and replacement of bad pixels are carried out by highlighting the squares “Fill dead pix” and “Offset Corr” in the main window. An example is shown in Figure 12-23.

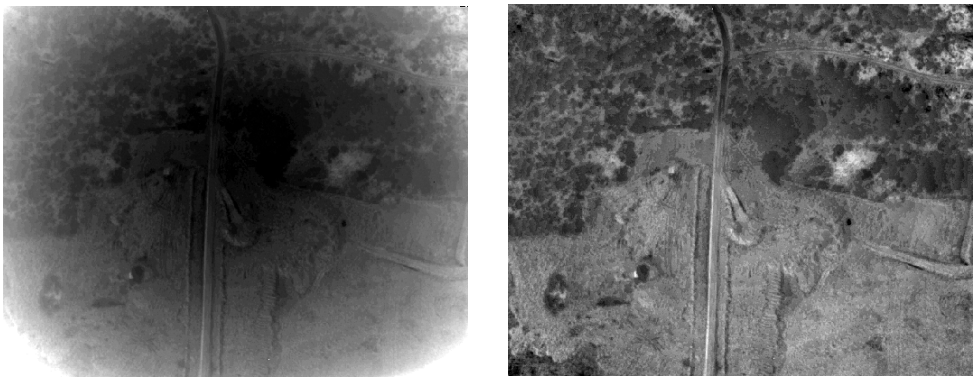

Figure 12-23. An airborne registration with Emerald from a trial in Kvarn 2008. The left image is before the correction; the right image shows the result after the offset correction and pixel replacement

12.2.3 Saving data

Images can be saved as jpg, tif, avi, mat or to workplace. Either of these can be selected in the box where it says “Save data” on the main window. A specific image sequence can be selected in the same box. At “Start” the user can chose a desirable image number and at “Count” the user can decide the number of images to be saved before and after the wanted image.

12.3 Signaturkalkyl

SignaturKalkyl, see Figure 12-24, is a graphical user interface in MATLAB for performing target detection, target signal integration in image data and radiometric calibration of calculated target signals. The GUI is built around CamViewer (see section 12.2) for loading and displaying images and takes image sequences (currently supported formats are hdr and ser), filter data (mat-format), atmospheric transmittance data (mat-format), range to target, aperture diameter, integration time settings and calibration constants as inputs. Non-uniformity correction can be applied to images from reference data or by scene-correction (an offset calibration). Targets can either be selected manually by drawing a rectangle in the display window or by employing target detection algorithms (currently two are implemented). SignaturKalkyl calculates target and background intensities (for up to three different targets) as well as thresholded target areas (in pixels as well as in m^2) as outputs. The results can be saved in mat-format for later continued evaluation and/or exported to ascii for further analysis in e.g. Excel or Origin.

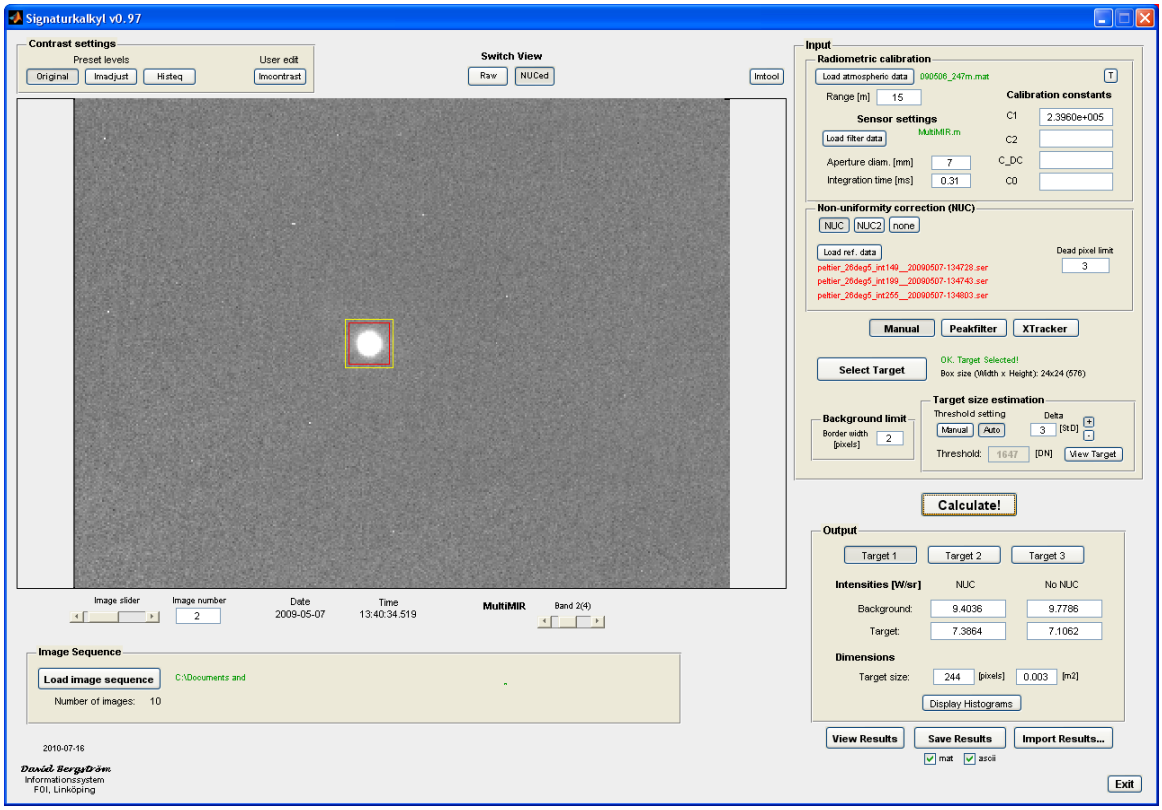

Figure 12-24. Main dialogue window of SignaturKalkyl (v0.97).

12.4 SensorSim

SensorSim is a graphical user interface in MATLAB, see Figure 12-25, for simulating sensor effects such as blurring and noise in images. It contains functions to read image data, add sensor effects and store degraded images. Effects that are supported in the latest version (v0.91) are diffraction, aberration, defocus, detector footprint and sampling, linear and random motion, sinusoidal and jitter vibrations, atmospheric turbulence and scattering as well as dead pixel noise (salt and pepper) [30]. Sensors are created and edited in the accompanying SensorEditor GUI, see Figure 12-26, where FPA geometry, spectral detector responsivity, filter transmissivities, etc., can be specified (either as user input or loaded from ascii input files). SensorSim can also be run as a script with a supplied configuration file, which can be created and saved in the GUI, for batchwise data processing.

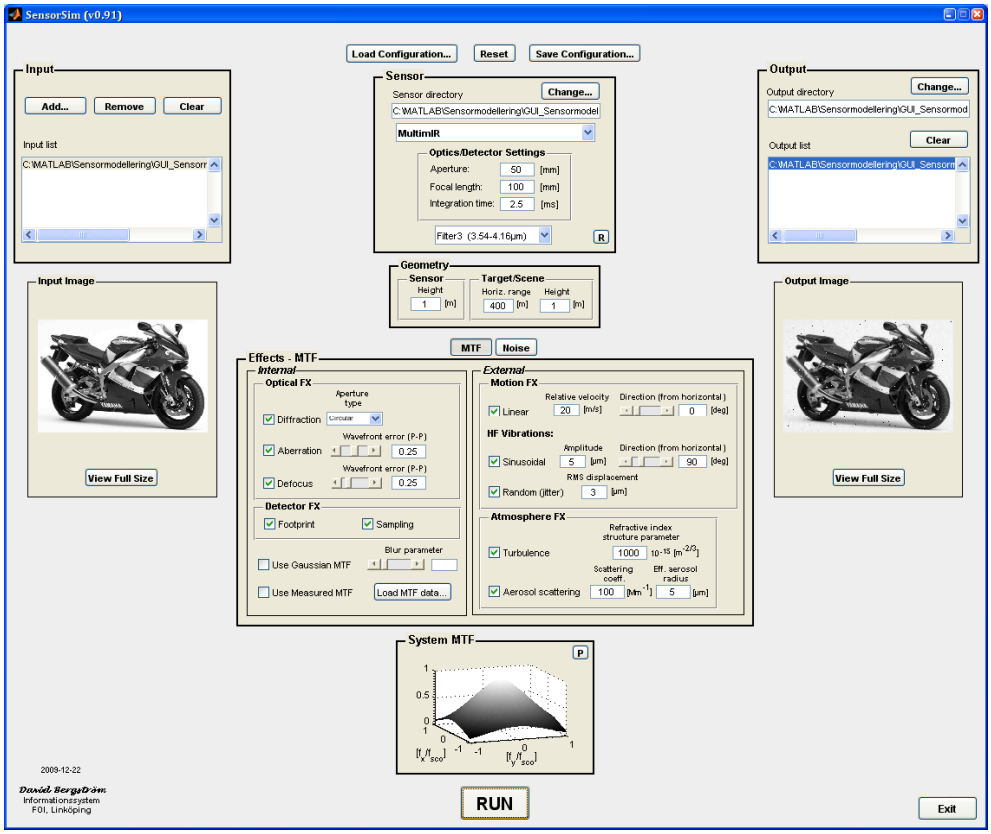

Figure 12-25. Main dialogue window of SensorSim (version 0.91).

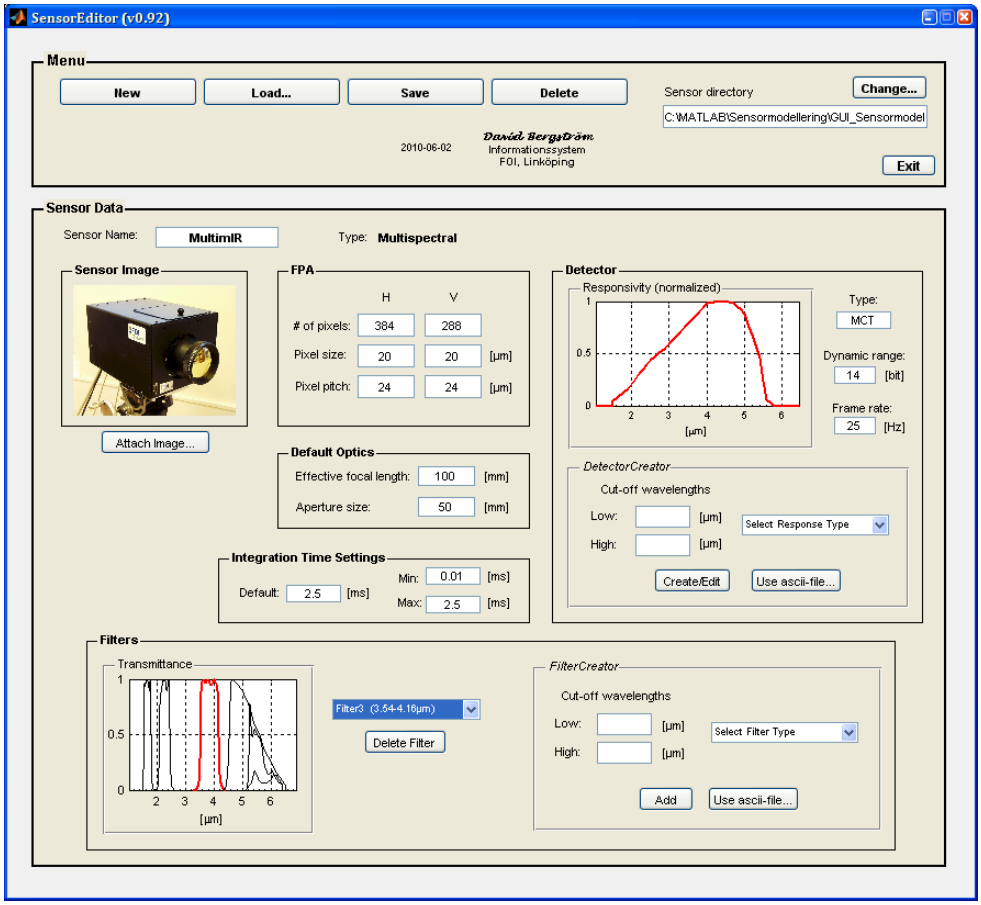

Figure 12-26. Sensors can be created and edited in the SensorEditor GUI (v0.92).

12.5 Edgefit

EDGEFIT (v2.0) is a program package in MATLAB used for evaluation of the spatial resolution of imaging sensors [31]. It takes images from the sensor as input, supported formats are TIFF, BMP and JPEG. In the main GUI window, see Figure 12-27, the user selects regions containing a straight edge by marking and EDGEFIT can then produce the corresponding edge response, point spread and modulation transfer functions (see Figure 12-28).

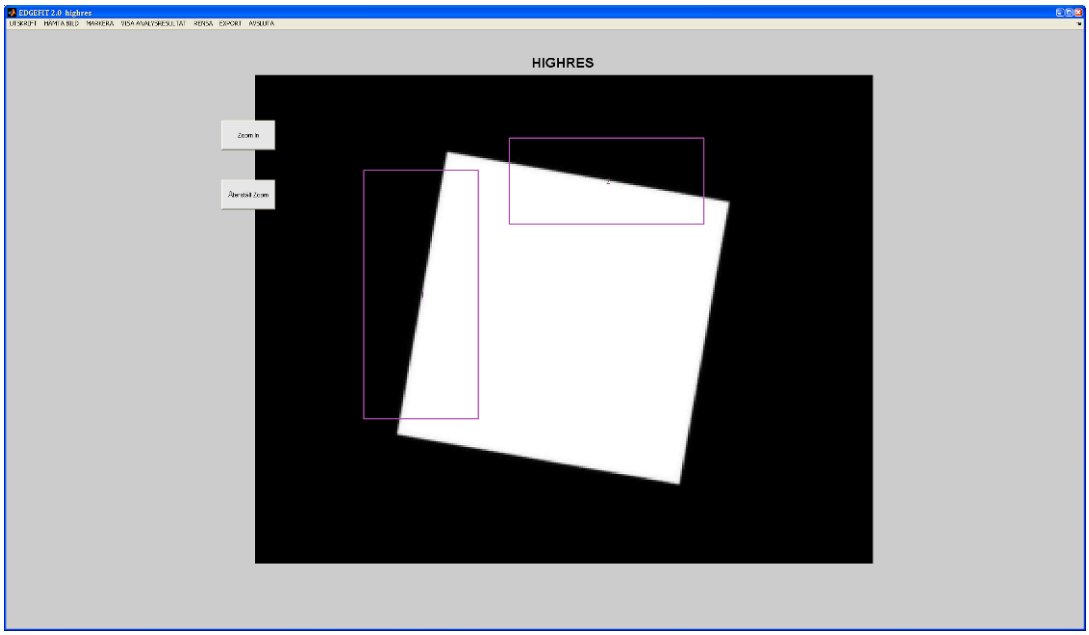

Figure 12-27. Main dialogue window of EDGEFIT (v2.0), showing two selected regions for analysis.

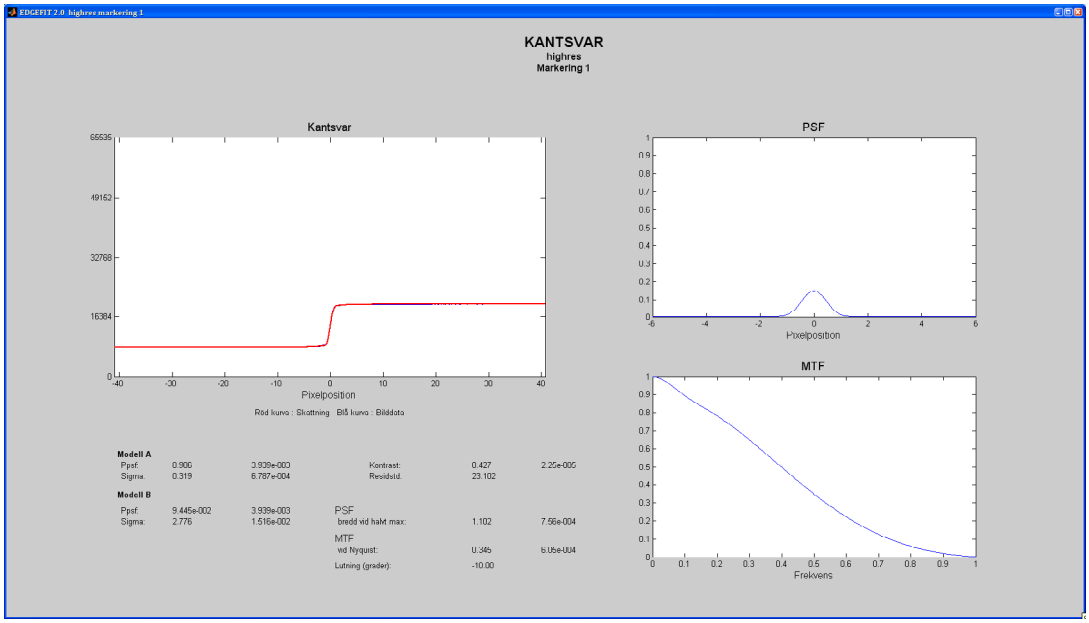

Figure 12-28. EDGEFIT results window showing edge response, point spread and modulation transfer functions of a selected region.

12.6 Hyperspectral Imaging (HSI) toolbox

The research on analysis of multi- and hyperspectral imaging indirectly results in software tools. Some of these tools, developed in Matlab, are packed in a toolbox available internally at FOI [32]. The HSI Toolbox includes a few graphical user interfaces (GUI) to facilitate examination of hyperspectral data (Figure 12-29).

The toolbox essentially consists of a set of classes each encapsulating certain functionalities. Additionally, there is a set of tools for common tasks, for example, principal components analysis, viewing hyperspectral image data, and file utilities for accessing imagery in the ENVI file formats.

The most basic functionalities include handling hyperspectral images (which tend to occupy large amounts of space on disk or in memory), regions of interest (typically, target masks), and receiver operating characteristics for assessing the performance of detection algorithms.

On top of that, functionality for spectral models is available. In the literature, it is very common to model the spectral variation of a specific target or background type as a linear subspace, a Gaussian distribution, a certain direction in spectral vector space, or a Gaussian mixture model. Thus, classes for each of these models have been implemented.

The different models often form the basis of target or anomaly detection schemes, which can be exploited by the anomaly detection tool or the different target detectors. The most common target detectors (ACE, ASD, AMF) from the literature are implemented as detector classes. Anomaly detection is executed by creating the suitable spectral model for the background, applying a spatial model (local or global), and measure the fit of the model to each investigated pixel.

For complex background models, typically Gaussian mixture models or cluster models, a set of training algorithms based on K-means or Expectation-Maximization are available.

The HSI Toolbox can also read output from MODTRAN and be used for fitting black- or graybody curves to spectral data and estimate/compensate for atmospheric transmission [33].

The HSI Toolbox is mainly developed in the Sensor Informatics Group.

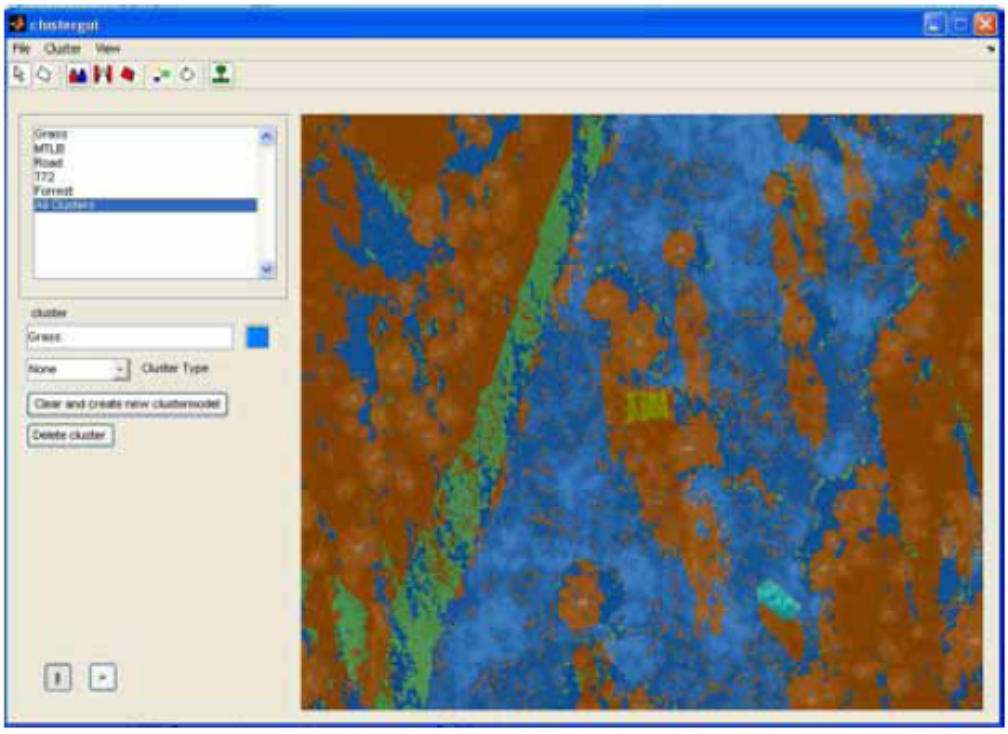

Figure 12-29. The spectral clustering dialog of the HSI Toolbox, here used for terrain classification.

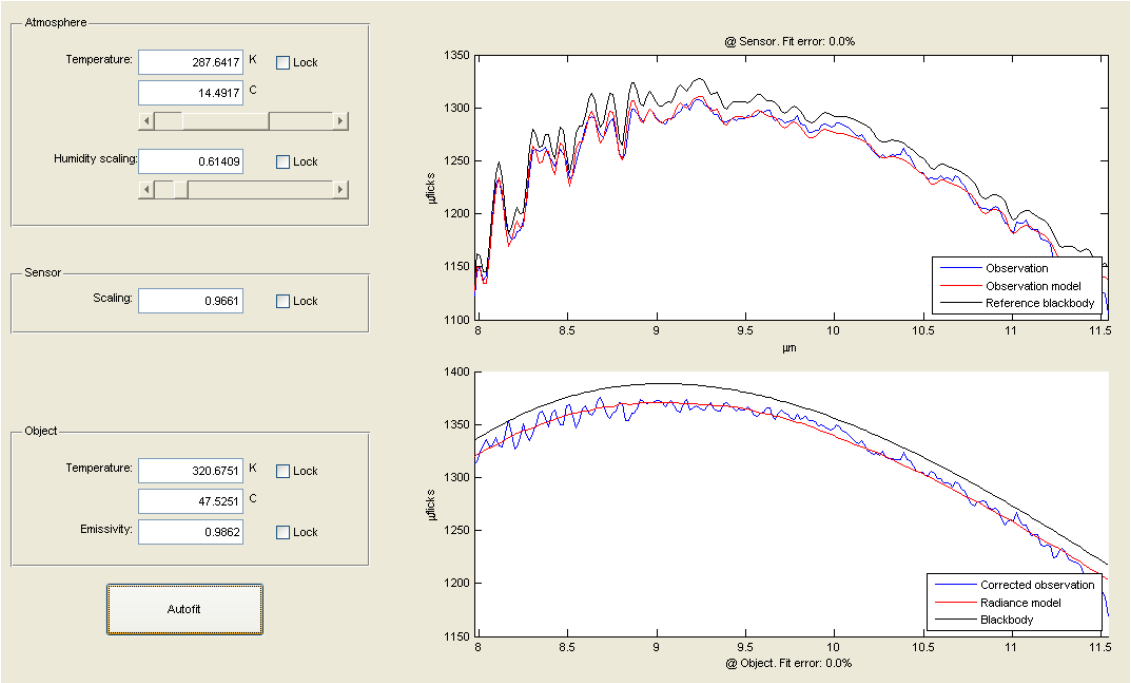

Figure 12-30. The atmosphere, temperature and emissivity GUI of the HSI Toolbox.

12.7 Modtran

At Air Force Geophysics Laboratory, Hanscom Air Force Base in Massachusetts (also denoted AFGL and Phillips Laboratory), an atmospheric model for describing the atmosphere's influence on radiation with optical wave lengths was developed. Both extinction and emission were described with low spectral resolution in the models. Later special laser wave lengths were included. The development of the models was initiated during the first half of the 70s. The first models consisted of a number of tables and graphs, from which the searched values could be estimated. Later, they became computer models named LOWTRAN and HITRAN for low resolution and laser model respectively. A number of versions of the LOWTRAN model were released and named with a number. The first version was released in 1971 and was updated several times until 1983 when LOWTRAN6 came. LOWTRAN7 was released in 1988 with several improvements. The following year, the more advanced model, MODTRAN (MODerate resolution TRANsmission), was presented [34, 35].

The last update of LOWTRAN was version 7. This version, as well as version 2 (and later) of MODTRAN has also been sold commercially as a PC program. The use of LOWTRAN today is due to the need of comparing new and old estimations. Though the model is considered old, it can still be run within MODRAN as an option.

The models estimate the atmosphere's transmission, background radiance, single scattered radiation from sun and moon, direct irradiance from sun and moon and multiplied scattered solar and thermal IR radiation from the atmosphere itself. The spectral resolution of LOWTRAN7 is 20 cm^{-1} (FWHM). Data is provided at each 5cm^{-1} in the spectral range of 0-50000cm^{-1}, e.g. 0.2 μm - ∞ (in praxis the limit is set by the resolution). The resolution in MODTRAN is 2 cm^{-1} with data at each 1 cm^{-1}. The models differ in the way of calculating the molecular transmission. LOWTRAN uses a single-parameter model (air pressure) while MODTRAN uses a three-parameter model (air pressure, temperature and line width). The data bases with 5 cm^{-1} and 1 cm^{-1} resolution has been established with HITRAN as a foundation. Later, as HITRAN became available in new improved versions, LOWTRAN and MODTRAN have been updated.

Now the latest version for PC, MODTRAN5 is available. This version was released in July 2009. It was co-developed by the US AFRL and Spectral Sciences Inc. In July 2010, Ontar released the PcModWin5 v1.3.0 (MODTRAN5). MODTRAN5 has many improvements such as increased spectral resolution to 0.1 cm^{-1} in the calculations. Besides the MODTRAN model, PcModWin5 contains modules for: defining input data, storing the data as files, studying results in form of tables and graphs. It is also possible to define filters for a detector's spectral sensitivity and include one or more filters with a calculated result from MODTRAN. In the program package help functions are provided. A significant addition in version 4 and 5 is the support for the model NOVAM standing for Navy Oceanic Vertical Aerosol Model. MODTRAN already contains, since earlier, the NAM model (Navy Aerosol

Model). NOVAM is a detached program and is run in PCModWin as a separate program module that delivers a result file.

NOVAM models aerosols from the sea surface up to 6 km's height within the spectral range 0.2 µm – 40 µm. The input data for the model includes: sea surface temperature, air temperature, relative humidity, visibility, wind, average wind speed the past 24 hours, air mass (30 different types), clouds, the IR extinction at 10.6 µm and an additional number of parameters. NOVAM functions with three types of meteorological profiles, characterised by none, one or two temperature inversions. The marine aerosols are modelled as four classes that consist of different mixtures of aerosols with three size modes: 0.03 µm, 0.24 µm and 2.0 µm.

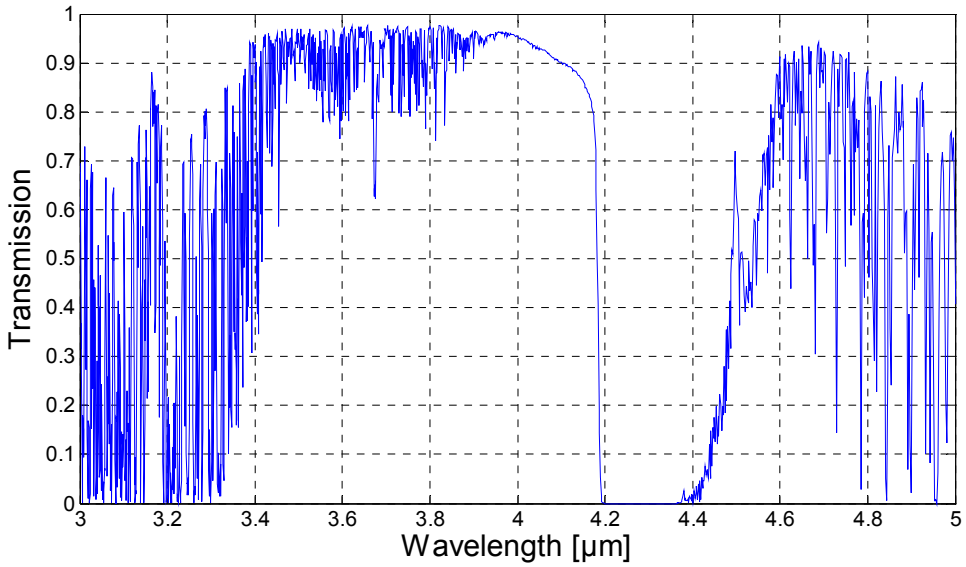

Figure 12-31. Example of a Modtran calculation of the atmospheric transmission at the sea surface; path length: 1 km

The accuracy of LOWTRAN's estimated transmittance values were stated to be ± 5%. The accuray of MODTRAN is stated to be better (not explicitly stated).

MODTRAN estimates the absorption and scatter in the atmosphere for a chosen distance. Absorption consists of linear absorption, where radiation is absorbed into the molecules, and continuum absorption, which also depends on molecular absorption but with other qualities. To estimate linear absorption the model uses atmosphere pressure, temperature and a line width. The scatter of radiation of atmosphere's aerosols can be estimated from the size distribution of the aerosol particles. A number of different aerosol models can be found in the program, for example: Urban, Rural and Maritime.

The atmosphere models are divided into different layers from 0 km to 120 km where a number of parameters are given for each height. The spherical refraction and the earth curvature are considered in the estimation of the

moderation along, for example, slant beam paths. The representative atmospheric models are Tropical Model, MidLatitude Summer, MidLatitude Winter, SubArctic Summer, SubArctic Winter and 1976 U.S. Standard. For each of these models, temperature, atmosphere pressure, density and mixture ratios for molecules like H_2O, O_3, CH_4, CO and N_2O, are given. CO_2 and O_3 are considered to be season-dependent and exist together with approximately 18 other molecules in the U.S. Standard Atmosphere model. The most common molecule in air, N_2, is present in the model but, since it has no dipole moment, is not optically active.

12.8 Tools for estimation of sensor performance

There are several tools intended for performance estimation of passive optronic systems, for example: **NVTherm, TRM, pcSitoS, IGOSS** and **TERRTEX** [36, 37, 38, 39, 40].

Software like **NVTherm** (Night Vision Thermal Imaging System Performance Model - developed by U.S Army Night Vision and Electronic Sensor Directorate) and **TRM** (Thermal Range Model - developed by FGAN) have proven to be useful in development and procurement of thermal imaging systems. It is not possible, however, to generate images with these programs. NVTherm and TRM estimate probability of detection, recognition and identification as functions of distance in the 3-12 μm spectral range from fundamental parameters such as noise, temperature resolution and modulation functions. The programs use somewhat different methodology. NVTherm has been further developed and is now a part of a program package called NVESD that includes:

- NVThermIP - Night Vision's Thermal and Image Processing model
- SSCamIP - Solid State Camera and Image Processing model
- IICamIP - Image Intensified Camera and Image Processing model
- IINVD - Image Intensified Night Vision Device model
- NVLaserD - NVESD Laser Designator model
- CN2 - Cn2-atmospheric refractive index structure constant calculator
- MRTSim - Minimum Resolvable Temperature Simulation

NVThermIP was introduced in 2006 with latest update in 2008. In this version a rectangular bar-target pattern is used (instead of the sinusoidal pattern used earlier) to calculate MRT and, with a new method (instead of Johnson criterion), estimate target detection distance. Generally, there is a good correspondence between predicted and actual ranges. Yet there are limitations that may become notable in some target/background combinations, some weather types and evaluation of signal and image handling techniques. To overcome these limitations, the **pcSitoS** software has been exerted by FGAN-FOM [38]. pcSitoS is implemented in Matlab. Output consists of images or image sequences generated from target and background data.

IGOSS (Image Generation in Optronic Sensor Systems) was advanced at FOI to describe image generation in optronic systems. The program is compatible with Windows NT and Windows 95 and can be used with or without indata. In the latter, the program is used to simulate a sensor system’s ranges for objects

with a given size and temperature difference between target and background. Like in many other models, decision of range is based on the Johnson criterion and an MRTD function.

TERRTEX is another program developed at FOI for finding target and background qualities in sensor images. The tool has been modified several times and now includes an estimation of the probability of exploration of a target as a function of distance. The program does not treat recognition and identification; instead it involves background and its variations.

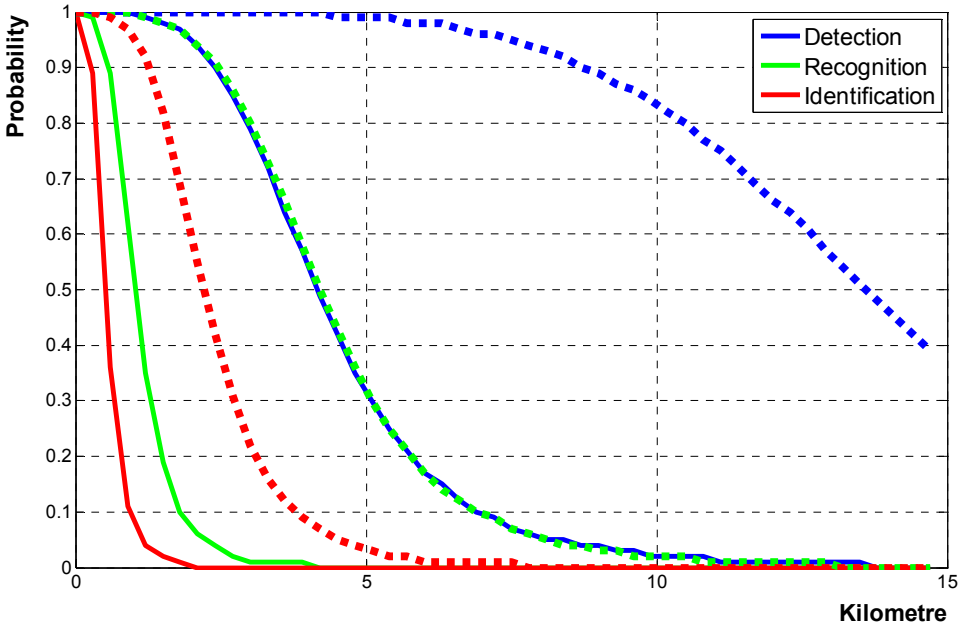

Figure 12-32. Example: detection (blue), recognition (green) and identification (red) ranges for a tank (2m x 5m) at clear weather conditions obtained with NVTherm (Sep2002). Sensor: Emerald (section 3.2.1) with a 50 mm (—) and a 250 mm lens (·····).

13 References

[1] Claes Nelsson, Pär Nilsson, *Measurement Equipment at the department of IR Systems*, FOA report, FOA-R--99-01111-615--SE (April 1999)

[2] E.L.Dereniak, G.D.Boreman. *Infrared detectors and systems*, John Wiley & Sons, Inc. (1996)

[3] G.C. Holst, *Electro-optical imaging system performance*, Fifth edition, JCD Publishing Co (2008)

[4] EMVA Standard 1288: http://emva.org

[5] I. Renhorn, *Modelling of Imaging Spectral Sensors*, FOI-R--2118--SE (2006)

[6] http://www.thermoteknix.com

[7] http://www.flir.com

[8] http://www.xenics.com

[9] http://www.qimaging.com

[10] Wilhelm Isoz, T.Svensson, I.Renhorn, *Nonuniformity correction of infrared focal plane arrays*, Infrared Technology and Applications XXXI, SPIE 5783-119, (2005)

[11] J.Ahlberg, I.Renhorn, T.Svensson, T.Winzell, G.Carlsson, *Multispektrala IR- & EO-sensorer*, FOI-rapport, FOI-R--1815--SE (2005)

[12] Renhorn I., Svensson T., Carlsson G., Letalick D., Larsson H., Steinvall O., *Försök med multispektrala aktiva/passiva sensorer,* FOI-R--0290--SE, teknisk rapport (2001)

[13] T.Svensson, I.Renhorn, *Multispectral MWIR imaging sensor*, Infrared Technology and Applications XXVIII, SPIE 4820-13, (2002)

[14] T.Svensson, I.Renhorn, P.Broberg. *Evaluation of a method to radiometric calibrate hot target image data by using simple reference sources close to ambient temperatures*, Infrared Imaging Systems: Design, analysis, modeling and testing XXI, Proc. of SPIE vol.7662, 76620X (2010)

[15] P.Broberg. *Kalibrering och modellering av multispektrala IR-kameror*,

Examensarbete vid FOI och LTU, LTU-EX--09/023--SE (2009)

[16] Thomas Svensson och Göran Carlsson. *Mätrapport från Semark fältförsök i Kvarn nov-dec 2005*, FOI report, FOI-R--2246--SE (2007)

[17] http://www.specim.fi

[18] Claes Nelsson. *Characterization of the polarimetric Imspec,* FOI-D--0284--SE (2007)

[19] Tomas Chevalier, *Samverkande sensorer - Illustrerat exempel med hyperspektral kamera och 3D-laserradar*, FOI-R--2325--SE (2007)

[20] http://www.abb.com

[21] Claes Nelsson. *MR304SC FTIR spectrometer. A system description and user guide,* FOI-D--0336--SE (2009)

[22] http://www.sphereoptics.com

[23] http://www.scintec.com

[24] I.Renhorn, T.Svensson, G.Carlsson, S.Cronström, *Inverkan av atmosfärsturbulens vid småmålsdetektion*, FOI-R--0715--SE (2002)

[25] I.Renhorn, T.Svensson, G.Carlsson, S.Cronström, G.Boreman, *Infrared image scintillation: comparison of modeling and measurement*, Optical Engineering Vol.45 (2006)

[26] http://www.davisnet.com/

[27] http://www.konikaminolta.com

[28] Cronström Staffan, Svensson Thomas, Renhorn Ingmar. *D8 – an image capturing software for advanced applications including temporal synchronization of imaging sensors*, Infrared Imaging Systems: Design, analysis, modeling and testing XXI, Proc. of SPIE vol.7662, 766216 (2010)

[29] T.Svensson, J.Ahlberg, L. Allard, S. Björklund, L Carlsson, S. Cronström, J. Fagerström, N. Karlsson, R. Lindell, I. Renhorn, N. Wadströmer. *Multi- och hyperspektral spaning 2006-2008—slutrapport*, FOI-R--2642--SE (2008)

[30] T. Winzell, *Basic optical sensor model*, FOI-R--2135--SE (2006)

[31] N-U. Jonsson, D. Murdin, *EDGEFIT Users Manual*, ISSN 1650-1942 (2008)

[32] J. Ahlberg, *A Matlab Toolbox for Analysis of Multi/Hyperspectral Imagery*, FOI-R--1962--SE (2006)

[33] Jörgen Ahlberg, *Estimating atmosphere parameters in hyperspectral data*, *Proceedings of SPIE* Vol. 7695 (Algorithms and Technologies for Multispectral, Hyperspectral, and Ultraspectral Imagery XVI), 76952A, 2010.

[34] L.W. Abreau, G.P. Anderson, *The MODTRAN 2/3 Report and LOWTRAN 7 Model*. Phillips Laboratory, Geophysics Directorate, PL/GPOS, Hanscom AFB, MA 01731-3010, USA (1996).

[35] A. Berk, G.P. Anderson, P.K. Acharya, E.P. Shettle, *MODTRAN®5.2.0.0 USER'S MANUAL*, (2008)

[36] F. Näsström et.al. *Metodik för teknisk värdering av sensorsystem med MSSLab*, FOI-R--3004--SE (2010)

[37] Bijl P., Hogervorst M.A., Valeton J.M., *TOD, NVTherm, and TRM3 model calculations: a comparison*, Proc. SPIE Vol. 4719, p. 51-62, Infrared and Passive Millimeter-wave Imaging Systems, 2002, FOI-R--3004--SE (2010)

[38] T.Maurer, R.G.Driggers, R.Vollmerhousen, M.Friedman, *NVTherm improvements*, Proc. SPIE Vol. 4719, FOI-R--3004--SE (2010)

[39] C. Wigren, *IGOSS Model of Image Generation in Optronic Sensor Systems*, FOA-R--97-00582-616--SE (1997)

[40] S. Nyberg, *Models used in assessment of optical sensors*, FOI-R--2290--SE (2007)

[41] L. Lindskog, *Mätvärdesbehandling och rapportering av mätresultat*. Hjo: Sandtorp Consult AB, 1994, ISBN 91-972122-8-8

[42] Claes Nelsson, *Kalibrering av data från Thermovision 900 i TP 86 Sabreliner*, FOA-R--99-01073-408--SE (1999)

14 Appendix A: Characterization of Cheetah-640CL

The EMVA model (section 2) is here applied on image data collected with Cheetah-640CL (section 3.1.4) using sub-windowing, 352 by 448 pixels. Prior to the calculations, the image data was cropped and an area of 150 by 150 pixels was retained in the middle of each image.

Table A-1. Measured and calculated EMVA parameters for Cheetah-640CL, T_{exp} = 498 µs, (frame rate = 2000 Hz), F/# = 1.4.

Parameter	**Value**	**Value**	**Value**	**Value**
μ_y [DN]	1069	1321	1777	2360
L [W m^{-2} sr^{-1}]	0.409	0.545	0.818	1.090
S [W]	6.5557e-11	8.7356e-11	1.3111e-10	1.7471e-10
μ_p [photons]	2.5145e+5	3.3506e+5	5.0290e+5	6.7013e+5
$\sigma^2_{y,temp}$ [DN]^2	14.5	16.0	18.7	22.5
$\sigma^2_{y,spat}$ [DN]^2	385	503	804	1497

(2-6): A diagram of μ_y vs. μ_p gives the dark current $\mu_{y,dark}$ and $K\eta$ (Figure A-1).

(2-10): A diagram of $\sigma^2_{y,temp}$ vs. μ_p gives $\sigma^2_{y.temp.dark}$ (Figure A-2).

(2-12): A diagram of $\sigma^2_{y,spat}$ vs. $\mu_p{}^2$ gives $\sigma^2_{y,spat,dark}$ (Figure A-3).

(2-14): A diagram of $\sigma^2_{y.temp}$-$\sigma^2_{y.temp.dark}$ vs. μ_y-$\mu_{y.dark}$ gives the gain K (Figure A-4).

(2-16): A diagram of $\sqrt{\sigma^2_{y,spat} - \sigma^2_{y,spat,dark}}$ vs. $\mu_y - \mu_{y,dark}$ gives S_g (Figure A-5)

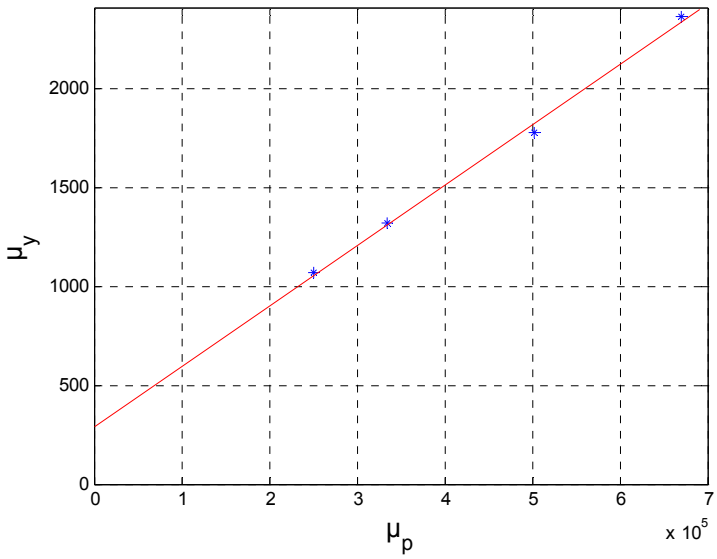

Figure A-1. $K\eta$ = 0.003048; $\mu_{y,dark}$ = 290.8

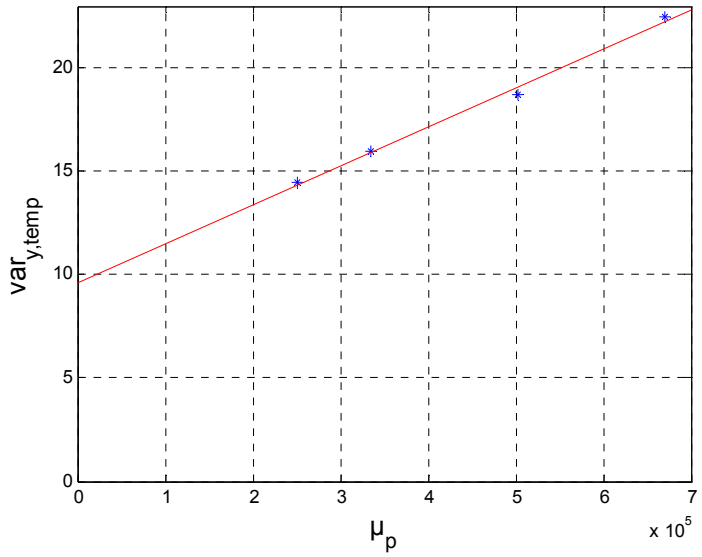

Figure A-2. $\sigma^2_{y.temp.dark} = 9.64$, $(slope = 1.88 \cdot 10^{-5})$

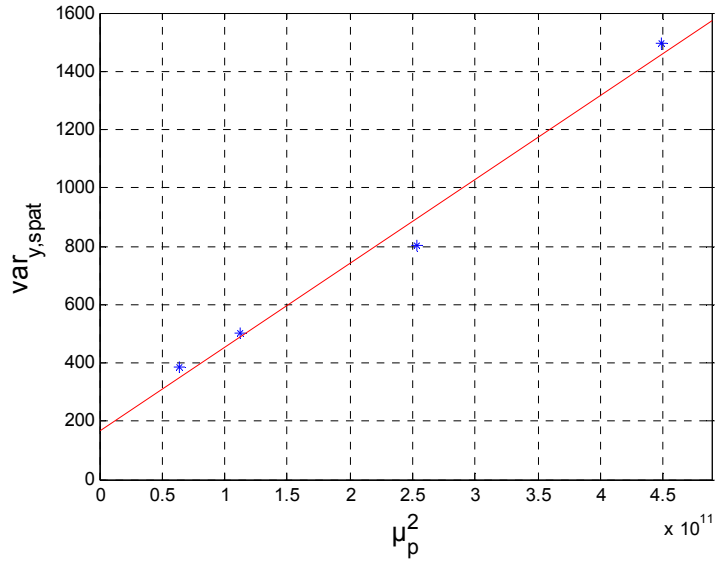

Figure A-3. $\sigma^2_{y,spat,dark} = 169$, $(slope = 2.68 \cdot 10^{-9})$

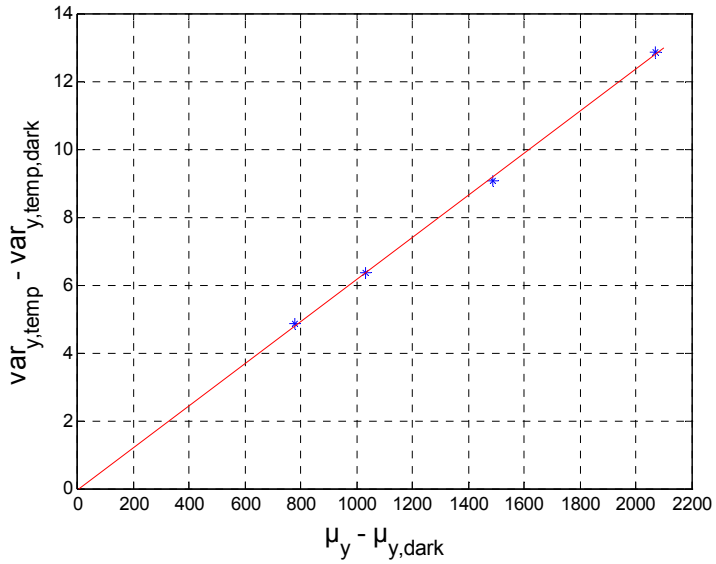

Figure A-4. K = 0.00618

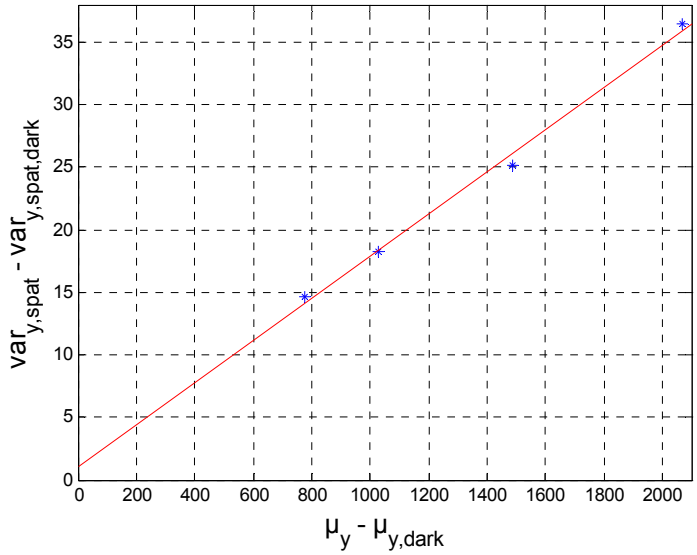

Figure A-5. S_g = 0.0173

Figure A-1 and A-4: $\eta = 0.493$ (49.3 %)

Figure A-2 and A-4: $\sigma_d = \frac{\sigma_{y,temp,dark}}{K} = 502.4$

Figure A-3 and A-4: $\sigma_0 = \frac{\sigma_{y,spat,dark}}{K} = 2104$

SNR, given by (2-20), is plotted vs. S [W] in Figure A-7. The sensitivity threshold is given at an SNR value equal to unity.

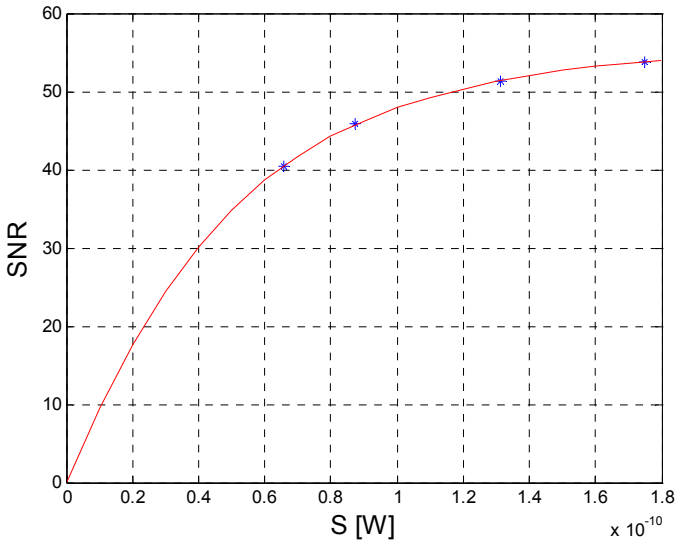

Figure A-6. SNR vs. incident power S [W]. The relation has been approximated by a 4th degree polynomial (red line). At SNR = 1, S = 1.04·10^{-12} W

(2-24): At room temperature a typical D* value of the InGaAs detector is 5 × 10^{12} cm·Hz^{½}·W^{-1}. With $A_d = (20 \cdot 10^{-4})^2$ cm^2 and $\Delta f = 1/(2 \cdot 0.000498)$ Hz, an NEP value = $2.83 \cdot 10^{-13}$ W is obtained.

In Figure A-7, SNR, given by (2-20), is plotted vs. μ_y. The maximum achievable SNR is reached at the saturation level.

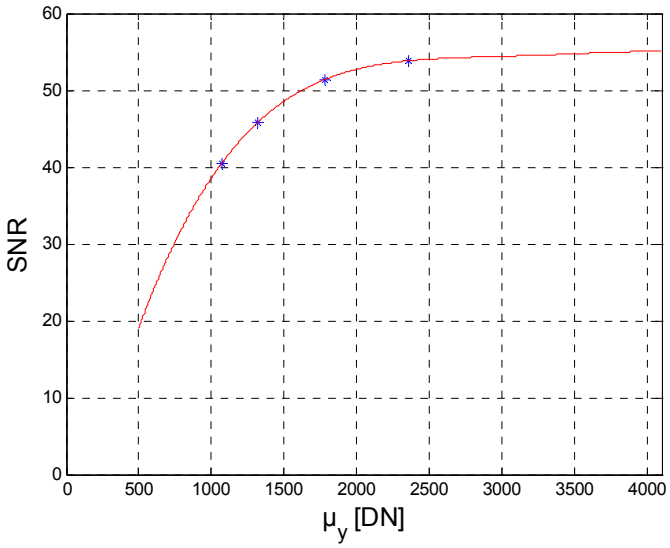

Figure A-7. SNR vs. μ_y [DN]. The relation has been approximated by a 4th degree polynomial (red line). A maximum SNR = 55 is obtained at the saturation level μ_y = 4095 (2^{12}-1).

In Figure A-8 the SNR for an ideal sensor, given by (2-5), is compared to the measured SNR for a real sensor, given by (2-20). Disregarding the spatial noise there are two limiting cases:

1. $SNR \approx \frac{\eta\mu_p}{\sqrt{\sigma_d^2}}$; $\eta\mu_p << \sigma_d^2$ (low photon range)

2. $SNR \approx \sqrt{\eta\mu_p}$; $\eta\mu_p >> \sigma_d^2$ (high photon range)

The slope of the SNR curve is therefore expected to change from a linear increase at low radiation to a slower, square root increase at high radiation.

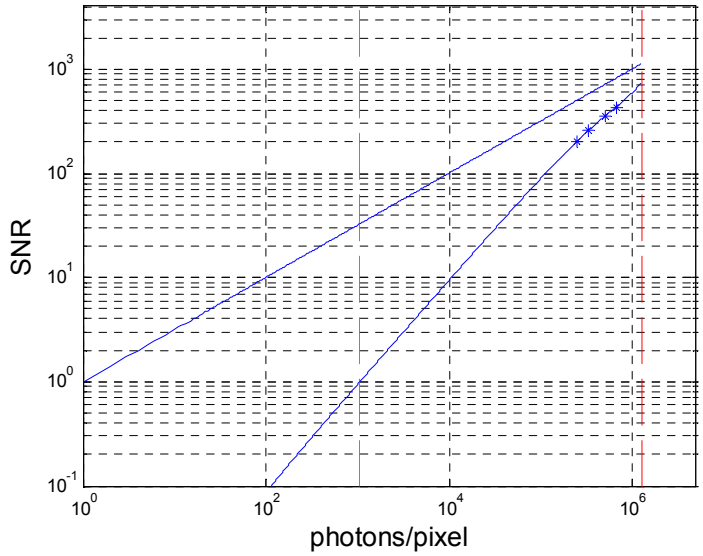

*Figure A-8. The figure compares the SNR of an ideal sensor (upper curve) with the measured SNR of a real sensor (lower curve), disregarding the spatial noise (the non-uniformity). A 2nd degree polynomial was fitted to the data points (marked *). A linear relation was assumed in the region between 10^2 and $2.5 \cdot 10^5$ photons/pixel (where no measurement data were available). The red, vertical lines mark the sensitivity (left line) and the saturation (right line) thresholds. The maximum achievable SNR values are 1017 for the ideal sensor and about 650 for the real sensor.*

Calculated spatial variances

At 50% saturation, $\mu_{y.50}$ is 2048 (4095/2). In the calculation below, image data with μ_y = 2360 ($\approx\mu_{y.50}$) was used.

(2-25): $DSNU_{1288}$ = 3860 [e^-] or $DSNU_{1288}$ = 23.9 [DN]

(2-26): $PRNU_{1288}$ = 8.7215

Calculated defect pixels

Semilogarithmic histograms for DSNU and PRNU images are shown in Figure A-9 and A-10. The PRNU image was not highpass-filtered before the calculation and Figure A-10 therefore shows the raw data results.

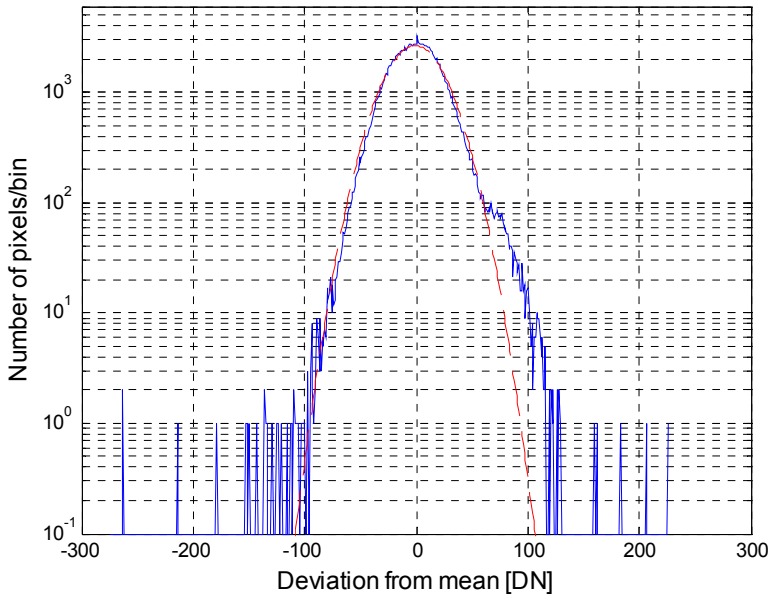

Figure A-9. Semilogarithmic histogram for the DSNU image with the normal probability distribution added (red dashed line)

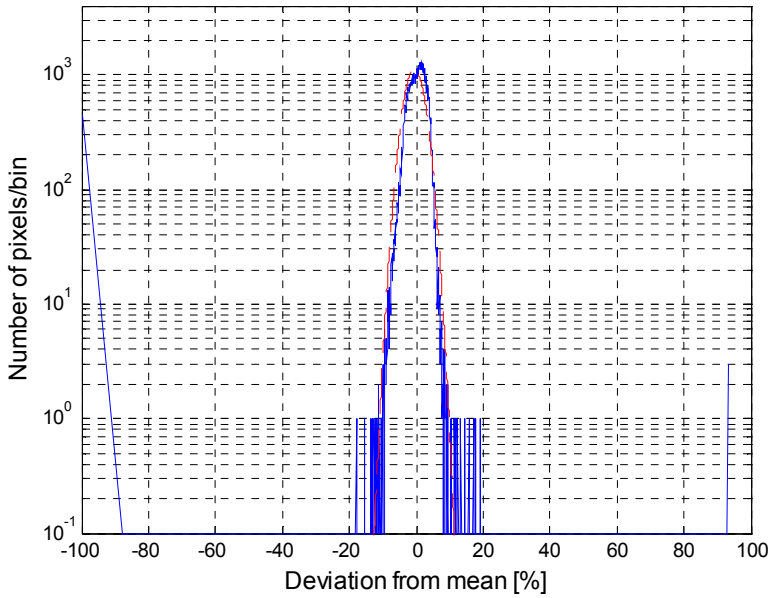

Figure A-10. Semilogarithmic histogram for the PRNU image with the normal probability distribution added (red dashed line). There are 495 pixels with the value 0. 3 pixels have significantly larger values than the mean value. The total number of pixels is 157696.

15 Appendix B: Measurement quality

"A measurement of any kind is incomplete, unless it is accompanied with an estimate of the uncertainty associated with that measurement." James M. Palmer

This section is based on [41] which uses GUM, *Guide to the Expression of Uncertainty in Measurement*, to report measurement results. An uncertainty analysis following the GUM method is found in [42].

X is the unknown quantity desired and x is the measurement result. The standard uncertainty is obtainable by two methods, type A or type B. Type A is based on statistical analysis and type B on all other methods e.g. estimates of the uncertainty.

For type A the standard uncertainty for x is

$$u(x) = \sqrt{\frac{1}{n-1}\sum_{i=1}^{n}\left(x_i - \bar{x}\right)^2} \qquad \text{(B-1)}$$

where x_i are measurement results and $\bar{x}$ is the mean value. The standard uncertainty for the mean value $\bar{x}$ is expressed in

$$u(\bar{x}) = \sqrt{\frac{1}{n(n-1)}\sum_{i=1}^{n}\left(x_i - \bar{x}\right)^2} \qquad \text{(B-2)}$$

In most cases the final result Y is a function of several measured quantities X_i

$$Y = f\left(X_1, X_2, ...X_n\right) \qquad \text{(B-3)}$$

The measurement result y is then obtained from

$$y = f\left(x_1, x_2, ...x_n\right) \qquad \text{(B-4)}$$

In this case a combined standard uncertainty $u_c(y)$ is calculated. If the quantities are non-correlated $u_c(y)$ is given by

$$u_c\left(y\right) = \sqrt{\sum_{i=1}^{n}\left(\frac{\delta f}{\delta x_i}\right)^2 u^2\left(x_i\right)} \qquad \text{(B-5)}$$

It is often required to use a measure of uncertainty that defines an interval about the measurement result y within which the value of Y can be confidently asserted to lie.

Then an expanded uncertainty, U, is used instead. It is calculated by multiplying the combined standard uncertainty (or standard uncertainty) with a coverage factor, k

$$U = k \cdot u_c(y) \tag{B-6}$$

The table below shows some coverage factors often used and which level of confidence they correspond to.

Table B-1. Coverage factors

Coverage factor	Level of confidence [%]
1.645	90
1.960	95
2.576	99

Sometimes the final result Y is a product of several measured quantities X_i

$$Y = X_1^{p_1} \cdot X_2^{p_2} ... X_n^{p_n} \tag{B-7}$$

The measurement result is then given by

$$y = x_1^{p_1} \cdot x_2^{p_2} ... x_n^{p_n} \tag{B-8}$$

Calculation of $\delta y/\delta x_i$ gives

$$\frac{\delta y}{\delta x_i} = x_1^{p_1} \cdot x_2^{p_2} ... p_i x_n^{p_{n-1}} ... x_n^{p_2} = y \frac{p_i}{x_i} \tag{B-9}$$

By substituting $\delta y/\delta x_i$ instead of $\delta f/\delta x_i$ in (5), $u_c(y)$ is given by

$$u_c(y) = \sqrt{\sum_{i=1}^{n} \left(y \frac{p_i}{x_i} u(x_i) \right)^2} \tag{B-10}$$

(B-10) can be rewritten:

$$\frac{u_c(y)}{y} = \sqrt{\sum_{i=1}^{n} \left(p_i \frac{u(x_i)}{x_i} \right)^2} \tag{B-11}$$

where $u_c(y)/y$ is the relative combined standard uncertainty.